4-24-2024

Development and Structure of Spinal Interneuron Connectivity in Larval Zebrafish

Saul Bello Rojas
Washington University in St. Louis

WASHINGTON UNIVERSITY IN ST. LOUIS

Division of Biology and Biomedical Sciences
Neurosciences

Dissertation Examination Committee:
Martha W. Bagnall, Chair
Andreas Burkhalter
Bruce A. Carlson
Aaron DiAntonio
David McLean

Development and Structure of Spinal Interneuron Connectivity in Larval Zebrafish

by
Saul Bello Rojas

A dissertation presented to
Washington University in St. Louis
in partial fulfillment of the
requirements for the degree
of Doctor of Philosophy

May 2024
St. Louis, Missouri

Table of Contents

List of Figures

Chapter 1

Chapter 2

Chapter 3

Chapter 4

List of Tables

Acknowledgments

The path towards earning a PhD was neither quick nor easy, and I have to thank so many people for their help along the way. My experience to get this point would not have been possible without your support. I will begin in chronological order to ensure that everyone gets their acknowledgment. I would like to begin by thanking my high school guidance counselor, Mrs. Samiah Garcia. It was thanks to her that I was encouraged to apply to college and pursue my love of science. Without her, I do not think that I would have attended college, so she was truly the first catalyst in my journey here.

I attended Lake Forest College with no idea what I wanted to do with my life. All I knew was that I wanted to study neuroscience. Thankfully, I was educated by several amazing professors: Dr. Shubhik DebBurman, Dr. Anne Houde, Dr. Matthew Kelley, Dr. Douglas Light, and Dr. Susan Long. You all were instrumental in helping me obtain the basic knowledge to enter the neuroscience field. Furthermore, I would like to thank Dr. DebBurman for giving me my first real lab opportunity after being let go from my first lab position. In the DebBurman lab, I would like to thank my bench mentors, friends, and now doctors, Dr. Natalie Kukulka and Dr. Maiwase Tembo. You both taught me everything that I needed to know about working in a lab, but additionally, you both taught me how to be a great lab mentor and lab personality. I always enjoyed going into lab when I knew that you all would be there. You were both kind, considerate, intelligent, and sincere, and more importantly, you showed me what type of lab mate and mentor I wanted to be. I need to thank my first lab mentees, Logan Graham and Peyton Schrag. Both students made working in the lab so much fun, and both were great students to mentor. Team Splice Variant for life. Lastly, I need to thank my college friends: Morgan Marshall, Benjamin Weiss, Daniel Lopez, Cesar Cardenas, John Vinkavich, and Taylor Jones.

You all were some of the best friends that someone could ask and really helped me get out of my shell.

I would like to acknowledge people from my time at Northwestern University beginning with Dr. Cassandra VanDunk and Dr. Sally McIver who ran the NeuroPREP program. You two were incredibly instrumental in my drive to attend graduate school by being supportive and encouraging me to apply to WashU. Furthermore, you made being a post-bac so much fun, and you put an amazing group together with Sierra, Andrew, Leah, and Chad. I know that all of us are incredibly grateful to have been a part of the program. Next, I need give a huge shout out to Dr. Dave McLean and the entire McLean lab (Sandeep, Mike, Cindy, Elisa, Moneeza). Without a doubt, Dave is one of the most influential people in my life. He was incredibly supportive, smart, and kind. He has a knack for taking any project and making it exciting, and in return he can make you enthusiastic about any project. It was his love for science that really convinced me to stay in the spinal cord and zebrafish field. I need to give special thanks to Sandeep, Mike, and Cindy. They were the postdocs in the lab, and they really pushed me to better myself as a scientist and excel to their level. Additionally, I enjoyed our beer and dinner outings, and it was great that you all wanted to hang out with a lowly post-bac.

From Washington University, I need to begin by acknowledging Dr. Martha Bagnall. She was the main reason that I wanted to apply and ultimately attend WashU. Martha is an amazing scientist who thinks critically about her work, but she is also an amazing teacher. I have learned so much from her during my time in her lab. Furthermore, she is a one of kind person who is very considerate, passionate, and empathetic. It is very hard to find a research adviser that can be your boss, friend, and at times, big sister. My time in the lab was truly special and meant so much to me. It was great to see her get promoted, which was very well deserved, and I am

excited to see what all comes out from her lab after I am gone. In addition to her mentoring style, Martha put together an amazing lab culture by recruiting a fun and supportive group of people. I want to thank all of the Bagnall lab members (Rich, Rebecca, Mohini, Zhikai, Vamsi, Yizhen, Zoe, Alaina, Mary, Devon, Peter, and Olivia) for their support. It has been a pleasure and honor to have worked with you all, and I am happy that you all are doing amazing things with your lives now. I still think that we should have gotten lab tattoos, but maybe we can table that again in the future.

I need to thank my other committee members: Dr. Bruce Carlson, Dr. Andreas Burkhalter, and Dr. Aaron DiAntonio. Thank you all for the support and feedback these past few years. Andreas, thank you for being a great teacher during systems. Aaron, thank you for letting me rotate in your lab and not getting mad about me leaving after ~3 weeks. Bruce, thank you for encouraging me to come to WashU. I apologize for not rotating, but I appreciate all of your advice as my chair. Next, I need to thank all of my friends from WashU. There are too many to name them all, but I need to give some special thanks to my cohort: Chas Pfeifer, Jiwon Yi, Katie Lefton, Marwa Mikati, Melvin King, Pingchuan Ma, Bobbie Brown, Zelun Wang, and honorary neuro student, Shashank Anand. I could not think of a better group of people to have started graduate school with. Everyone here is incredibly smart and talented, and everyone is going to do such amazing things in their lives. Our El Burro trips and "Let's just get one drink" nights will always be memorable even if most of them ended up being pretty hazy. Next, I need to thank the 4530 Crew (Adalee Lube, Ryan Raut, Lorenzo Lones, Allison Soung, and Melvin King). Living in the same building made graduate school seem like college. It was so much fun to have semi – weekly movies, game nights, and hiking trips. I need to thank the Sunday Crew: Chas Pfeifer, Ryan Bowen, Tomasz Kaszuba, Martin Jarzyna, Yizhen Jia, and Rick Reneau. We

started this Sunday tradition during COVID, and I am happy that it stuck around long after. It always made Sundays my favorite day to look forward to, and I look forward to continuing our annual trips to Arrowhead Stadium.

Lastly, I need to thank my family beginning with my parents. Even though you two did not fully understand what I was doing, your support never wavered. I appreciate all of your love, and it is truly special to see that your sacrifices and efforts got me this far. Kara, I love you very much, and I am excited for our new life in Portland. Thank you for putting up with my scientific ramblings. Additionally, thank you for being such a great pet mom to our four boys (Mosley, Les, Bucky, and Cap). The boys would be lost without you, and I know that they love you very much just like I do.

Saul Bello Rojas

Washington University in St. Louis
May 2024

Dedicated to mi familia.

ABSTRACT OF THE DISSERTATION

Development and Structure of Spinal Interneuron Connectivity in Larval Zebrafish

by

Saul Bello Rojas

Doctor of Philosophy in Biology and Biomedical Sciences

Neurosciences

Washington University in St. Louis, 2024

Professor Martha Bagnall, Chair

In vertebrates, spinal interneurons are essential for the initiation and propagation of locomotor activity with each class of interneurons serving its own unique role. Ipsilateral interneurons function to control locomotor speed; whereas, commissural interneurons aid in left – right alternation. To date, most studies have been aimed at studying the impact of each individual class of interneurons onto motor neurons. However, not much work has revolved around studying interneuron – interneuron connectivity among the various cardinal classes. Furthermore, it remains unknown how the connectivity of interneurons changes along their entire axonal reach. This thesis aims to address the developmental patterns and structure of interneuron connectivity along the spinal cord. Among the various types of interneurons, two major groups of ipsilaterally projecting interneurons emerge from the same progenitor cell yet diverge into distinct cell types due to differences in Notch signaling. V2a (NotchOFF) neurons and V2b (NotchON) neurons provide glutamatergic and GABAergic/glycinergic input onto motor neurons, respectively. Given their shared origin, it was important to evaluate their developmental connectivity because previous work showed that sisters neurons exhibit stereotypic patterns of

connectivity. In mammals, sister neurons assemble into shared microcircuits, whereas in Drosophila, Notch-differentiated sister neurons integrate into distinct circuits. Using an in vivo labeling approach, we identified pairs of sister V2a/b neurons born from individual Vsx1+ progenitors in the zebrafish spinal cord. We used paired whole-cell electrophysiology and optogenetics to reveal that sister V2a/b neurons do not communicate with each other, receive input from different presynaptic sources, and connect to distinct targets. These results resemble the divergent connectivity in Drosophila and represent the first evidence of Notch-differentiated circuit integration in vertebrates.

The scarcity of shared targets revealed potential differences in connectivity between V2a and V2b neurons. Prior research on the mapping of V2b postsynaptic targets revealed a connectivity preference for short range targets, but to date, there has been no systematic assessment of V2a postsynaptic targets. Direct assessment of V2a postsynaptic targets using optogenetics revealed that connections from V2a neurons are weighted to longer ranges, explaining the lack of shared targets. Not only did V2a neurons elicit more EPSCs onto target neurons at longer ranges (> 4 muscle segments away from the target neuron), the strength of the evoked EPSC events were larger than any of the observed local connections. Given the scarcity and strength of local connections, it is unlikely that V2a neurons function as the recurrent and rhythmogenic source in the unit burst generator model, but instead, the propensity to form long range connections could result from the need to ensure propagation of an excitatory wave down the spinal cord during locomotion and provide patterned input, such as directing turns.

Chapter 1: Introduction

1.1 Spinal Cord Function and Development

Locomotion is the primary means by which organisms engage and interact with their environments. Locomotor output is produced by the spinal cord and generated through neuronal networks comprised of various populations of excitatory and inhibitory interneurons. These networks then act in concert to govern the firing patterns of motor neurons (Goulding, 2009; Jankowska, 2001; Jankowska & Edgley, 1993; Kiehn, 2006; Sengupta & Bagnall, 2023). Motor neurons integrate neuronal input from various interneurons and provide the final output to skeletal muscles, producing locomotion and a wide range of other behaviors (Eccles, 1957; Henneman, 1957; Sherrington, 1904). The ability of spinal cord to produce these rhythmic movements is innate given that spinalized organisms are still able to produce rhythmic movements, demonstrating that higher order input is not needed for spinal cord rhythmicity (Fedirchuk et al., 1998; Grillner, 1985). Further evidence that spinal cord is intrinsically rhythmic came from the demonstration that isolated spinal cords in a dish were still able to produce rhythmic outputs (Cangiano & Grillner, 2003). These results suggest that there are intrinsic central pattern generators (CPGs) within the spinal cord that are able produce rhythmicity which is most likely established by the various interneurons in the spinal cord (Goulding, 2009; Grillner, 2003; Kiehn, 2006; Wilson & Wyman, 1965).

The organization of these spinal populations occurs early in embryo development. Genetic studies revealed that the activity of two morphogen gradients along the dorsal-ventral axis of the developing spinal cord establishes the order of the emerging progenitor groups (Goulding, 2009; Jessell, 2000; Le Dréau & Martí, 2012; Lee & Jessell, 1999). In the ventral

portion of the developing spinal cord, notochord and floor plate excrete Sonic hedgehog (Dessaud et al., 2008; Jessell, 2000; Yang et al., 2019), while the dorsal portion, the epidermis and roof plate release Bone Morphogenic Proteins (Cucun et al., 2024; Lee & Jessell, 1999). These opposing gradients are then responsible for initiating the developing neural programs within the spinal cord progenitor domains, leading to the diversity in cell type identity within the spinal cord (Cucun et al., 2024; Le Dréau & Martí, 2012; Sagner & Briscoe, 2019). Ultimately, the spinal cord is composed of five dorsally derived sensory population domains (dI1 – dI5) and six ventrally derived motor population domains (dI6, V0, V1, V2, V3, and motor neurons) with each cardinal class of neurons expressing unique molecular profiles (Goulding, 2009; Sagner & Briscoe, 2019). With our interest in locomotor control, we will be focusing on the ventrally derived populations.

1.2 Motor Neuron Connectivity and Firing Patterns

Motor neurons are a ventrally derived population and are the final step in the spinal cord's path to produce locomotion. This is accomplished through the release of acetylcholine from motor neurons onto the neuromuscular junction (Heckman & Enoka, 2012). In vertebrates, motor neurons are organized into motor units consisting of one motor neuron and all of the muscle fibers that it innervates (Heckman & Enoka, 2012; Henneman, 1957; Henneman et al., 1974; Henneman et al., 1965). These units are then organized and characterized by the type of muscle fibers that they innervate and the locomotor force produced (Heckman & Enoka, 2012). In total, there are three broad classes of motor units (Fast-twitch fatigable, Fast-twitch fatigue-resistant, and slow-twitch fatigue-resistant). Fast-twitch fatigable motor units are composed of the largest of muscles in addition to being innervated by the largest motor neurons; meanwhile, slow-twitch fatigue-resistant motor units consist of the smallest muscle fibers and the smallest motor neurons

(Heckman & Enoka, 2012; Henneman & Mendell). Fast-twitch fatigue-resistant motor neurons fall in between the previous two groups. According the size principle and recruitment properties, the slow-twitch motor units are recruited first given that their motor neurons have the highest input resistance, thus requiring the least of amount of excitatory input to reach firing threshold (Henneman, 1957; Henneman et al., 1974; Henneman et al., 1965). As the intensity of the movement increases, more excitatory input is driven onto motor neurons, and eventually, the fast-twitch fatigue-resistant motor units are recruited. Ultimately, once the excitatory input onto motor neurons becomes large enough, the large fast-twitch fatigable muscle, whose neurons have the lowest input resistances, get recruited (Henneman, 1957; Henneman et al., 1974; Henneman et al., 1965).

In addition to this recruitment order and differences in input resistance, the various types of motor neurons also exhibit other electrophysiological differences such as firing patterns (Henneman, 1957; Menelaou & McLean, 2012). In larval zebrafish, which is the model system used in our studies, the slow motor neurons, also known as s-type secondary motor neurons, have higher input resistances and exhibit a bursting firing pattern (Bello-Rojas et al., 2019; Menelaou & McLean, 2012). The combination of these properties suggest that s-type secondary motor neurons are more intrinsically rhythmic and do not need much input to shape their oscillatory drive (Menelaou & McLean, 2012). However, fast muscle innervating motor neurons, also known as primary motor neurons, have lower input resistances and exhibit a tonic firing pattern (Eisen et al., 1990; Menelaou & McLean, 2012). The combination of these two properties suggest that large motor neurons are not inherently rhythmic and require more synaptic drive to be recruited and generate their rhythmicity. Thus, the patterned input that the various interneuron

groups in the spinal cord provide to motor neurons is crucial for establishing the rhythmic drive needed to allow motor neurons to function properly.

1.3 Ipsilateral Interneuron Input onto Motor Neurons

The ventral spinal cord possesses two broad classes of ipsilaterally projecting interneurons, V1 and V2 neurons (Fig 1.1, Table 1.1). V1 neurons are an inhibitory cell type that are marked by the expression *en1* and have long ascending axons (Alvarez et al., 2005; Higashijima et al., 2004; Li et al., 2004; Saueressig et al., 1999; Wenner et al., 2000). V1 neurons have been shown to provide reciprocal inhibition onto local motor circuits in addition to aiding in flexor/extensor alternation in limbed organisms (Britz et al., 2015; Zhang et al., 2014). V1 neurons fire in phase with motor neuron activity as a means to provide rapid inhibition onto motor pools (Jay et al., 2023; Kimura & Higashijima, 2019). This inhibitory circuit is believed to aid in the transition from slow to fast movements. This hypothesis was further supported when loss of V1 neurons in both mouse and zebrafish showed that organisms were unable to move at faster speeds (Falgairolle & O'Donovan, 2019; Gosgnach et al., 2006; Kimura & Higashijima, 2019). Recently, new subclasses of V1 neurons have been identified with each subclass expressing their own unique molecular markers (Bikoff et al., 2016; Worthy et al., 2023); however, it remains unknown how each these various subclasses contributes to the overall locomotor circuit.

The last cardinal class of ipsilaterally projecting interneurons are V2 neurons (Al-Mosawie et al., 2007; Lundfald et al., 2007; Peng et al., 2007). The V2 class of interneurons is composed of three distinct subclasses (V2a, V2b, and V2c mouse/V2s zebrafish). V2a neurons are glutamatergic and express the transcription factor, *chx10* (Hayashi et al., 2018; Kimura et al., 2006; Li et al., 2009; McLean & Fetcho, 2009; Menelaou et al., 2014). Activation of V2a neurons has been shown to increase excitability of locomotor populations in the spinal cord

(Hägglund et al., 2010; Hayashi et al., 2018; Menelaou & McLean, 2019; Menelaou et al., 2014). Furthermore, loss of V2a neurons has been linked to decreases in locomotor output and the inability to drive motor neuron recruitment (Crone et al., 2008; Crone et al., 2009; Eklöf-Ljunggren et al., 2012). Thus, V2a neurons are an important cell type in the spinal cord given their ability to promote excitability of the locomotor circuit. Anatomical evidence later confirmed that V2a neurons form synaptic contacts onto motor neurons, directly driving excitability of motor populations in addition to other spinal groups (Crone et al., 2008; Kimura et al., 2006; Menelaou & McLean, 2019; Song et al., 2018; Song et al., 2020). Further anatomical and electrophysiological evidence revealed that V2a neurons can be divided into two distinct subclasses (Type I and Type II). Type I V2a neurons only have intraspinal projections and form preferential connections onto other V2a neurons (Hayashi et al., 2018; Menelaou & McLean, 2019; Menelaou et al., 2014). Type II V2a neurons have both intraspinal and supraspinal projections and mostly synapse onto motor neurons (Hayashi et al., 2018; Menelaou & McLean, 2019; Menelaou et al., 2014). Given these differences in connectivity, it is hypothesized that Type I V2a neurons are mostly involved in rhythmogenesis and maintaining the rhythmic nature of the spinal cord (Agha et al., 2024; Menelaou & McLean, 2019). Type II V2a neurons are believed to involved in pattern generation and recruitment of motor neurons (Agha et al., 2024; Menelaou & McLean, 2019). However, the role of supraspinal Type II V2a projections remains unknown.

V2b neurons are inhibitory interneurons that express *gata3* and are thought to play a role in inter-limb coordination (Callahan et al., 2019; Lundfald et al., 2007; Sengupta & Bagnall, 2022). Similar to V1 neurons, V2b neurons have been shown to enforce flexor – extensor alternation (Zhang et al., 2014). Furthermore, there is evidence in zebrafish that suggests that

V2b neurons function as locomotor brakes by providing short range inhibition onto motor neurons and V2a neurons (Callahan et al., 2019). Lastly, V2c/s neurons have been more recently discovered. Both V2c/s neurons are ipsilaterally projecting, glycinergic neurons that express *sox1*; however, their contributions to locomotion remain unknown (Cucun et al., 2024; Gerber et al., 2019; Li et al., 2010; Panayi et al., 2010). Altogether, ipsilaterally projecting interneurons serve to provide input in – phase with locomotor activity to either initiate or reduce locomotor output (Jay et al., 2023; Kimura & Higashijima, 2019; Menelaou & McLean, 2019).

1.4 Commissural Interneuron Input onto Motor Neurons

Motor neurons are rhythmically active during locomotion, and this activity is driven by an alternating pattern of excitation to promote firing and inhibition to suppress firing (Kiehn, 2016; Kjaerulff & Kiehn, 1997). This alternating pattern of excitation and inhibition is accomplished through several classes of commissural innervating neurons inhibitory (dI6 and V0d) neurons (Goulding, 2009; Lanuza et al., 2004; Satou et al., 2012; Satou et al., 2020; Stokke et al., 2002; Talpalar et al., 2013) (Fig 1.1, Table 1.1). Both dI6 and V0d neurons have been shown to form monosynaptic connections onto motor neurons (Satou et al., 2020; Talpalar et al., 2013). These connections aid in left – right alternation within the spinal cord by providing inhibition to contralateral motor populations during activation of ipsilateral motor neurons (Kiehn, 2016; Satou et al., 2020). V0d neurons were shown to be more active during stronger/faster movements in zebrafish; whereas, a subset of dI6 neurons labeled by the expression of *dmrt3a* transcription factor were more active at slow and intermediate speeds (Satou et al., 2020). The recruitment of dI6 neurons at slow locomotor speeds was further supported when horses with mutations in dI6 neurons were able to produce faster speeds (Andersson et al., 2012). This suggests that there are speed and frequency dependent recruitment properties within these interneuron populations as

means of locomotor control, and ablation or inactivation of these neurons would have different effects on movement given the locomotor speed being produced (Kishore et al., 2020; Satou et al., 2020).

V0v and V3 neurons are the two groups of excitatory commissural interneurons in the spinal cord which are believed to aid general spinal cord excitability and locomotor strength (Kawano et al., 2022; Zhang et al., 2008). V0v neurons are defined by the expression of both *dbx*, which labels all V0 neurons, and *evx1*, which only labels the excitatory subset (Juárez-Morales et al., 2016; Kawano et al., 2022; Pierani et al., 2001), while V3 neurons are labeled by the transcription factor *sim1* (Blacklaws et al., 2015; Borowska et al., 2015; Borowska et al., 2013; Zhang et al., 2008). V0v neurons have been shown to be exclusively recruited in slow swim in both larval and adult zebrafish and are thought to promote general spinal cord excitability (Björnfors & El Manira, 2016; Kawano et al., 2022) More recently, it has been reported that V0v neurons play an important role in trunk and head stability at slow speeds by helping maintain the stereotyped S-shaped body bend in fish (Kawano et al., 2022). Loss of V0v neurons not only led to head instability, but it also caused an inability for the fish to produce their S-shaped body bends during swim. Meanwhile, V3 neurons are believed to be involved in modulating the strength of movement (Böhm et al., 2022; Zhang et al., 2022; Zhang et al., 2008). V3 neurons' ability to control strength of movement could be a result of their synaptic connections onto motor neurons and recurrent excitatory connection onto other V3 neurons (Chopek et al., 2018; Zhang et al., 2008). This recurrent excitatory circuit sets up a means to provide more electrical input onto the locomotor bout as needed with more powerful movements by recruiting more V3 neurons (Chopek et al., 2018). This claim was further supported when loss of V3 neurons resulted in a reduction of locomotor bouts (Böhm et al., 2022; Zhang et al., 2022).

Ultimately, commissural interneurons play crucial roles in left – right alternation and frequency dependent movements produced by locomotor circuits; however, a lot remains unknown given the technical difficulties of assessing commissural connectivity (Sengupta & Bagnall, 2023).

1.5 Coordination and Connectivity Between Interneurons

Due to the importance of motor neuron modulation in locomotor output, most researchers have focused on the impact of each interneuron class onto motor neurons; however, only recently have researchers begun to assess the connectivity between the various interneurons onto each other (Grillner et al., 2007; Sengupta & Bagnall, 2023; Zhang et al., 2008). Thus far, researchers have relied on the use of rabies tracing and inducible Cre transgenic lines to label neurons in the spinal cord (Hayashi et al., 2018; Li et al., 2010; Talpalar et al., 2013; Worthy et al., 2023). In part, these labeling methods have made it difficult to capture the entire extent of interneuron populations given that rabies tracing can be unreliable at crossing all synapses equally. Additionally, it is difficult to control the spread of the injected viruses, leading to non-specific and/or aberrant labeling (Willenberg & Steward, 2015; Worthy et al., 2023). Furthermore, recent work has revealed subtype heterogeneity within the various cardinal classes, leaving several subtypes under labeled or simply unidentifiable (Worthy et al., 2023). However, this should not overshadow the importance of understanding the various connections among interneurons. In fact, most computational models of the CPG network rely on the interconnectivity of interneuron cell types to function properly (Danner et al., 2017; Grillner et al., 2007; Roussel et al., 2021) Thus, it is imperative for the field to further evaluate the various connections between interneuron groups.

Furthermore, interconnectivity among the various interneuron groups has been implicated in an organism's ability to adapt their locomotor speeds (Kimura & Higashijima, 2019; Satou et

al., 2020; Talpalar et al., 2013). Thus far, most interneuron – interneuron connections have been shown to aid in the transition from slow to fast speeds, wherein subsets of interneurons such as slow – recruited V1 neurons inhibit slow – recruited V2a neurons in order for the organism to reach its top speeds (Kimura & Higashijima, 2019). This is just one example of speed – specific interneuron – interneuron interactions, but it reveals how important understanding these intraspinal connections are to a functioning organism. To date, most of the interneuron – interneuron interconnectivity has been observed and measured by using paired recordings (Chopek et al., 2018; Menelaou & McLean, 2019; Radosevic et al., 2019; Song et al., 2018; Song et al., 2020). Although this is powerful tool to measure direct connectivity, it is a very low throughput method for identifying all of the interneuron connections within the spinal cord. The challenges of identifying potential interneuron – interneuron connections are further exacerbated by the scarcity of connections within the spinal cord (Radosevic et al., 2019). New optogenetic protocols have attempted to aid in providing higher throughput methods of assessing interneuron connectivity (Hayashi et al., 2023; Hayashi et al., 2018; Sengupta & Bagnall, 2022; Sengupta et al., 2021). However, the inability to assess direct monosynaptic connections due to antidromic spiking and induced polysynaptic connections have hindered the viability of these protocols and identification of these connections (Hayashi et al., 2023). Thus, better and more selective protocols need to be established to improve the accessibility of these experiments. Although it may be difficult to identify all of interneuron connections due to the scarcity or selectivity of these contacts, any evidence will elucidate the machinations of the spinal cord network and further aid in work revolved around re-establishing spinal cord function post injury (Li et al., 2023; Zholudeva et al., 2017).

1.6 Developmental Origins Shape Circuit Modules

What factors aid in the assembly of spinal cord connectivity? Developmental timing and birth order allow for proper integration of neurons into functional speed - dependent locomotor circuits in spinal cord (McLean et al., 2007; McLean & Fetcho, 2009). In zebrafish, it has been well established that motor neurons and interneurons born during the same developmental periods form distinct circuit modules with each other. During locomotion, these temporally linked circuit modules get recruited at similar speeds (Ampatzis et al., 2014; McLean et al., 2007). Similar developmental windows have now been observed in mice where different subtypes of a cardinal class of interneurons (i.e. V1 and V3 neurons) are born during different developmental periods (Deska-Gauthier et al., 2020; Russ et al., 2021; Worthy et al., 2023). These temporally distinct subtypes end up expressing unique molecular profiles and occupy different regions of the spinal cord. Further evaluation will help determine whether these unique subtypes are also important for specific locomotor movements or recruited for different speeds. Thus, developmental birthdate helps establish the heterogeneity of cellular cell type and function within the spinal cord by establishing unique topographical maps of recruitment and functions. This feature is not unique to spinal cord, and in fact, the nervous system utilizes developmental topographic maps of organization for sensory systems as well such as the vision, auditory, and vestibular systems (Kandler et al., 2009; Liu et al., 2022; Tootell et al., 1982).

In recent years, there has been more attention in evaluating the relationship between circuit connectivity and ancestral origin within the nervous system. In particular, researchers have begun to evaluate the impact of how being derived from a shared lineage (i.e. common progenitors) impacts a cell's circuit connectivity. In part, this is due to the new technical ability of being able to tag and sort developing progenitors to identify commonly derived neurons post

mitotically (Mayer et al., 2015; Xu et al., 2014; Yu et al., 2009; Zhang et al., 2017). In mouse cortex, lineage tracing experiments have revealed that neurons which are clonally related (i.e. originate from the same progenitor cell) have a greater likelihood of being integrated within the same microcircuit than neurons that are not clonally related (Xu et al., 2014; Yu et al., 2009; Zhang et al., 2017). In this case, excitatory sister neurons were more likely to synapse onto each other than neurons that were not clonally related in mouse cortex (Yu et al., 2009). This result was not the only outcome of preferential connectivity among sister neurons. In the hippocampus, sister pyramidal neurons were more likely to receive input from the same presynaptic source than non - sister neurons (Xu et al., 2014). Lastly, sister inhibitory neurons in cortex are more likely to connect to the same downstream postsynaptic targets than non - sister cells (Zhang et al., 2017). However, this last claim has been disputed given contradictory evidence between different research groups, suggesting that sister inhibitory interneurons do not preferentially connect to same downstream targets (Mayer et al., 2016; Mayer et al., 2015). These contradictory results bring into question the reliability and viability of labeling clonally related sister neurons using Cre viruses given potential off – target effects even with techniques such as sparse labeling. Although these labeling methods have advanced our understanding of lineage tracing, direct ancestry can only be inferred given the *in utero* development of the nervous system in mammalian models. Thus, a more direct method to observe shared lineage would be needed to resolve these inconsistencies.

Special circuit relationships among clonally related neurons have also been observed in invertebrates. In *Drosophila*, developing sister neurons undergo Notch – mediated differentiation giving rise to distinct sister neurons (Artavanis-Tsakonas et al., 1999; Endo et al., 2007; Harris et al., 2015; Lacin et al., 2019). In this scenario, one sister neuron undergoes an upregulation of

Notch ($Notch^{ON}$), whereas the other sister neuron undergoes a downregulation of Notch ($Notch^{OFF}$) (Harris et al., 2015; Lacin et al., 2019; Lacin & Truman, 2016). Upon developing, clonally related, Notch-differentiated sister neurons integrate into distinct Notch hemilineages, extending to different regions of the *Drosophila* nervous system. These results demonstrate that despite their clonal relationship, Notch-differentiated sister neurons are actively being separated and integrated into distinct circuits. However, the question remains whether these intrinsic properties are determined by the differences between vertebrate vs invertebrate systems or if it is related to the Notch-mediated developmental component.

As described above, neuronal birthdate plays an important role in locomotor circuit formation with neurons born during similar time periods being recruited for similar behaviors. As such, there is strong possibility that many of the speed - dependent locomotor microcircuits established in the spinal cord utilize some form of clonal relationships/identity to establish functional circuits. This hypothesis will be tested using clonally related, Notch-differentiated V2a/b neurons and presented in Chapter 2.

1.7 Longitudinal Structure of Spinal Cord Connectivity

A key to proper locomotor output is the ability to coordinate the locomotor signal down the entire length of the spinal cord (Bonnot et al., 2002; Wiggin et al., 2014; Wolf et al., 2009). This requires both inhibitory and excitatory signals to be organized along the longitudinal axis of the spinal cord as the locomotor wave originates in the most rostral portion of the cord and later travels and terminates caudally (Grillner, 2003; Kiehn, 2006, 2016; Kozlov et al., 2009; Tunstall & Roberts, 1994). Coordination is accomplished by the various groups of interneurons some of which span the entire rostral-caudal extent of the spinal cord. However, in some cardinal classes, variability does exist in form of preferential connectivity among the various subtypes to specific

postsynaptic populations (Hayashi et al., 2018; Menelaou & McLean, 2019; Satou et al., 2020; Sengupta & Bagnall, 2022; Sengupta et al., 2021). For example, it has been shown that V1 neurons target motor populations (motor neurons and V2a neurons) locally but target sensory populations further away from the V1 cell body in larval zebrafish (Sengupta et al., 2021). Thus, the variability seen along the rostral-caudal axis of the spinal cord suggests important structural dynamics which have not been fully addressed. In part, this is due to the technical difficulties involved with using mammalian models where electrophysiology recordings are performed either in slice or *ex vivo* preps (Ampatzis et al., 2014; Kiehn, 2016; Sengupta & Bagnall, 2023).

These technical issues have made it difficult to test computational models such as the CPG network model, in which V2a neurons have been hypothesized to play a major role (Grillner & Manira, 2020; Song et al., 2020). V2a neurons are glutamatergic and excite both motor neurons and other V2a neurons (Kimura et al., 2006; Menelaou & McLean, 2019; Song et al., 2018; Song et al., 2020). V2a neurons are found across the entire rostral-caudal axis of the spinal cord (Hayashi et al., 2018; Menelaou et al., 2014), and furthermore, loss of V2a neurons have shown to greatly reduce the recruitment of motor populations (Crone et al., 2008; Crone et al., 2009; Eklöf-Ljunggren et al., 2012). These results have made V2a neurons an important cell type to study in the context of CPG model given that V2a neurons satisfy the key features of the unit burst generator hypothesis: (1) an ipsilateral excitatory cell type that can provide both (2) recurrent excitation onto itself and (3) excitatory input onto motor neurons. This hypothesis was later supported by work in adult zebrafish which revealed that V2a neurons provide excitation to local V2a neurons (recurrence) and onto local motor neurons (output) (Song et al., 2020). Given the identified local preference of V2a neurons to target both V2a and motor neurons and the anatomical evidence that V2a neurons extend along the full longitudinal axis of the spinal cord, it

is possible that other preferential connections onto other cell types exist along the longitudinal axis of the spinal cord. Thus, a comprehensive analysis of postsynaptic targets of V2a neurons, and the structure of these connections along the rostral - caudal axis, can assess both how well V2a neurons fit with their proposed role in rhythmogenesis, as well as their potential roles in other forms of locomotor control. These questions will be addressed in Chapter 3 of this thesis.

1.8 Figures and Legends

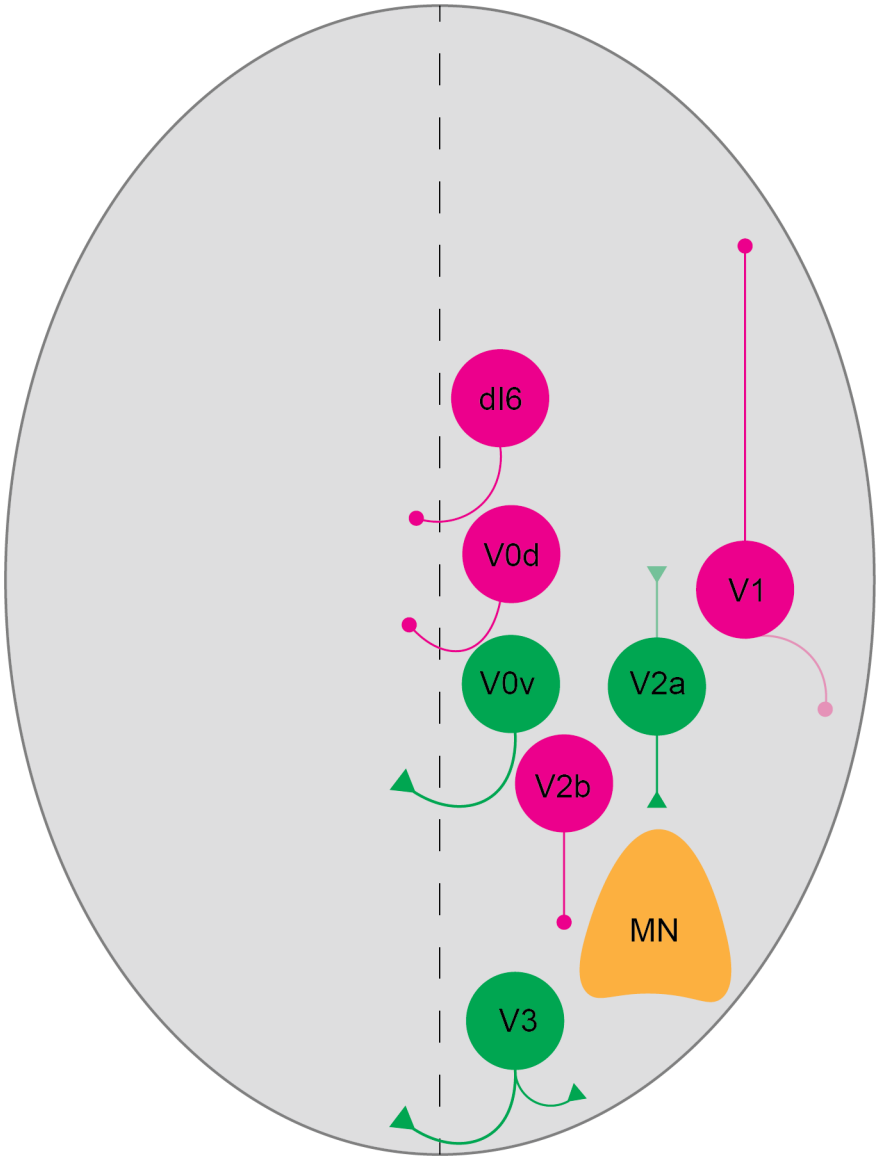

Figure 1.1 Schematic of spinal cord and the ventrally derived cell types.

Cross section of the spinal cord showing the various cardinal classes of neurons. Excitatory (glutamatergic) neurons are shown in green. Inhibitory (glycinergic and GABAergic) neurons shown in magenta. Motor neurons (cholinergic) are shown in yellow. Adapted from (Sengupta & Bagnall, 2023)

1.9 Tables

Cell Type	Neurotransmitter	Transcription Factor	Function
dI6	Glycine	*dmrt3a, wt1*	Speed dependent left – right alternation
V0d	GABA	*dbx1*	Speed dependent left – right alternation
V0v	Glutamate	*dbx1, evx1*	Head stability; General excitability; Left – right coordination
V1	GABA; Glycine	*en1*	Reciprocal inhibition; Flexor/Extensor alternation
V2a	Glutamate	*chx10*	In – phase excitation
V2b	GABA; Glycine	*gata3*	Flexor/Extensor alternation; In – phase inhibition
Motor Neurons	Acetylcholine	*mnx1*	Excitation of muscle fibers
V3	Glutamate	*sim1*	Recurrent excitation; Modulation of locomotor strength

Table 1.1 Ventral spinal cord population summary

Table listing the various ventral spinal cell types, their neurotransmitter, expressed transcription factors, and general function.

Chapter 2: Clonally related, Notch-differentiated spinal neurons integrate into distinct circuits

This chapter is adapted from the following publication:

Bello-Rojas, S. & Bagnall, M.W. (2022). Clonally related, Notch-differentiated spinal neurons integrate into distinct circuits. *eLife*, 11:e83680

2.1 Abstract

Shared lineage has diverse effects on patterns of neuronal connectivity. In mammalian cortex, excitatory sister neurons assemble into shared microcircuits. In Drosophila, in contrast, sister neurons with different levels of Notch expression ($Notch^{ON}$/$Notch^{OFF}$) develop distinct identities and diverge into separate circuits. Notch-differentiated sister neurons have been observed in vertebrate spinal cord and cerebellum, but whether they integrate into shared or distinct circuits remains unknown. Here we evaluate the connectivity between sister V2a ($Notch^{OFF}$) / V2b ($Notch^{ON}$) neurons in the zebrafish spinal cord. Using an *in vivo* labeling approach, we identified pairs of sister V2a/b neurons born from individual Vsx1+ progenitors and observed that they have somata in close proximity to each other and similar axonal trajectories. However, paired whole-cell electrophysiology and optogenetics revealed that sister V2a/b neurons receive input from distinct presynaptic sources, do not communicate with each other, and connect to largely distinct targets. These results resemble the divergent connectivity in Drosophila and represent the first evidence of Notch-differentiated circuit integration in a vertebrate system.

2.2 Introduction

How does shared lineage affect neuronal circuitry? Neurons arising from common progenitors are more likely to exhibit stereotypic patterns of connectivity, in two models from vertebrate and invertebrate systems. In mouse cortex, clonally related excitatory sister neurons preferentially form connections within a shared microcircuit (Xu et al., 2014; Yu et al., 2009). In contrast, clonally related sister neurons in Drosophila form distinct Notch^{ON} and Notch^{OFF} hemilineages which innervate distinct targets and often express different neurotransmitters (Artavanis-Tsakonas et al., 1999; Endo et al., 2007; Harris et al., 2015; Lacin et al., 2019; Lacin & Truman, 2016; Mark et al., 2021; Pinto-Teixeira & Desplan, 2014; Skeath & Doe, 1998).

Notch-differentiated clonally related sister neurons have been observed in the vertebrate spinal cord and cerebellum (Kimura et al., 2008; Peng et al., 2007; Zhang et al., 2021), but it remains unknown whether these clonally related neurons integrate into shared circuits. In ventral spinal cord, motor neurons and interneurons develop from five progenitor domains (p0, p1, p2, pMN, p3) (Goulding, 2009; Goulding & Lamar, 2000; Jessell, 2000). Progenitors in the p2 domain transiently express the transcription factor Vsx1 (Kimura et al., 2008; Passini et al., 1998). Each p2 progenitor makes a final paired division into an excitatory V2a (Notch^{OFF}) and an inhibitory V2b (Notch^{ON}) neuron, via asymmetric expression of Delta ligands and subsequent Notch-mediated lateral inhibition (Del Barrio et al., 2007; Francius et al., 2016; Kimura et al., 2008; Okigawa et al., 2014; Peng et al., 2007).

Although both V2a and V2b neurons project axons ipsilaterally and caudally, these neuron classes differ in other aspects. V2a interneurons express *vsx2* (referred to as *chx10* in this paper for clarity) and provide glutamatergic drive onto motor populations (Kimura et al., 2006), whereas V2b interneurons express *gata3* and provide glycinergic and GABAergic inhibition onto

motor populations (Andrzejczuk et al., 2018; Callahan et al., 2019). V2b neurons also support flexor/extensor alternation through reciprocal inhibition in limb circuits (Britz et al., 2015; Zhang et al., 2014). Given their shared origin but divergent cellular identities, it remains unknown whether these V2a/b sister neurons integrate into shared or distinct functional spinal circuits. We investigated whether V2a/b sister neurons in zebrafish spinal cord preferentially integrate in shared circuits, as with clonally related cortical neurons, or distinct circuits, as with Notch-differentiated hemilineages in Drosophila. Using a sparse labeling approach, we directly observed and identified individual pairs of sister V2a/b neurons arising from a single progenitor. Our morphological and electrophysiological analyses reveal that although sister V2a/b neurons share anatomical characteristics, these sister neurons diverge into separate circuits, with largely distinct presynaptic and postsynaptic partners. To the best of our knowledge, this is the first assessment of circuit integration of Notch-differentiated clonally related neurons in vertebrate models.

2.3 Results

Micro-injection of vsx1 plasmid allows for clonal pair tracking in vivo

In both zebrafish and mice, *vsx1+* progenitors give rise to two distinct daughter populations, V2a and V2b neurons (Kimura et al., 2008; Peng et al., 2007). Using transgenic zebrafish, individual *vsx1+* progenitors have been shown to undergo a final paired division into one V2a ($Notch^{OFF}$) and one V2b neuron ($Notch^{ON}$) (Fig. 1A) (Kimura et al., 2008). We aimed to develop a protocol to label and identify individual clonal pairs resulting from this division *in vivo*. To label individual pairs, we micro-injected titrated amounts of a bacterial artificial chromosome (BAC) construct, *vsx1:GFP*, into fertilized zebrafish embryos at the single-cell stage (Fig. 1B). At the 21-somite stage, larval zebrafish were screened for *vsx1* GFP+

progenitors and then imaged every 5 minutes to capture the progenitor division (Fig. 1C). Progenitors become elongated before dividing into two distinct cells.

When the fish become free swimming at 4 days post fertilization (dpf), *vsx1* GFP+ pairs were assessed for co-expression of known V2a/b transcription factors (*chx10/gata3*) to verify their neuronal identities, using transgenic fish *Tg*(*chx10:lox-dsRed-lox:GFP)* (Kimura et al., 2006) or *Tg*(*gata3:lox-dsRed-lox:GFP)* (Callahan et al., 2019) (Fig. 1D). For simplicity, these fish lines will be referred to as *chx10:Red* and *gata3:Red.* We assayed these in separate experiments due to overlap in fluorescence from reporter lines. Fig. 1D presents example images of *vsx1* GFP+ pairs in which one of the two neurons in the pair expresses the appropriate marker: a clonal pair (green) where one neuron co-expresses the V2a marker Chx10 (left), and a different clonal pair in which one neuron co-expresses the V2b marker Gata3 (middle). Based on previous work, we expected that every *vsx1* GFP+ pair would consist of one V2a and one V2b neuron (Kimura et al., 2008). However, among clonal pairs imaged in the *chx10:Red* background, only 61/92 (66.3%) of *vsx1* GFP+ pairs included one identified V2a neuron (Fig. 1E). In contrast, in the *gata3:Red* background, 35/38 (92.1%) of *vsx1* GFP+ pairs included one identified V2b neuron (Fig. 1E). Rarely, both *vsx1 GFP+* neurons in a pair expressed both Chx10 or Gata3 markers (<10%). However, in 25% of *vsx1* GFP+ pairs in *chx10:Red* fish, neither neuron expressed the V2a marker.

A possible explanation for the lower rate of V2a marker expression could be under-labeling in the fluorescent reporter line. Alternatively, there is at least one additional population of neurons to emerge from the V2 domain. In zebrafish, the V2s population is glycinergic and expresses Sox1a (Gerber et al., 2019). V2s neurons resemble V2c neurons in mice in that they both express Sox1a and arise after V2a/b development; however, V2c neurons are GABAergic

while V2s neurons are purely glycinergic (Gerber et al., 2019; Panayi et al., 2010). Using the *Tg*(*sox1a:dmrt3a-gata2a:EFP(ka705)*) reporter line, here referred to as *sox1*:*GFP*, (Gerber et al., 2019), we assayed the presence of *sox1+*/*vsx1+* neurons by injecting a *vsx1:mCherry* BAC in embryos at the single-cell stage. In 16/65 (24.6%) of *vsx1* mCherry+ pairs, one of the two sister neurons co-labeled with *sox1a* (Fig. 1D, right), and in 49/65 (75.4%) of *vsx1* mCherry+ pairs, neither neuron co-labeled with *sox1a* (Fig. 1E). These results suggest that not all *vsx1+* progenitors differentiate into V2a/b pairs. Instead, approximately 75% of *vsx1* progenitors divide into V2a/b pairs while the remainder divide into V2b/s pairs. We did not see any *vsx1+* triplets or singlets in co-label experiments (0/195), suggesting that *vsx1* progenitors only undergo a single, terminal division. Based on these results, we conclude that our stochastic labeling approach successfully labeled clonally related V2 neurons, but required a *chx10* co-label to properly identify *vsx1* pairs as V2a/b neurons *in vivo*.

Sister V2a/b neurons remain in close proximity to each other

Immediately after progenitor division around 1 dpf, sister V2a/b neurons are located in close proximity to each other (Kimura et al., 2008), but they have not been followed out to 3-5 dpf when the spinal circuit transitions from spontaneous coiling during embryonic stages to the beat-and-glide locomotion at the larval stage. To assess somatic relationships between sister V2 neurons at larval stages, we measured inter-soma distances among sister and non-sister pairs. In an example fish (Fig. 2A), the inter-soma distance between the GFP-only sister neuron (presumed V2b) to the GFP/Chx10:Red co-labeled V2a neuron (dark red arrow) was shorter than the distance between non-sister neurons (white arrows). Across animals, sister V2 neurons were usually closer neighbors than non-sister V2 neurons, whether measured in the V2a or V2b reporter lines (Fig. 2B). Sister *vsx1+* neurons remained in close proximity to each other

throughout embryonic and larval development. Beginning at 24 hpf, we embedded embryos in low melting point agarose, imaged, and then re-imaged at 48 hpf. At 24 hpf, sister neuron centers were ~7 μm apart, or effectively adjacent. By 48 hpf, this inter-soma distance increased slightly to ~9 μm (Fig. 2C). In a separate set of experiments, we tracked *vsx1*+ sister neurons from 48 – 96 hpf by embedding fish for imaging at 48 hpf, freeing from agarose after imaging, and re-embedding at 96 hpf. The distance between somata increased slightly, but still remained relatively short (Fig. 2C). Because V2a/b somata are ~10 μm in size (Callahan et al., 2019; Kimura et al., 2006; Menelaou et al., 2014), our data suggest that sister V2 neurons usually remain adjacent. Lastly, restricting our analysis to sister V2a/b neurons using *chx10:Red* fish, we found that V2b neurons were typically positioned more dorsally than their sister V2a counterparts (Fig. 2D), consistent with previous work showing inhibitory populations are located more dorsally than excitatory neurons in spinal cord (Kimura et al., 2006; McLean et al., 2007). Altogether, our data demonstrate that sister V2a/b neurons develop and remain close to each other during larval stages. As a result, in subsequent experiments we inferred that sparsely labeled *vsx1* GFP+ neurons located close to each other at 3-4 dpf represented sister pairs.

Though V2a axons are consistently longer, sister V2a/b axons travel along similar trajectories

As V2a/b neurons both project descending, ipsilateral axons, we next assessed whether the axons of clonally-related V2a/b neurons exhibited any consistent morphological characteristics. *Vsx1* GFP+ pairs were labeled in *chx10:Red* fish using a *vsx1*:GFP plasmid and later imaged on a confocal microscope. V2a/b axons were reconstructed (Fig. 3A), and the descending axon length of each clonal V2a/b neuron was measured. Sister V2a neurons exhibited axons that were on average 61% longer than their V2b counterparts (Fig. 3B), consistent with

work showing that Notch expression attenuates axon growth (Mark et al., 2021; Mizoguchi et al., 2020). There was no relationship between the length of the axons and their location along the rostral-caudal axis of the fish (Fig. 3B). To measure axon proximity, the shortest distance between the V2b and V2a axon was calculated along each point of the V2b neuron, beginning at the axon hillock (Fig. 3C, inset). The fraction of those inter-axon distances within 5 μm was calculated for each pair. Indeed, clonally related V2a/b neurons send axons along a similar trajectory, with a median of 37.1% of the V2b axon length within 5 μm of the V2a axon (Fig. 3C). Because the axons follow similar paths, these results suggest a possibility for sister V2a/b neurons to contact shared synaptic targets.

Sister V2a/b neurons receive input from distinct synaptic circuits

Work in hippocampus has shown that sister neurons are more likely to receive synaptic input from shared presynaptic partners than non-sister neurons (Xu et al., 2014). In contrast, $Notch^{ON}$ and $Notch^{OFF}$ sister neurons in Drosophila integrate into separate hemilineages that segregate spatially, although whether they receive shared input is not known (Harris et al., 2015). To evaluate whether sister V2a/b neurons receive input from shared or distinct presynaptic partners *in vivo*, we performed paired whole-cell electrophysiology in voltage clamp from clonally related pairs of V2a/b neurons identified as above (Fig. 4A, B) (Bagnall & McLean, 2014). Both sister neurons were held at -80 mV, the chloride reversal potential, to isolate excitatory postsynaptic currents (EPSCs), while a bright-field stimulus was used to elicit fictive swim (Fig. 4C). The timing of EPSCs arriving in each neuron of the pair was asynchronous, as exemplified by an overlay of several hundred EPSCs from either a V2a/b and the associated EPSC-triggered average in its sister neuron (Fig. 4D, E). A summary of the amplitudes of detected EPSCs and associated EPSC-triggered averages for this example neuron is shown in

Fig. 4F. Across recordings from 13 clonally related pairs *in vivo*, we consistently saw little to no synchronous synaptic input (Fig. 4G).

Lastly, we wanted to compare whether this asynchrony in EPSC input was present in non-sister V2a/b neurons from the same segment. Using the same analysis, it appeared that non-sister V2a/b neurons from the same spinal segment receive input from distinct synaptic sources as well (Fig. 4H). The asynchronous timing of these inputs suggests that they cannot be arriving from a shared presynaptic source, but rather, different presynaptic sources which fire at different times (Bagnall & McLean, 2014). Altogether, these data show that not only sister V2a/b neurons, but any V2a-V2b pair, clonal or non-clonal, from the same segment receives input from distinct presynaptic sources during light-evoked locomotion at slow to medium locomotor speeds. We cannot rule out the possibility that sister neurons receive shared inputs from circuits for fast locomotion or specialized behaviors.

Sister V2a/b neurons do not form synaptic connections with each other

Clonal pair analysis in cortex has shown that sister neurons preferentially form synapses onto each other (Yu et al., 2009; Zhang et al., 2017). To identify whether sister V2a/b neurons form synaptic connections with each other, paired *in vivo* whole-cell recordings were performed in *chx10*:*Red* fish as described above (Fig. 5A). Spiking was elicited by depolarizing current steps in either the V2a or the V2b neuron while the other neuron was held in voltage clamp to measure synaptic responses (V_{hold} of –80 mV in V2b neurons to measure EPSCs, V_{hold} of 0 mV in V2a neurons to measure IPSCs). In both cases, there were no detectable evoked currents, showing that sister V2a/b neurons do not connect with each other (Fig. 5C). Similarly, non-clonally related V2a/b neurons exhibited no interconnectivity (Fig. 5D). Therefore, V2a/b neurons in the same segment do not form direct synapses with each other. Any connectivity

among V2a and V2b neurons likely occurs between neurons in different segments (Sengupta & Bagnall, 2022).

Sister V2a/b neurons provide asymmetric input onto downstream neurons in spinal cord

Research in cortex has shown that clonally related inhibitory interneurons form synaptic connections with shared downstream targets (Zhang et al., 2017), although this claim is disputed (Mayer et al., 2016). Given the proximity of sister V2a/b axons (Fig. 3), it was plausible that they share common downstream targets. To address this question, we micro-injected a *vsx1*:Gal4 BAC and a *UAS:CoChR2-tdTomato* plasmid (Antinucci et al., 2020; Schild & Glauser, 2015) in embryos at the single-cell stage to drive stochastic expression of this channelrhodopsin variant in *vsx1* sister neurons (Fig. 6A) for selective optical stimulation of sister neurons. To distinguish presumed V2a/b pairs from V2b/s pairs, we screened *CoChR2-tdTomato+ vsx1* sister pairs for morphological characteristics (Methods). We validated that the optical stimuli effectively elicited spiking in *CoChR2-tdTomato+ vsx1* sister neurons by performing cell-attached recordings while providing a 10 ms light pulse (Fig. 6B). All *CoChR2-tdTomato+ vsx1* neurons fired action potentials in response to optical stimulation (Fig. 6C, n = 13 neurons from 12 fish). Spiking was elicited in both V2a and V2b *CoChR2-tdTomato+* neurons (Fig. 6D). Similar experiments were performed on nearby *CochR2-tdTomato(-)* neurons to ensure that optical stimuli evoked spiking only in neurons expressing *CoChR2-tdTomato.* All *CoChR2-tdTomato(-)* neurons remained inactive during the light stimulus (Fig. 6C, n =22 neurons from 18 fish). In CoChR2-tdTomato+ neurons, most light-evoked spikes were observed throughout the duration of the stimulus, with some spiking following the stimulus window (Fig. 6 C, E). This prolonged activity is most likely due to the long inactivation kinetics of the *CoChR2* variant (Antinucci et al., 2020). Altogether,

our optogenetic approach is a feasible method for assessing downstream connectivity of sister V2a/b neurons.

Having validated our optogenetic approach, we proceeded to perform whole-cell patch clamp recordings on known V2a/b neuron downstream spinal targets (i.e. motor neurons, V1, V2a, V2b neurons) which were located 1-4 segments caudal to the V2a/b sister pair in voltage clamp mode using a cesium-based internal solution (Fig. 7A) (Bagnall & McLean, 2014; Callahan et al., 2019; Kimura et al., 2006; Menelaou & McLean, 2019). Because sister *vsx1+* neurons are close to each other, our optogenetic stimulus would activate both neurons simultaneously. However, by clamping the target neuron at different reversal potentials, we could isolate either evoked EPSCs or inhibitory postsynaptic currents (IPSCs) (Fig. 7B-D). In most recorded neurons, optical stimuli evoked neither EPSCs nor IPSCs, consistent with sparse connectivity in the spinal cord (n = 85/99; Fig. 7E, F). In six target neurons, we recorded evoked EPSCs (V_{hold} -80mV) but not IPSCs, demonstrating that the target neuron received synaptic input from the CoChR2-labeled V2a neuron but not the V2b (Fig. 7B, E). In another six target neurons, we detected evoked IPSCs (V_{hold} 0 mV) but no EPSCs, demonstrating that the target neuron received synaptic input from the V2b but not the V2a neuron (Fig. 7C, E). In a subset of experiments, NBQX/APV or strychnine were used to block responses and confirm glutamatergic or glycinergic connections, respectively (Fig. 7B, n = 2; Fig 7C, n = 4). In two instances, a target neuron received both evoked EPSCs and IPSCs, with the magnitude of IPSCs ~5-fold larger than the magnitude of the EPSCs, suggesting an asymmetric connection from sister V2a/b neurons (Fig. 7E).

In ten neurons, we detected a slow depolarizing current when target neurons were held at -80 mV (Fig. 7D, F gray), but not at 0 mV. This evoked current had a lower amplitude and longer rise

time than fast evoked EPSCs (Fig. 7G). This slow excitatory current may be caused by a weak di-synaptic electrical connection (Menelaou & McLean, 2019), but we were not able to eliminate it with gap junction blockers (carbenoxylone and 18-β-glycyrrhetinic acid). We summarize the identities of target neurons receiving synaptic input from sister V2a/b neurons in Table 1. Target neurons were evenly divided between motor neurons (early and late born), and excitatory and inhibitory interneurons. Overall, these results demonstrate that clonally-related V2a/b neurons do not preferentially form synaptic connections with shared targets.

2.4 Discussion

In this study, we showed that clonally related V2a/b neurons exhibit similar morphological characteristics, but form synapses with and receive information from largely distinct neuronal partners. Through our use of plasmid injections and time lapse imaging, we definitively identified individual pairs of clonally related V2a/b neurons born from a single *vsx1+* progenitor cell *in vivo* (Fig. 7H). Additionally, some *vsx1+* progenitors appear to divide into V2b/s pairs. Within V2a/b pairs, we saw that sister neuron somata remain in close proximity to each other and send their axons along similar trajectories. However, our electrophysiological data showed that these sister neurons integrate into distinct circuits. Clonally related V2a/b neurons do not communicate with each other, do not receive input from similar sources, and infrequently connect to the same downstream target. This connectivity pattern resembles circuitry seen in Drosophila Notch-differentiated hemilineages (Fig. 7I). Our results represent the first evidence of Notch-differentiated circuit integration in a vertebrate system, and may reflect a means of cell-type and circuit diversification in earlier evolved neural structures.

Notch determines cellular identity of vsx1+ sister neurons

Notch is an important regulator in V2a/b differentiation, and during *vsx1+* progenitor division, differences in Notch expression result in the onset of V2a ($Notch^{OFF}$) or V2b ($Notch^{ON}$) programming (Batista et al., 2008; Debrulle et al., 2020; Kimura et al., 2008; Mizoguchi et al., 2020; Okigawa et al., 2014). However, it remains unknown whether Notch plays a role in sister V2a/b development beyond initiating cellular identity or if it functions as an intermediary step before other molecular factors determine cellular morphology post-mitotically (Kozak et al., 2020; Mizoguchi et al., 2020). Our morphological analysis showed differences in V2a/b axon lengths and dorso-ventral position (Fig. 2, 3). Further experiments are needed to evaluate whether these differences are a result of Notch signaling or intrinsic to post-mitotic cellular identity. Constitutive manipulation of Notch levels results in a skewing of V2a/b numbers (Mizoguchi et al., 2020). Therefore, a temporally controlled manipulation is needed to address the role of Notch in post-mitotic morphological and functional development of sister V2a/b neurons.

Similarly, the recently discovered V2s population relies on Notch signaling for its development with Notch KO mutants showing a decrease in *sox1a+* neurons (Gerber et al., 2019). We speculate that some *vsx1+* progenitors give rise to some V2b/s sister pairs in addition to the previously described V2a/b pairs. Our experiments in reporter lines (Fig 1) showed that ~75% of *vsx1* GFP+ progenitors divided into V2a/b sister neurons, whereas ~25% resulted in V2b/s neuron pairs. V2s neurons arise later than the initial wave of V2a/b pairs (Gerber et al., 2019). Because Notch has been shown to exhibit different effects on cellular identity during early and late development, we suggest that delayed Notch activity causes some later born *vsx1+* sister neurons to adopt a V2b/s identity which are both $Notch^{ON}$ (Jacobs et al., 2022a). Similarly, only early cerebellar progenitors appear to undergo Notch differentiation into distinct cell types,

the Purkinje and granule cells (Zhang et al., 2021). Notch overexpression experiments could have biased differentiation in favor of V2b/s pairs earlier in development, accounting for the increase in V2b and decrease in V2a numbers (Mizoguchi et al., 2020). However, these experiments have not looked at changes to V2s numbers, so selective evaluation of later born V2 progenitors is needed to identify whether V2b/s clonal pairs exist and if so whether they are temporally delayed relative to V2a/b pairs.

Notch-differentiation development influences circuit formation

Lineage pathfinding and innervation differences in Drosophila are well documented, and Notch-differentiated sister neurons in these organisms develop different axon trajectories, presumably connecting to different downstream targets (Harris et al., 2015; Truman et al., 2010). Similarly, our data show that *vsx1+* sister neurons in spinal cord have similar descending trajectories albeit different axon lengths (Fig. 3). Analysis of Notch-differentiated lineages in vertebrate cerebellum has shown that Notch mediates cerebellar progenitor differentiation into excitatory and inhibitory cerebellar cell types (Zhang et al., 2021), but it is not yet known whether the resulting neurons integrate into shared or distinct circuits. Our results are consistent with a framework in which the progeny of Notch-differentiated divisions preferentially integrate into distinct networks in both invertebrates and vertebrates. In contrast with cortical lineages, the divergent cellular identities of sister V2a/b neurons appear to determine that they participate in distinct circuits. We speculate that earlier evolved neural structures rely on Notch-differentiated divisions as a means to diversify neuronal populations during development. The presence of Notch-differentiated sister neurons in both cerebellum and spinal cord could represent an efficient mechanism to generate diverse cell types early in development, in contrast to cortical reliance on dedicated streams of excitatory and inhibitory neural progenitors (Goulding, 2009;

Leto et al., 2016; Ma et al., 2018). This would allow for the development of several neuronal cell-types, each governed by their own intrinsic molecular cues.

Shared vsx1+ progenitor birthdates do not lead to shared integration

Developmental timing allows for proper integration of neurons into functional speed dependent locomotor circuits. In zebrafish, motor neurons and interneurons born during similar developmental windows are active and recruited at similar speeds (McLean et al., 2007; McLean & Fetcho, 2009). These speed dependent microcircuits emerge in larvae and persist into adulthood (Ampatzis et al., 2014). By definition, *vsx1+* sister neurons share a birthdate, suggesting that both neurons are likely recruited at similar speeds and therefore might integrate into shared microcircuits. However, our work shows that *vsx1* sister neurons neither synapse onto each other, receive similar inputs, nor frequently target the same neurons. One possible explanation is that sister V2a/b divergence in cellular identity may cause integration into different hemilineage temporal cohorts, similar to Drosophila, which then determine their neuronal connectivity (Mark et al., 2021). Additionally, V2b neurons, whose recruitment patterns have not yet been described, may participate in different behaviors than V2a neurons. This separation of pathways driving excitatory and inhibitory neurons would allow for independent activation (accelerator) or inactivation (brake) of movement (Callahan et al., 2019; Eklöf-Ljunggren et al., 2012). It is worth noting that we measured synaptic inputs during fictive locomotion induced by bright-field stimuli, and that the possibility remains sister *vsx1* neurons do receive similar inputs under different behavioral paradigms, such as turns or escapes.

Lastly, the sister *vsx1* neurons infrequently connected to the same downstream targets (Fig. 7). Because we saw two examples of targets receiving input from both the V2a and V2b neuron of a clonal pair, it is unclear whether sister neurons are explicitly discouraged from

sharing downstream targets, or whether it is simply random. In either case, the observed connectivity divergence might function to coordinate antagonistic components during locomotion. Spinal V1 interneurons target different populations of neurons along the rostral-caudal length of the spinal cord (Sengupta et al., 2021). Even if non-clonally-related V2a and V2b neurons generally form synaptic contacts onto the same populations, such as motor neurons, they may exhibit different connectivity patterns in the longitudinal axis, preventing clonally-related pairs from sharing downstream targets. Mapping the rostrocaudal connectivity of V2a and V2b populations would address this hypothesis.

2.5 Acknowledgments

We thank Dr. Rebecca Callahan for initial contribution in experimental design and topic development, Dr. Mohini Sengupta for thoughtful critiques of the paper, Dr. Shin-ichi Higashijima for the *vsx1:GFP* BAC construct, and Dr. Uwe Strähle for the *sox1:GFP* fish line. We are grateful to Drs. Andreas Burkhalter and Haluk Lacin for insightful comments on manuscript. We also acknowledge the Washington University Zebrafish Facility for fish care and Washington University Center for Cellular Imaging (WUCCI) for supporting the confocal imaging experiments. This work is supported by funding through the National Institute of Health (NIH) R01 DC016413 (M.W.B.). M.W.B. is a Pew Biomedical Scholar and a McKnight Foundation Scholar.

2.6 Author contributions

S.B. and M.W.B. conceived the project. S.B. performed all experiments and data analysis. S.B. and M.B. interpreted the results and wrote the manuscript.

2.7 Materials and Methods

Experimental model and subject details

All fish used for experiments were at larval stage from 1-6 days post fertilization (dpf), before the onset of sexual maturation. All experiments and procedures were approved by the Animal Studies Committee at Washington University and adhere to NIH guidelines. Adult zebrafish (Danio rerio) were maintained at 28.5^{o}C with a 14:10 light:dark cycle in the Washington University Zebrafish Facility up to one year following standard care procedures. Larval zebrafish used for experiments were kept in Petri dishes in system water or housed with system water flow.

To target V2a and V2b neurons, the *Tg*(*chx10:loxP-dsRed-loxP:GFP*) (Kimura et al., 2006) (ZDB-ALT-061204-4) and *Tg*(*gata3:loxP-dsRed-loxP:GFP*) (Callahan et al., 2019) (ZDB-ALT-190724-4) lines were used. We visualized V2s neurons in *Tg*(*sox1a:dmrt3a-gata2a:EFP(ka705)*) (ZDB-ALT-191113-2) (Gerber et al., 2019), a gift from Dr. Uwe Strähle.

Stochastic single cell labeling by microinjections

Tg(*chx10:loxP-dsRed-loxP:GFP*) and *Tg*(*gata3:loxP-dsRed-loxP:GFP*) were injected with a *vsx1:GFP* bacterial artificial chromosome (BAC) at a final concentration of 5 ng/µL (a gift from Dr. Shin-ichi Higashijima). *Tg*(*sox1a:dmrt3a-gata2a:EFP(ka705)*) were injected with a *vsx1:mCherry* BAC at 15 ng/µL (generated by VectorBuilder, Inc.). To label clonal pairs with an optogenetic activator, wild-type embryos were injected with a *vsx1:Gal4* BAC and *UAS:CoChR2-tdTomato* plasmid (Addgene Catalog #: 124233) at 20 ng/µL and 25 ng/µL, respectively. The embryos were transferred to system water to develop. Embryos were screened between 1-4 dpf for sparse expression of Red/GFP fluorophores and selected for confocal imaging and electrophysiology. In this experiment, it was not feasible to use *Tg(chx10:Red)* animals to identify V2a neurons because of fluorophore overlap. Instead, we screened *CoChR2-tdTomato+ vsx1* sister neurons for distinguishable V2a morphology, specifically the presence of

an ascending collateral which is characteristic of V2a but not V2b or V2s neurons (Callahan et al., 2019; Gerber et al., 2019; Menelaou et al., 2014)

Confocal imaging

18-24 hour post fertilization (hpf) larvae were anesthetized in 0.02% MS-222 and embedded in low-melting point agarose (0.7%) in a 10 mm FluoroDish (WPI). Spinal segments with sparsely labeled progenitors were imaged with a time-lapse approach, consisting of one Z-stack every 5 min, under a spinning disk confocal microscope (Crest X-Light V2; laser line 470 nm; upright Scientifica microscope; 40X objective; imaged with Photometrics BSI Prime camera). After progenitor division, larvae were kept in the FluoroDish inside of an incubator and reimaged at a higher-resolution at 2 dpf with a laser confocal (Olympus FV1200, 488 nm laser, XLUMPlanFl-20x W/0.95 NA water immersion objective).

Larvae imaged beginning at 2 dpf were anesthetized in 0.02% MS-222 and embedded in low melting point agarose (1.5%) in a 10 mm FluoroDish (WPI). Images were acquired on an Olympus FV1200 Confocal microscope equipped with XLUMPlanFl-20x W/0.95 NA water immersion objective. A transmitted light image was obtained along with laser scanning fluorescent images to identify spinal segments. Sequential scanning used for multi-wavelength images. Fish were unembedded from the agarose and placed separately in labeled Petri dishes and later reimaged at 4 dpf as described above. In some cases, fish were only imaged at 4 dpf using the embedding methods described above. Transcription factor co-expression was quantified manually.

Image analysis

Confocal images were analyzed using Imaris (9.8, Bitplane) and ImageJ (1.53q, FIJI) (Schindelin et al., 2012). For axon tracing, stitched projection images were made with the

Pairwise stitching (Preibisch et al., 2009) ImageJ plugin. The overlap of the fused image was smoothed with linear blending and was registered based on the fill channel or the average of all channels. Three-dimensional (3D) images were reconstructed and analyzed using Imaris. Axon length measurements of each reconstructed neuron were obtained using the Filament function to trace over the 3D rendering. Axon length includes only the descending branches of the neuron, starting at the axon hillock. 3D axon coordinates of descending projections were exported from Imaris, and separation of axon distances was calculated as the shortest distance between sister V2b to sister V2a axons. Muscle segment number was counted under differential interference contrast (DIC). Inter-soma distances were measured in three dimensions using the Points function in Imaris. Each point was placed at the center of each soma. Normalized dorso-ventral soma position was calculated by measuring the height of the soma from the notochord and dividing by the total height of the spinal cord, with 0 as the ventral-most point.

Electrophysiological Recordings

Cell-attached recordings were targeted to stochastically labeled WT fish with *vsx1:Gal4* BAC and *UAS:CoChR2-tdTomato* plasmid to calibrate firing of *vsx1:Gal4;UAS:CoChR2-tdTomato vsx1+* pairs. Whole-cell patch-clamp recordings were performed in *Tg(chx10:loxP-dsRed-loxP:GFP)* injected with *vsx1:GFP* and *Tg*(*chx10:GFP;gata3:loxP-dsRed-loxP:GFP)* larvae at 4-6 dpf for paired clonal V2a/b and non-clonal V2a/b recordings, respectively. Additional, whole-cell patch-clamp recordings were performed in stochastically labeled *WT* fish with *vsx1:Gal4* BAC and *UAS:CoChR2-tdTomato* in downstream targets. Larvae were immobilized with 0.1% α-bungarotoxin and fixed to a Sylgard lined Petri dish with custom-sharpened tungsten pins. Each larva was then transferred to a microscope (Scientifica SliceScope Pro) equipped with infrared differential interface contrast optics, epifluorescence, and immersion

objectives (Olympus: 40X, 0.8 NA). One muscle segment overlaying the spinal cord was removed (segments 7-17) using a blunt end glass electrode and suction (Wen & Brehm, 2010). The bath solution consisted of (in mM): 134 NaCl, 2.9 KCl, 1.2 $MgCl_2$, 10 HEPES, 10 glucose, 2.1 $CaCl_2$. Osmolarity was adjusted to ~295 mOsm and pH to 7.5.

Patch pipettes (5-15 MΩ) were filled with internal solution for voltage and current clamp and cell-attached composed of (in mM): 125 K gluconate, 2 $MgCl_2$, 4 KCl, 10 HEPES, 10 EGTA, and 4 Na_2ATP). Whole-cell optogenetic and some paired recordings were performed using internal solution composed of (in mM): 122 cesium methanesulfonate, one tetraehtylammonium-Cl, 3 $MgCl_2$, 1 QX-314 Cl, 10 HEPES, 10 EGTA, and 4 Na_2ATP. Additionally, Alexa Fluor 647 hydrazide 0.05-0.1 mM or sulforhodamine (0.02%) was included to visualize morphology of recorded cells post hoc. Osmolarity was adjusted to ~285 mOsm and KOH or CsOH, respectively was used to bring the pH to 7.5. Patch recordings were made in whole-cell configuration using a Multiclamp 700B, filtered at 10 kHz (current clamp) or 2 kHz (voltage clamp). All recordings were digitized at 100 kHz with a Digidata 1440 (Molecular Devices) and acquired with pClamp 10 (Molecular Devices). The following drugs were bath applied where noted: strychnine (10 µM), NBQX (10 µM), APV (100 µM), 18-beta-glycyrrhetinic acid (150 µM), and carbenoxolone disodium salt (500 µM).

During paired electrophysiology recordings, fictive swimming sometimes occurred spontaneously and in other instances was elicited by white light illlumination of the animal. In optogenetic experiments examining channelrhodopsin firing and V2a/b targeting, light stimulation was provided with high intensity epifluorescent illumination (CoolLED pE-300), 10% intensity with a 40X (0.8 NA) water immersion objective for 10 ms. The objective was positioned over a single spinal segment prior to stimulus delivery.

Electrophysiology data were imported in Igor Pro 6.37 (Wavemetrics) using NeuroMatic (Rothman & Silver, 2018). The detection algorithm was based on the event detection instantiated in the SpAcAn environment for Igor Pro (Rousseau et al., 2012) and as previously described (Bagnall & McLean, 2014). All events detected were additionally screened manually to exclude spurious noise artifacts. EPSCs were analyzed using custom written codes in Igor and MATLAB. For synchronized input evaluation, recordings were excluded from analysis if we could not induce robust fictive locomotion.

Statistics

Statistical tests were performed using MATLAB (R2018a, MathWorks). Due to the non-normal distribution of physiological results, we used nonparametric statistics and tests for representations and comparisons. Details of statistical tests, p values, used, and sample sizes are described in the corresponding figure legends.

Data availability

All analyses generated during this study are included in the manuscript source data file. Computational analyses were performed using code available at https://github.com/bagnall-lab/Event-detection (Bagnall, 2022). Raw data is available on Dryad at the following DOI: https://doi.org/10.5061/dryad.4xgxd25dh. You may include lettered, numbered, or bulleted lists in your document. Use consistent punctuation and capitalization throughout each list. Lists may be indented.

2.8 Figures and Legends

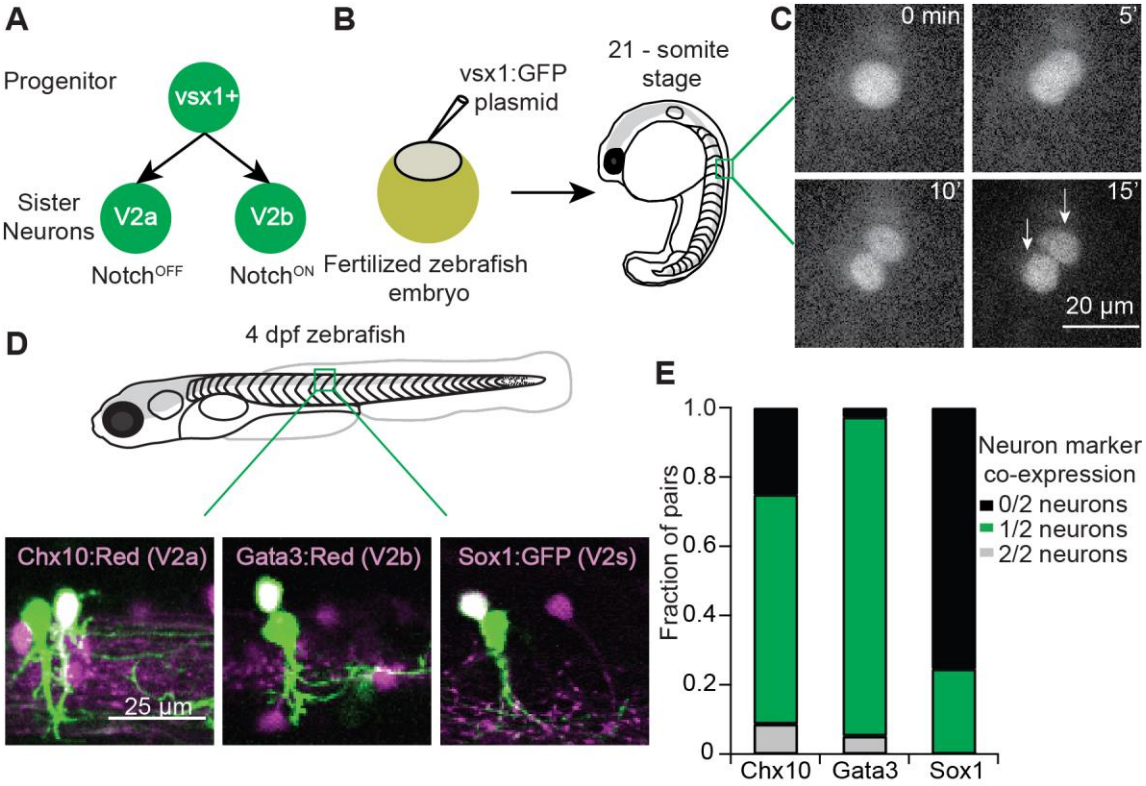

Figure 2.1. Sparse *vsx1*+ progenitor labeling allows for clonal pair tracking *in vivo.*

A. Schematic of *vsx1* GFP+ progenitor undergoing a final paired division into sister V2a/b neurons. B. Schematic of fertilized embryo injection and screening for *vsx1* GFP+ progenitors at the 21-somite stage. C. Time-lapse single-plane confocal images taken every 5 min as a *vsx1* GFP+ progenitor divides into two sister neurons, imaged at 24 hours post fertilization (hpf). D. Confocal imaging of *vsx1*+ sister neuron pairs in the spinal cord of 4 dpf larvae. Left, *vsx1* GFP+ sister pair in a *chx10:Red* larva. One sister neuron is co-labeled (white, V2a) while the other is a presumed V2b. Middle, *vsx1* GFP+ sister pair in a *gata3:Red* larva showing an identified V2b with a presumed V2a or V2s. Right, *vsx1* mCherry+ sister pair in a *sox1:GFP* larva, showing an identified V2s with a presumed V2b. Colors switched for label and image consistency. E. Bar graph displaying the fraction of *vsx1* GFP+ pairs in *chx10:Red* (n = 92), *gata3:Red* (n = 38), and *sox1:GFP* (n = 65) larvae in which either 0/2 sister neurons were co-labeled with the reporter (black), 1/2 sister neurons were co-labeled (green), or 2/2 sister neurons were co-labeled (gray).

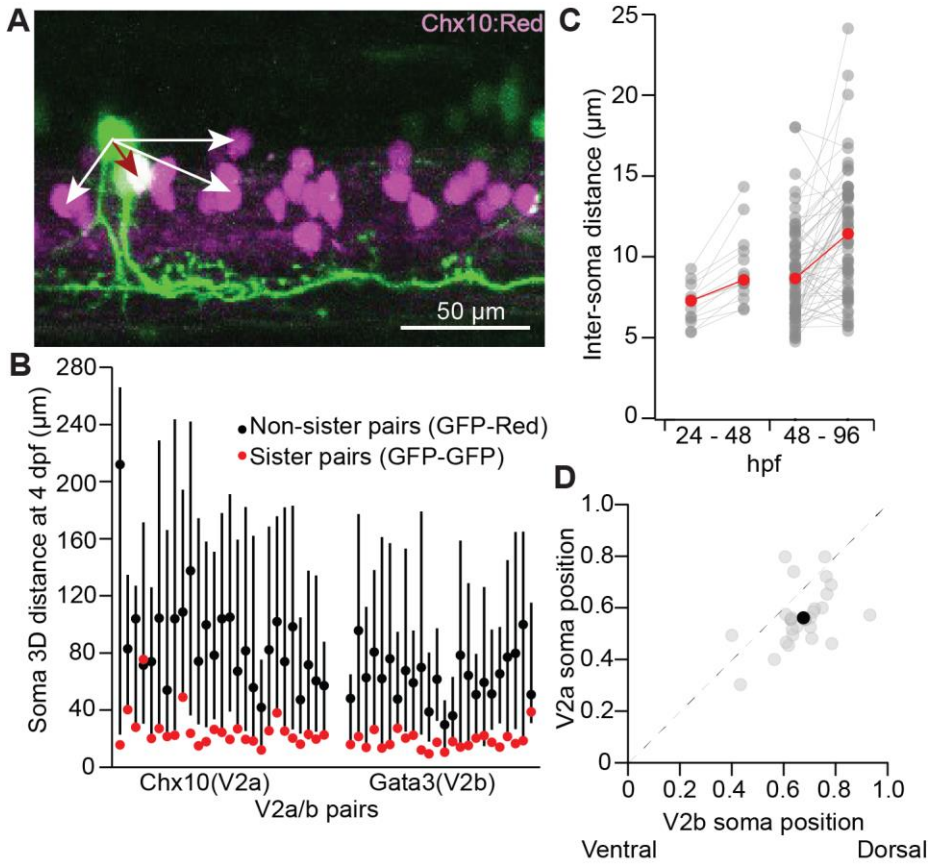

Figure 2.2 Sister V2a/b neurons remain in close proximity to each other.

A. Maximum intensity projection (50 planes, 50 µm) of *chx10:Red* with a single *vsx1* GFP+ clonal pair. The inter-soma distance between the GFP-only sister neuron to the GFP/Red co-labeled V2a neuron (dark red arrow) is smaller than the distance between non-sister neurons (white arrows). B. For each clonal pair in either the Chx10 reporter line (n = 27) or the Gata3 reporter line (n = 24), the 3D distance between the two sister neurons (GFP-GFP, red) and the median 3D distance between one sister neuron and its non-sister neurons in the same segment (GFP-Red). Black dot indicates median and lines show 5^{th} – 95^{th} percentiles. C. Paired line plot of inter-soma distances of individual *vsx1* GFP+ sister pairs first imaged at 24 hpf and later reimaged at 48 hpf (left) (n = 14) or first imaged at 48 hpf and later reimaged at 96 hpf (right) (n = 66). Red values indicate median distances at each time point. D. Scatterplot of normalized dorsal (1)-ventral (0) soma position for each of 27 sister V2a/b neurons. Dashed line indicates unity. Typically, the V2b neuron was located more dorsally than the V2a neuron. Black dot indicates the median V2a/b pair position. ** Wilcoxon signed rank test, $p = 5.2 \times 10^{-4}$, paired t-test, n = 27 pairs.

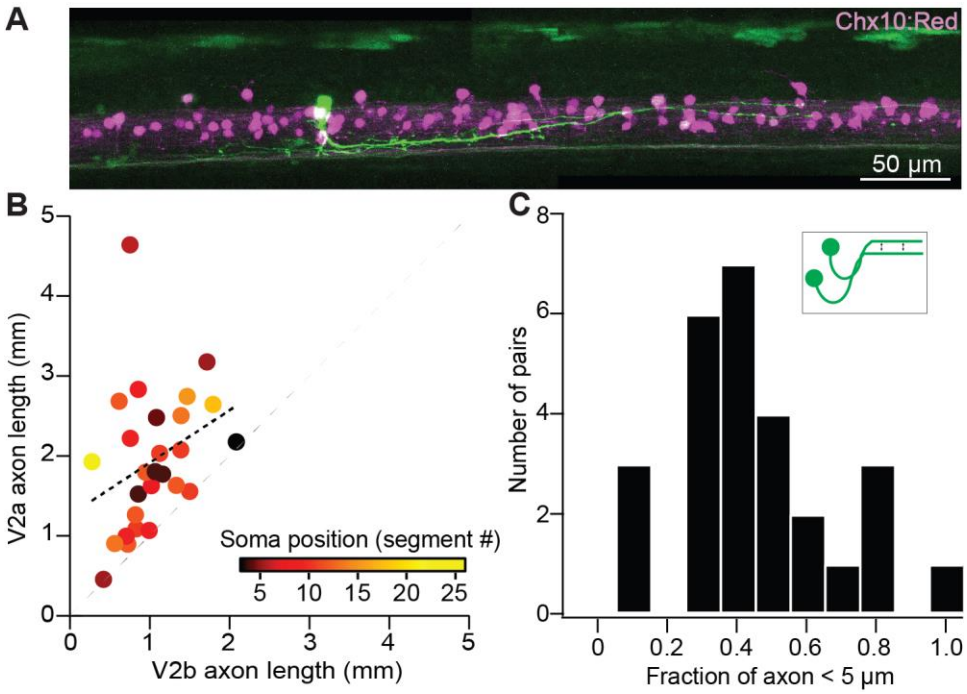

Figure 2.3 Sister V2a/b neurons project along similar trajectories, although V2a neurons are consistently longer.

A. Confocal image of *chx10:Red* larva exhibiting a single *vsx1* GFP+ clonal pair with long axons in close proximity to each other. Stitched maximum intensity projection over 74 z- planes (74 µm). B. Scatter plot of sister V2a axon length vs. sister V2b axon length (n = 27) for V2a/b pairs. Heat map depicts the muscle segment number where each clonal pair was located. Black line depicts Pearson correlation, $r = 0.32$, $p = 0.10$. V2a axons were invariably longer than sister V2b axons, as seen by each pair's position relative to the unity line (dashed gray). *** Wilcoxon signed rank test, $p = 1.9 \times 10^{-5}$, paired t-test n = 27 pairs. C. Histogram of clonal pairs showing the fraction of V2b axon that is within 5 µm of V2a axon. Inset schematic depicts how the distances were measured.

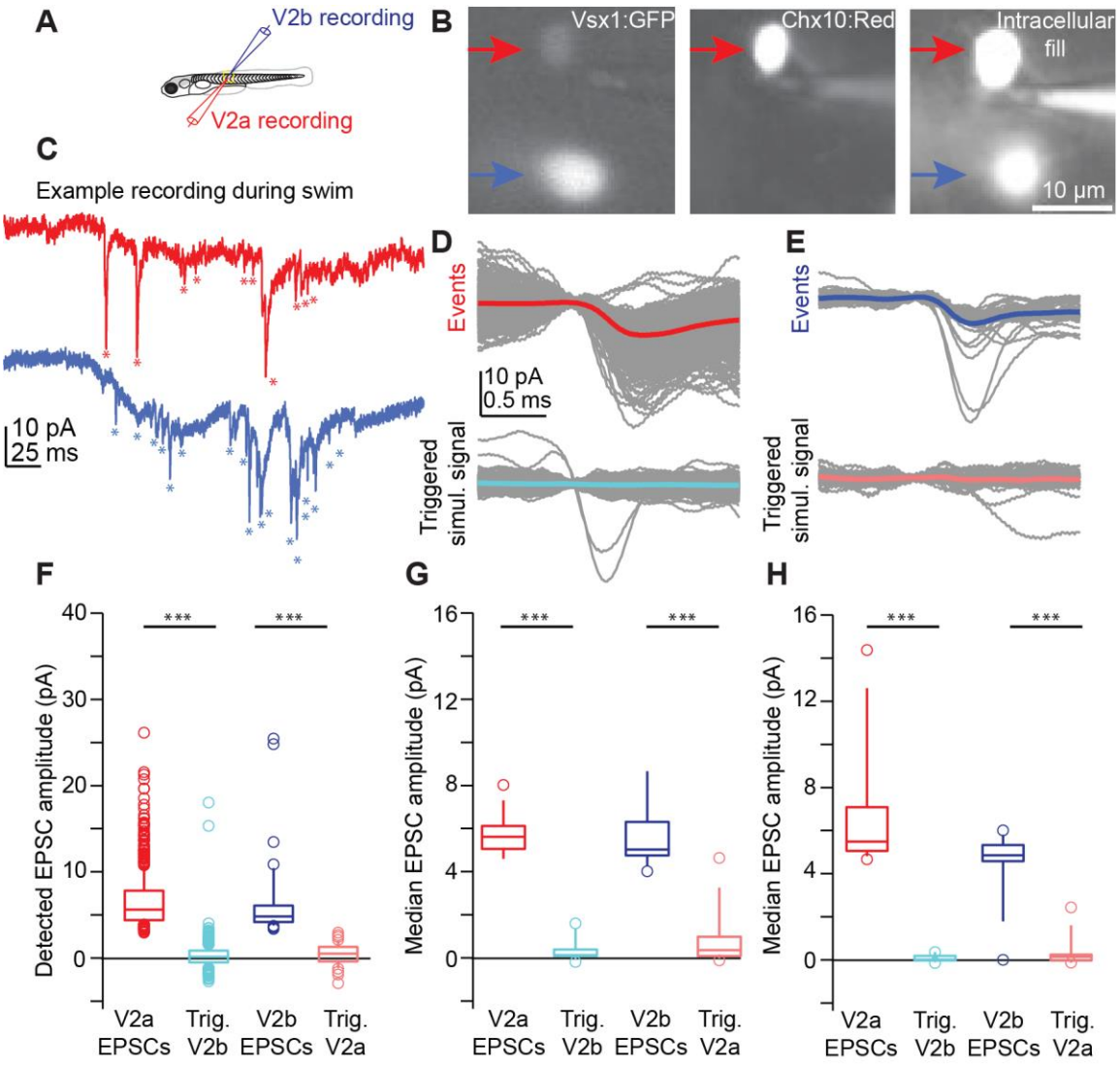

Figure 2.4 V2a/b sister neurons receive input from distinct synaptic circuits.

A. Schematic of larval zebrafish whole-cell paired recording (sister V2a in red and sister V2b in blue). B. Two sister neurons labeled with *vsx1*:GFP (left), filled with dye during whole-cell recording (right). One neuron co-labels with V2a marker *chx10:Red* (middle). Red arrow and blue arrow indicate sister V2a and presumed sister V2b, respectively. C. Example traces during swim of *vsx1* GFP+ sister neurons from V2a/b pair in voltage clamp configuration. Asterisks denote detected EPSC events. D. Overlaid detected EPSC events recorded from sister V2a neuron (top) and simultaneously recorded signal in the sister V2b neuron (bottom). Most detected EPSCs in the V2a do not occur synchronously with EPSCs in the V2b neuron. E. Overlaid detected EPSCs in V2b neuron (top) and simultaneously recorded signal in sister V2a neuron (bottom), also showing very few synchronous EPSCs. Colored traces represent averages of individual traces in gray. F. Data from one example sister V2a/b pair showing the EPSC amplitude of detected events and the amplitude of the simultaneously recorded signal in the other neuron (Trig). Boxes depict medians, 25th and 75th percentiles. Whiskers denote 10th and 90th

percentiles. Open circles depict EPSC values above and below the 10^{th} and 90^{th} percentiles. ***, Wilcoxon signed rank test, (V2a – V2b simul.) $p = 1.8 \times 10^{-206}$; (V2b – V2a simul.) $p = 6.7 \times 10^{-15}$ paired t-test. G. Summary data from all sister V2a/b pairs of recorded EPSC amplitudes and the EPSC-triggered simultaneously recorded signal in the other neuron. ***, Wilcoxon signed rank test, (V2a – V2b simul.) $p = 1.6 \times 10^{-5}$; (V2b – V2a simul.) $p = 2.6 \times 10^{-5}$ paired t-test, n = 13 pairs from 13 fish. H. As in (F), for non-sister V2a/b paired recordings from the same spinal segment. ***, Wilcoxon signed rank test, (V2a – V2b simul.) $p = 1.6 \times 10^{-5}$; (V2b – V2a simul.) $p = 1.3 \times 10^{-4}$ paired t-test, n = 13 pairs from 13 fish.

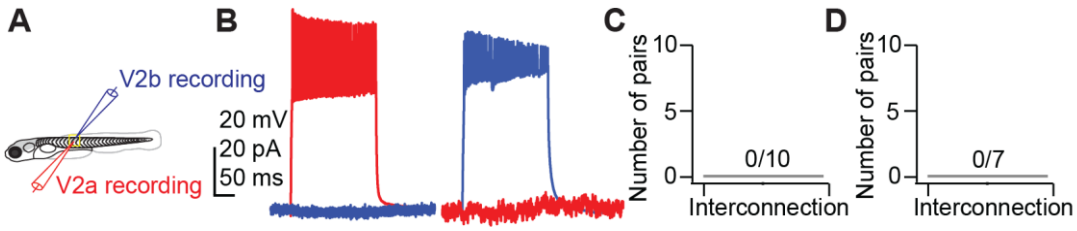

Figure 2.5 V2a/b sister neurons do not synapse with each other.

A. Schematic of larval zebrafish whole-cell paired recording. B. Simultaneous current clamp and voltage clamp recording of sister V2a/b neurons. Current step-evoked spiking in sister V2a neuron and simultaneous voltage clamp recording in V2b (left). Current step-evoked spiking in sister V2b neuron and simultaneous voltage clamp recording in V2a (right). No synaptic responses are seen in either case. C. Bar graph showing the number of clonal V2a/b interconnected pairs detected (n = 10 pairs from 10 fish). D. Bar graph showing the number of V2a/b interconnected pairs detected for non-sister pairs (n = 7 pairs from 7 fish).

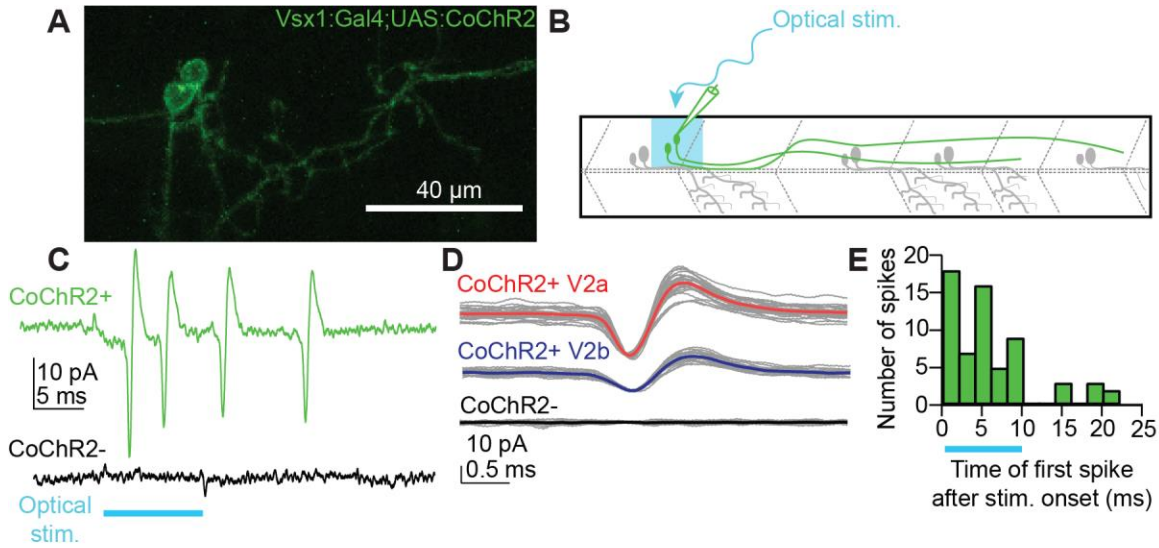

Figure 2.6. Optical stimulation elicits spiking in stochastically labeled *vsx1* sister neurons expressing CoChR2.

A. Maximum intensity projection (79 planes, 79 µm) of WT larva with a single *vsx1*:Gal4;UAS:*CoChR2-tdTomato*+ clonal pair. B. Schematic of cell-attached recording of *vsx1*:Gal4;UAS:*CoChR2-tdTomato*+ neurons using optical stimulation. C. Cell-attached example trace of *CoChR2*+ V2a neuron during optical stimulation (top, green) (n = 13 from 12 fish). Cell-attached example trace of nearby *CoChR2*- neuron during optical stimulation (bottom, black) (n = 22 from 18 fish). Both example traces are aligned to the start of the 10 ms optical stimulus (light blue). D. Averaged detected spike events recorded from an example *CoChR2*+ sister V2a neuron (top, red), *CoChR2*+ sister V2b neuron (middle, blue), and absence of response in nearby *CoChR2*- neuron (bottom, black). E. Histogram showing the number of spikes relative to the optical stimulus. Blue bar indicates the duration of the optical stimulus.

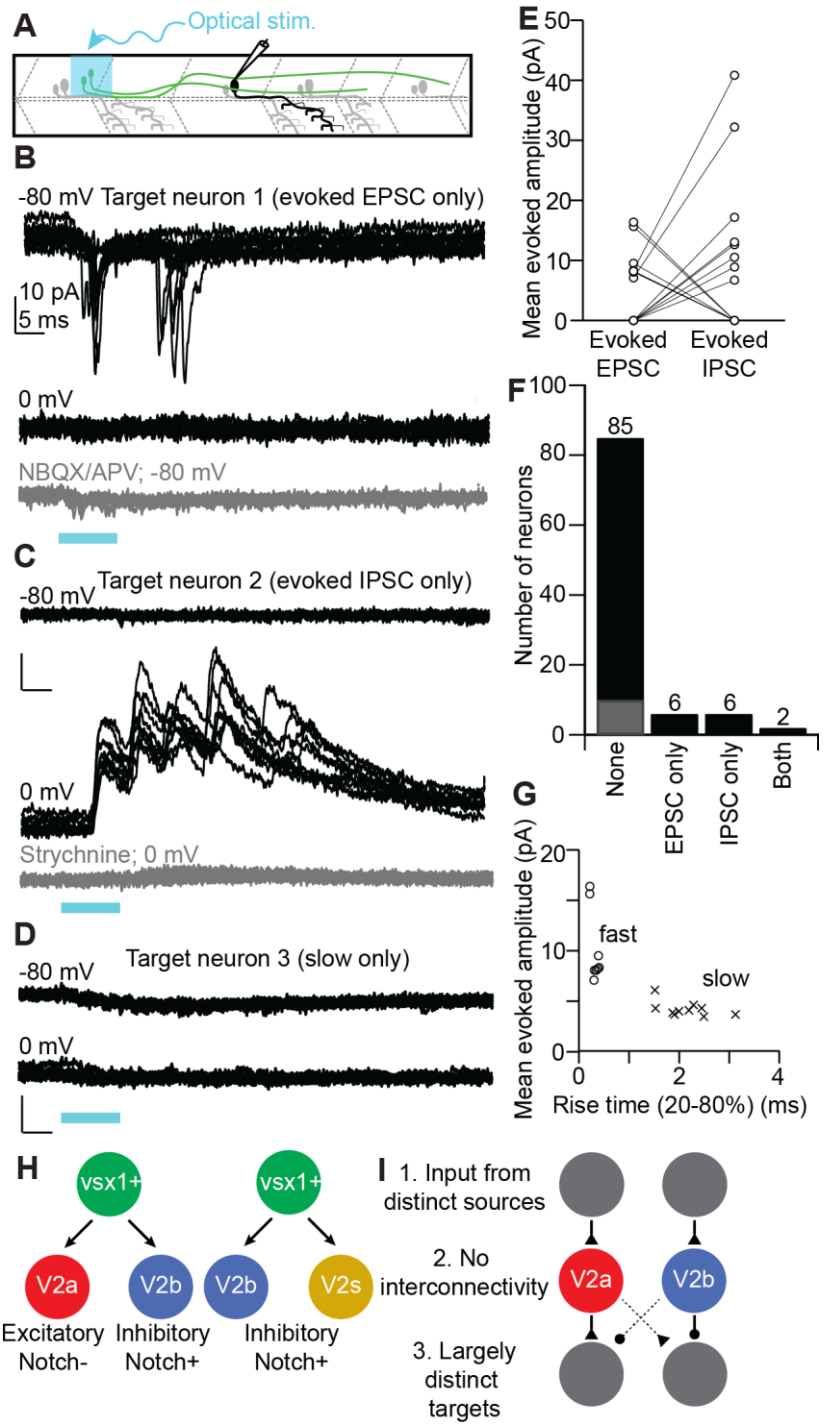

Figure 2.7. Sister V2a/b neurons provide asymmetric input onto downstream neurons in spinal cord.

A. Schematic of whole-cell recording of downstream neuronal targets of *vsx1*:Gal4;UAS:*CoChR2-tdTomato*+ neurons using optical stimulation. B. Example voltage clamp traces from a target neuron held at V_{hold} -80 mV or 0 mV during optical stimulation of the upstream sister neuron pair. Optical stimulation evoked EPSCs onto the target neuron (top) but

not IPSCs (middle), indicating connectivity from the V2a but not the V2b. Bottom, application of glutamatergic antagonists blocks the evoked EPSCs. C. As in (B) for another target neuron, this one showing evoked IPSCs but not EPSCs. IPSCs were abolished by application of strychnine (bottom). D. Example voltage clamp traces from a target neuron held at V_{hold} -80 mV or 0 mV. Trace showing a small, slow evoked EPSCs without any fast component. These are presumably due to indirect (polysynaptic) electrical connectivity from the optogenetically activated V2a neuron. E. Mean evoked amplitude of optogenetically-evoked EPSCs and IPSCs in each target neuron. 10/12 synaptically connected targets received only EPSCs or IPSCs, while 2/12 neurons received both EPSCs and IPSCs. F. Bar graph depicting the number of EPSC only (n = 6), IPSC only (n = 6), both EPSC/IPSC (n = 2), and no responses (n = 75) (black) or only slow presumed polysynaptic (gray) (n = 10) detected across all target neurons recorded. G. Scatterplot showing the distinction between mean evoked amplitude and 20-80% rise time for fast and slow evoked EPSC responses. H. Schematic depicting the two presumed types of *vsx1* GFP+ sister pairs observed. I. Summary of circuit integration pattern observed among sister V2a/b pairs.

2.9 Tables

Target Type	EPSC Only	IPSC Only	Both	Total
Primary MN	1	1	1	3
Secondary MN	2	1	0	3
V1	0	2	0	2
V2a	0	2	0	2
V2b	1	0	0	1
Unidentified	2	0	1	3

Table 2.1. Sister V2a/b identified postsynaptic targets.

Chapter 3: Defining the postsynaptic targets of V2a neurons in spinal cord

3.1 Abstract

In vertebrates, excitatory spinal interneurons are essential for the initiation and propagation of locomotor activity. Ipsilaterally projecting V2a (*chx*10+) neurons provide a major component of this excitatory wave. Activation of V2a neurons evokes motor activity, whereas V2a neuron ablation eliminates locomotor responses. Despite the importance of V2a neurons to locomotor network function, the specific targets and structure of connections along the rostral-caudal axis remain unknown. In this study, we used optogenetic stimulation of transgenic larval zebrafish with a digital micromirror device (DMD) to map synaptic outputs of V2a neurons onto several distinct classes of identified spinal neurons including excitatory interneurons, inhibitory interneurons, and motor neurons. We find that V2a neurons form both short and long range connections, but the strength of connectivity varies along the length of their axons. Connections from V2a neurons onto both motor and excitatory neuron populations are weighted to longer ranges with peak evoked synaptic activity occurring 4-6 muscle segments in the rostral direction, whereas connections onto inhibitory populations occur more locally, 3-4 segments away. We conclude that V2a neuron connectivity varies along the longitudinal axis, with peak synaptic output occurring at 3-6 segments caudal from the V2a cell body but with systematic variations in target identity. The lack of local connections makes it unlikely that V2a neurons function as the recurrent excitatory source proposed in the unit burst generator model. Instead, V2a neurons most likely function in propagation of excitatory wave and patterned output such as turning.

3.2 Introduction

Locomotion is a complex, rhythmic behavior which is produced through the balance of both inhibitory and excitatory signals onto diverse motor pools within the spinal cord. The modulation of both signals is mediated through evolutionarily conserved spinal interneurons, with each class of interneurons defined by unique electrophysiological and molecular profiles (Goulding, 2009; Jessell, 2000; Sengupta & Bagnall, 2023). Ultimately, these diverse cell types help the spinal cord produce locomotion. Locomotor output is determined by the spinal cord's innate ability to produce rhythmicity to drive movement which is established through the diverse cell types in the spinal cord (Grillner, 2003; Grillner & Manira, 2020; Kiehn, 2016). The source of this rhythmogenesis has been investigated with a range of approaches. For example, the use of spinalized animals revealed that the rhythmogenic population is housed within the spinal cord and not imposed by higher order brain networks (Fedirchuk et al., 1998; Grillner, 1985). The use of spinalized hemicords revealed that rhythmogenesis must be established by an ipsilaterally innervating rather than a commissurally innervating cell type (Cangiano & Grillner, 2003). Furthermore, application of inhibitory antagonists did not abolish rhythmicity, suggesting that the rhythmogenic neuron must be an excitatory cell type (Cangiano & Grillner, 2003; Grillner, 2003; Grillner & Manira, 2020; Kiehn, 2016). Ultimately, this central idea became known as the unit burst generator model where the rhythmogenic producing cell type provides local recurrent excitatory drive which feeds back to excite both the source of the population (i.e. itself), as means to establish rhythmicity, and the motor population (i.e. motor neurons) to establish output (Grillner, 2003; Grillner & Manira, 2020; Li et al., 2009; Li et al., 2006; Menelaou & McLean, 2019; Song et al., 2018; Song et al., 2020).

Recent work has explored the molecular identity of this rhythmogenic class of neurons with the candidates needing to be both excitatory and ipsilaterally innervating cell types. Among the various groups assessed, *vsx2+*, hereafter referred to as *chx10+*, V2a neurons emerged as a viable candidate because they are both glutamatergic and ipsilaterally projecting (Hayashi et al., 2018; Kimura et al., 2006; Menelaou & McLean, 2019; Song et al., 2018; Song et al., 2020). V2a neurons are located throughout the entire rostral-caudal axis of the spinal cord (Hayashi et al., 2018; Menelaou et al., 2014). Anatomical studies revealed that some V2a neurons only have intraspinal projections (Type I V2a neurons); whereas, some V2a neurons have both intraspinal and supraspinal projections (Type II V2a neurons) (Hayashi et al., 2018; Menelaou & McLean, 2019; Menelaou et al., 2014). Anatomical tracing revealed that V2a neurons form monosynaptic connections onto several populations within the spinal cord (Crone et al., 2008; Guan et al., 2021; Hayashi et al., 2018; Kimura et al., 2006; Menelaou & McLean, 2019). These populations include commissural innervating populations such as inhibitory dI6 and V0d neurons, and excitatory V0v neurons (Crone et al., 2008; Guan et al., 2021). These monosynaptic connections onto commissural populations have suggested that V2a neurons aid in the coordination of left-right alternation in spinal cord circuits (Crone et al., 2008). However, it is the connectivity of V2a neurons onto other V2a neurons and motor neurons that has caught the interest of researchers in recent years (Hayashi et al., 2018; Menelaou & McLean, 2019; Song et al., 2018; Song et al., 2020). Across vertebrates, V2a neurons form monosynaptic connections onto other V2a neurons (recurrence) (Hayashi et al., 2018; Menelaou & McLean, 2019; Song et al., 2020). Additionally, V2a neurons form monosynaptic connections onto motor neurons to drive motor neuron recruitment (output) (Eklöf-Ljunggren et al., 2012; Hayashi et al., 2018; Menelaou & McLean, 2019; Menelaou et al., 2014; Song et al., 2018). Furthermore, the loss of V2a neurons

has shown to greatly reduce the overall locomotor output among vertebrates (Crone et al., 2008; Eklöf-Ljunggren et al., 2012), suggesting that V2a neurons are essential for the spinal cord to produce locomotion. As a result, V2a neurons became a prime candidate as the rhythmogenic producing cell type within the spinal cord (Grillner & Manira, 2020; Kiehn, 2016; Song et al., 2020). As previously stated, V2a neurons extend long axons along the full longitudinal axis of the spinal cord, forming synapses along their entire axon (Menelaou et al., 2014). Recent work revealed that the preferential targets of spinal interneurons change along the rostral-caudal axis, suggesting compartmentalization of interneuron function at different locations along the axon (Sengupta & Bagnall, 2022; Sengupta et al., 2021). Given the importance of V2a neurons, it was imperative to evaluate the rostral-caudal connectivity onto both known and unknown postsynaptic targets to reveal any potential specialization of V2a function along the rostral-caudal axis.

Here, we take advantage of the transparency and accessibility of the intact spinal cord in larval zebrafish to map the rostral-caudal connectivity of V2a neurons as previously performed in V1 neurons (Sengupta et al., 2021) to construct a comprehensive map of V2a postsynaptic targets. Using a combination of optogenetics and electrophysiology, we mapped the synaptic connectivity from V2a neurons to six spinal populations (V2a neurons, fast motor neurons, slow motor neurons, V1 neurons, dI6 neurons, and V0v neurons). Our results reveal that V2a neurons exhibit preferential long range outputs (> 4 segments) onto a wide variety of spinal populations, including motor neurons and other V2a neurons. These connectivity results are at odds with the model in which high local, recurrent V2a output is the primary source of rhythmogenesis. Instead, we suggest that V2a neurons are mostly involved in the propagation of the excitatory

wave down the spinal cord with contribution to pattern generation such as turning (Cregg et al., 2020; Jay et al., 2023).

3.3 Results

Optogenetic calibration of V2a spiking in zebrafish spinal cord

To create a map of V2a connectivity via optical stimulation, we generated a transgenic larval zebrafish line, Tg(*chx10:Gal4:UAS:CatCh*), where all V2a neurons expressed CatCh, a calcium permeable cationic channelrhodopsin (Fig. 3.1A). First, we designed and calibrated an optogenetic approach that would allow us to evoke minimal V2a spiking using a digital micromirror device (DMD). To validate the efficacy of this approach, we recorded evoked spiking from V2a neurons in whole-cell current clamp configuration during presentation of a 6x5 grid of localized optical stimuli over a single segment. This highly localized stimulation evoked spiking in V2a neurons only when the stimulus was presented directly over the soma (Fig. 3.1B, inset red traces). Elsewhere within the same segment, optical stimulation evoked only subthreshold responses (Fig. 3.1B, inset black traces). Furthermore, only stimulation within the same segment as the recorded neuron successfully evoked V2a spiking. No spiking was elicited when the stimulus was presented 1-2 segments rostral or caudal to the recording site (Fig. 3.1C). In 3/21 neurons where spiking was elicited by stimulation one segment rostral or caudal to the recording site, the recorded V2a was on the muscle segment boundary, meaning that neuron was located within the stimulus grid in Segment 0 and Segment 1R/1C. These results demonstrate that optogenetic activation of CatCh+ V2a axons does not elicit antidromic spiking, and furthermore that this sparse optogenetic approach can be used to activate V2a neurons sparsely in the illuminated segment.

To determine the time period over which postsynaptic neurons would be likely to receive direct synaptic input from these optically activated V2a neurons, we measured the duration of elicited spiking. Most optically activated V2a neurons spiked within 20 ms of stimulus onset, and 96% of spikes were elicited within 100 ms after stimulus onset (Fig. 3.1D). We therefore used a 100 ms analysis window to detect optically evoked EPSC events in our target neurons.

One of the goals in the study was to establish that the evoked EPSCs observed were monosynaptic. To test whether the inputs measured were monosynaptic in nature, we performed some current clamp recordings while providing a 20 Hz train of three 20 ms pulses to ensure repetitive firing of V2a neurons as previously performed (Sengupta et al., 2021). If CatCh+ V2a neurons evoked three consecutive spikes with this train application (Fig 3.1E), then we would expect to reliably observe three consecutive barrages of EPSCs onto our target neuron. From these trials, V2a neurons received reliable V2a input during this high frequency stimulation, demonstrating monosynaptic connectivity (Fig 3.1E).

Longitudinal assessment of V2a postsynaptic targets

V2a – V2a Interneuron Connectivity

Anatomical and physiological studies indicate that V2a neurons provide input onto other V2a neurons (Hayashi et al., 2018; Menelaou & McLean, 2019; Song et al., 2020), so we began our assessment of postsynaptic targets by testing the longitudinal connectivity within V2a neurons. To examine the spatial extent of V2a excitation, V2a neurons were targeted using the Tg(*chx10:Gal4;UAS:CatCh*) line where all V2a neurons expressed a CatCh-YFP+ fluorophore (Fig 3.2A). In this and subsequent experiments, neurons in whole-cell voltage clamp configuration were held at -80 mV with a potassium-gluconate based internal solution to isolate EPSCs. The patterned optical stimulus was delivered one segment at time, rostrally up to 7

segments and caudally up to 6 segments relative to the recording site, while recording light evoked EPSCs (Fig. 3.2A,B). We were not able to assess evoked EPSCs within the recording site (segment 0) given the large depolarizing current caused by activating the opsin within the recording segment. Fig. 3.2B shows representative traces of evoked EPSCs in V2a neurons when the optical stimulus was presented in 2, 4, and 6 segments rostral and 2 segments caudal to the recording site, respectively. Surprisingly, V2a neurons did not receive robust EPSCs when local V2a neurons were stimulated (Segments 1 – 2). Instead, we observed a slow inward current and few fast electrical/chemical EPSCs (Fig 3.2B, segment 2R). Optical activation of V2a neurons located 3 segments rostral to the recording site evoked EPSCs with input peaking between 5 - 7 muscle segments rostral to the recording site (Fig. 3.2B,C). V2a neurons did not receive any input from caudally located V2a neurons, consistent with previous findings (Menelaou & McLean, 2019). These results indicate that V2a neurons mostly provide appreciable long-range excitation onto V2a neurons with little direct synaptic input locally.

V2a – Motor Neuron Connectivity

Next, we evaluated the longitudinal connectivity of V2a neurons onto fast and slow motor neurons which are considered a primary target of V2a neurons in the spinal cord (Fig. 3.3A) (Eklöf-Ljunggren et al., 2012; Menelaou & McLean, 2019; Menelaou et al., 2014; Song et al., 2018; Song et al., 2020). Fast motor neurons are identifiable by their large, laterally placed somata, low input resistances, and axon arborization, which we validated by post-hoc cell fills (Menelaou & McLean, 2012). Similarly, slow motor neurons were identified using their higher input resistances and unique arborization patterns (Bello-Rojas et al., 2019; Menelaou & McLean, 2012). Similar to the results from V2a – V2a connectivity, optical activation of V2a neurons located 4 – 6 segments rostral to recording site evoked more robust EPSCs than local

stimulation (Fig. 3.3B,C). Among slow motor neurons, optical activation of V2a neurons located 3 – 5 muscle segments rostral to the recording site produced the larger number of EPSCs (Fig. 3.4A,B); however, we began to see some input from V2a neurons onto slow motor neurons in the caudal direction, meaning that slow motor neurons are a target of ascending V2a input (Fig 3.4C). Altogether, it appears that V2a interneurons provide long range excitatory input onto motor populations with minimal ascending input onto slow motor neurons. Local stimulation evoked only a slow inward current in motor neurons, similar to that seen in V2a neurons (Menelaou & McLean, 2019). This slow current is likely to be a result of polysynaptic electrical connection, as we address below. These results demonstrate that both fast and slow motor neuron receive most of their ipsilateral, excitatory input from long range V2a neurons rather than short range connections.

V2a – V1 Interneuron Connectivity

Ipsilaterally projecting, inhibitory V1 interneurons, which have been shown to provide reciprocal inhibition onto motor circuits, are important for flexor/extensor alternation and production of fast locomotor speeds (Bhumbra et al., 2014; Higashijima et al., 2004; Kimura & Higashijima, 2019; Roussel et al., 2021). Computational models have accordingly predicted connections between V2a and V1 neurons; however, no direct V2a – V1 electrophysiological assays have been performed (Roussel et al., 2021). Using the same optogenetic strategy as above, we targeted V1 neurons for recording under fluorescence in a transgenic fish line Tg*(chx10:Gal4;UAS:CatCh;en1:LRL:GFP*) (Fig. 3.5A). Optical stimulation of V2a neurons local to the recording site (0-2 segments rostral or caudal) did not evoke appreciable EPSCs in V1 neurons. Stimulation of more rostrally located V2a neurons (3 – 4 segments) evoked robust EPSCs, while stimulation of more caudally located V2a neurons did not elicit synaptic responses

(Fig 3.4B,C). Optogenetic activation of V2a neurons located 3 – 4 segments rostral to the recording site evoked more EPSCs as opposed to 5 – 6 segments, suggesting that V2a neurons provide medium range excitation onto V1 neurons (Fig. 3.5C).

V2a – Commissural Interneuron Connectivity

Lastly, we evaluated the connectivity between V2a neurons and two groups of commissurally, innervating interneurons. The first group was V0v neurons, which are glutamatergic and have been implicated in coordination of movement across the body midline (Crone et al., 2008; Kawano et al., 2022; Talpalar et al., 2013). To label V0v neurons in the spinal cord, we generated an *evx1:*mCherry plasmid (Juárez-Morales et al., 2016) which was injected into zebrafish embryos of Tg(*chx10:Gal4;UAS:CatCh*) fish at the single-cell stage. Larval zebrafish were screened for both CatCh and mCherry expression (Fig 6A). Fluorescent RNA in situs were performed to validate *evx1* expression in the labeled RFP+ neurons (Fig 3.6B). Both rostral and caudal optogenetic activation of V2a neurons did not evoke significant excitatory input onto V0v neurons. The median summed evoked excitatory input from V2a neurons onto V0v was consistently observed to be around 0 for rostral-caudal positions tested, demonstrating no clear rostral-caudal connectivity relationships (Fig 3.6C,D). The second commissural interneuron group was *dmrt3a+* dI6 neurons which inhibit motor populations (Crone et al., 2008; Kishore et al., 2020; Satou et al., 2020; Uemura et al., 2020). *dmrt3a+* dI6 neurons were labeled by microinjecting a *dmrt3a*:mCherry BAC plasmid into zebrafish embryos of Tg(*chx10:Gal4;UAS:CatCh*) fish at the single-cell stage and validated by fluorescent *in situs* (Fig 3.7 A,B). Similarly, there were no clear rostral-caudal relationships between V2a and dI6 neurons (Fig 3.7 C,D). In both commissural populations, we did identify a few neurons that received optically evoked input from V2a neurons. Although it is likely that V2a input on these

few select neurons may result from biological variability, there is a possibility that specific subsets of V0v and dI6 neurons receive preferential input from V2a neurons which is consistent with previous literature (Crone et al., 2008; Guan et al., 2021). However, further work would be needed to verify this result.

3.4 Discussion

Our study demonstrates that V2a neurons preferentially form synapses at long distances within the spinal cord, mostly forming descending synapses onto ventral populations of spinal neurons 4 – 6 muscle segments caudal to the V2a cell body (Fig 3.8). Optogenetic activation of V2a neurons located 3 – 5 muscle segments rostral from the recording site of fast and slow motor neurons evoked the largest excitatory responses. To V1 neurons, optogenetic activation of V2a neurons located 3 – 4 muscle segments rostral from the recording site evoked the largest excitatory responses. Although V2a neurons provide input onto some commissural interneurons, V0v and dI6 neurons, there was no clear connectivity trend observed, suggesting subtype variability within these commissural populations. We conclude that V2a neuron connectivity varies along the longitudinal axis, with peak synaptic output occurring at 3 – 6 segments caudal from the V2a cell body but with systematic variations in target identity. Our results imply that V2a neurons provide long range input to ensure propagation of the excitatory wave down the spinal cord. Previous work suggested that V2a neurons provide short range local excitation to facilitate recurrent excitation and establish rhythmogenesis within the locomotor circuit (Grillner & Manira, 2020; Song et al., 2020). However, our work raises questions as to whether V2a neurons serve as the local central pattern generators given the scarcity of direct local excitation.

Long range connectivity onto postsynaptic excitatory and motor populations

As previously stated, V2a neurons are found throughout the entire rostral-caudal axis of the spinal cord, making synapses onto both motor neuron populations and other V2a neurons (Hayashi et al., 2018; Menelaou & McLean, 2019; Song et al., 2018; Song et al., 2020). Direct physiological assessment using whole-cell physiology and optogenetics across several species have revealed that V2a neurons are important glutamatergic drivers of locomotion through activation of motor neurons and other V2a neurons. Our assessment revealed that V2a neurons form long range synapses onto both early- and late-born motor neurons. Optogenetic activation of V2a neuron populations located 3 – 5 muscle segments rostral from the recording site of fast and slow motor neurons and V2a neurons evoked the largest excitatory responses. In vertebrates, hindbrain *chx10+* neurons innervate the spinal cord, providing higher order excitatory input onto the cord (Carbo-Tano et al., 2023; Cregg et al., 2020; Huang et al., 2013; Usseglio et al., 2020). It is possible that the hindbrain is responsible for providing input onto the initial spinal cord segments in zebrafish, and therefore, emerging V2a neurons in the first few muscle segments would then be responsible for tiling the excitatory drive to motor populations further down the spinal cord, given that the later developing muscle segments would not have established connections. This developmental pattern would account for the long range inputs seen onto motor populations with less frequent, short range inputs being mixed in. Although we identified some short range inputs from V2a neurons located 1 – 2 segments from the recording site, long range input was more consistently observed, suggesting that short range inputs from V2a neurons only provide a small amount of excitatory input relative long range input. It is also possible that the few V2a or motor neurons that receive short range preferential input from V2a neurons perform some specialized function, but further evaluation and better identification of these targets would be needed to address this scenario.

The lack of optically evoked input from V2a neurons onto other V2a and motor neurons locally was unexpected given that previous modeling experiments proposed V2a neurons as the population tasked with providing local recurrent excitation for rhythmogenesis (Grillner & Manira, 2020; Song et al., 2020). In fact, both fast and slow motor neurons and V2a neurons received more optically evoked EPSCs from long range V2a neurons (4 – 5 muscle segments from the recording site) than from local V2a neurons (0 – 1 muscle segments from the recording site). (Fig 3.9A,C,E). Most of the evoked events observed onto motor neurons and V2a neurons locally were large, slow inward currents with very few fast synaptic events (Fig 3.4,5,6). Furthermore, the few fast detected events in local segments had smaller amplitudes, where the 95th percentile of the median evoked EPSC amplitudes was 12.73 pA for fast motor neurons and 6.39 pA for slow motor neurons, compared to the evoked events in long range segments, where the 95th percentile of the median evoked EPSC amplitudes was 41.35 pA for fast motor neurons and 19.80 pA for slow motor neurons. Based on the target neuron input resistances, these fast synaptic conductances in local segments would be likely to drive EPSPs in the range of 3.15 mV in fast motor neurons (Fig 3.9B) to 2.51 mV in slow motor neurons (Fig 3.9D). Meanwhile, long range fast synaptic conductances from V2a neurons onto fast and slow motor neurons would likely drive EPSPs in the range of 9.92mV and 7.79 mV, respectively (Fig 3.9B,D). This trend in evoked EPSC amplitude was also consistent within V2a – V2a neuron connections, where the 95th percentile of the median evoked fast EPSC amplitude was 9.39 pA (4.92 mV EPSP) (Fig 3.9F) for short range V2a input versus 16.61 pA (8.70 mV EPSP) for fast long range V2a input (Fig 3.9F). In totality, long range V2a neurons are providing a greater quantity of fast, robust input to both motor neurons and V2a neurons (Fig 3.9).

Although V2a neurons do not provide as much local, fast input onto motor neurons and V2a neurons, the local, slow inward current observed could still play a role in membrane depolarization and recruitment of these neurons. Preliminary work performing current clamp recordings using the same optogenetic protocol where evoking both local (segment 0) and long range input (segment 4) onto fast motor neurons (n = 7) have revealed that the observed slow inward current evoked by local V2a neurons is enough to depolarize a motor neuron by ~3 mV. In contrast, long range V2a neurons, which do not provide as many slow conductances, only depolarize the motor neurons ~2 mV via this slow component. These results contrast with the fast synaptic inputs provided by long range and local V2a neurons in this data set which depolarize motor neurons by ~9 mV and ~6 mV, respectively.

Because we see few, if any, fast evoked EPSCs from local stimulation, this slow current is unlikely due to monosynaptic connectivity. As hypothesized by Menelaou and McLean (2019), we think that the most likely explanation for this current is indirect electrical coupling through an intermediate neuron. This intermediate neuron would likely receive electrical input from V2a neurons and then contribute electrical input onto both local motor neurons and V2a neurons, explaining the hypothesized polysynaptic connection seen in Menelaou and McLean (2019). This would also explain the modest connection observed in adult zebrafish using paired whole-cell recordings which has similar kinetics to the slow current observed in larval zebrafish (Song et al., 2018; Song et al., 2020). However, an alternative explanation that we cannot rule out based on our optogenetic stimulation is that our optogenetic protocol is causing some subthreshold depolarization of V2a axons that are near our target neuron. This subthreshold depolarization is then responsible for the slow inward component seen locally in our data set. The use of a soma-targeted opsin label would help rule out this possibility (Forli et al., 2018). By

driving expression of a soma-targeted opsin, we would restrict the opsin to the cell body. Then if we still observed the slow inward current, we could rule out the possibility of it being caused by depolarization of V2a axons given that only the cell body would be expressing the opsin. Instead, it would further support the hypothesis that there is an intermediate neuron that provides local monosynaptic input onto both V2a neurons and motor neurons.

At the moment, it can be inferred that the stronger inputs provided from long range V2a neurons function as the key drivers to allow V2a and motor neurons to be recruited rather than the smaller, short range evoked currents, which could participate in some form of recurrent, albeit indirect, excitation (Song et al., 2020). More current clamp experiments measuring the recruitment of V2a and motor neurons would be needed to evaluate the impact of long range vs short range inputs on these populations. Ultimately, our optical mapping casts some doubt as to whether V2a neurons function as the main recurrent excitatory source proposed in the unit burst generator hypothesis given that their main contribution to the locomotor circuit occurs over long ranges rather than locally (Grillner, 1985; Kiehn, 2016; Song et al., 2020). Although it is still possible that V2a neurons function as a source of recurrent excitation, it would necessarily be through indirect channels such as the weak slow polysynaptic signal observed (Menelaou & McLean, 2019). Instead, it is possible that V2a neurons are more likely to be important for the propagation of the excitatory wave and locomotor patterning such as turns (Cregg et al., 2020; Jay et al., 2023).

V2a neurons form direct synaptic connections onto V1 neurons

Connections from V1 neurons onto V2a neurons had been previously documented, showing that V1 neurons provide short-range inhibition onto V2a neurons to slow down locomotion (Bhumbra et al., 2014; Kimura & Higashijima, 2019; Li et al., 2004). However, the connection from V2a

neurons onto V1 neurons had not been observed through either physiology nor anatomy, but instead was only predicted through computational modeling (Roussel et al., 2021). Thus, this project was the first direct assessment of V2a input onto V1 neurons. Our work revealed that optogenetic activation of V2a neurons located 3 – 4 muscle segments rostral from the recording site provided the most input onto V1 neurons. This suggests that V2a neurons provide medium range input onto V1 neurons in the spinal cord.

Previous rostral – caudal assessment of V1 neurons revealed that V1 neurons make local connections onto motor neurons and V2a neuron as means to provide fine – tuned, short range inhibition during locomotion (Sengupta et al., 2021). This previous work combined with our work revealed a potential excitatory-inhibitory loop which allows for a sequential activation an excitatory wave down the spinal cord given the layout of peak evoked input (Fig 3.10). Through this process, the initial excitatory wave caused from a V2a neuron (V2a 1^0) would reach a motor neuron (MN) 5 – 6 segments caudally; meanwhile, a V1 neuron ($V1^0$) would receive excitatory input 3 – 4 segments away from the V2a 1^0 and reduce the activity of another V2a neuron (V2a 2^0) located 1 – 2 segments away from the initial activation point. This would prevent hyper-excitability of locomotor circuits through uncoordinated excitatory waves down the length of the spinal cord. This organization would also enable a V2a 2^0 to excite a V1 2^0 neuron located within the muscle segment of the motor neuron activated by the V2a 1^0 to be shutdown, thus closing its excitatory loop. Unfortunately, given the timing of V1 neuron recruitment and the fast conduction velocity of V2a neurons, this explanation seems unlikely. Instead, other electrophysiological factors such as the holding charge of membrane potentials may be dampening and slowing down the activation of V1 neurons (Jay et al., 2023; Kimura & Higashijima, 2019).

Although most V1 neurons received synaptic input from spinal V2a neurons, some V1 neurons (5/20) received zero or minimal excitatory input from spinal V2a neurons. Instead, we observed that 3/5 of these V1 neurons received preferential input from *chx10+* neurons located in the hindbrain (Fig 3.10). We did not perform hindbrain recordings in the other two neurons. Further evaluation of hindbrain *chx10+* neuron input on V1 neurons revealed more examples of preferential hindbrain input onto subsets of V1 neurons (Fig 3.11). Therefore, some V1 neurons may be driven less by patterned spinal input and instead by descending populations. This finding could indicate that there are subsets of V1 neurons that are responsible for integrating higher order information from the hindbrain into the spinal circuit, but it remains unknown what that function could be. It will be interesting to determine whether these V1 neurons align with distinct subclasses or clades as identified by molecular and developmental profiling (Bikoff et al., 2016; Worthy et al., 2023). Distinct clades of V1 neurons have been identified in mammalian spinal cord with each clade expressing different transcription factors, unique synaptic partners, and different birth periods (Worthy et al., 2023). These clades have not been identified or described in zebrafish; however, our connectivity data suggests that V1 subclasses could exist in zebrafish. To date, V1 neurons in zebrafish have only been classified as either fast or slow recruited, and molecular distinctions between the two groups have not been identified. It is possible that fast and slow V1 neurons innately express different transcription factors, and it is possible that hindbrain selective V1 neurons could fall into one of those classes or represent an entirely new population. Further genetic screening of these V1 populations will be needed to determine whether connectivity is linked to molecular identity.

V2a neurons connect to subsets of commissural interneurons

Our data revealed that V2a neurons form, albeit infrequent, connections onto some dI6 (7/21) and V0v (6/13) neurons, suggesting a possible subtype specificity within these commissural populations. From previous studies, it has been shown that dI6 and V0v neurons exhibit very distinct morphologies within each other (Satou et al., 2012; Satou et al., 2020), so it is possible that each morphologically distinct subclass of dI6 and V0v neurons exhibit unique connectivity profiles and functions. From our experiments, we could not address this because we could not always achieve a clear axonal fill during our recordings to identify morphological subtypes of these neurons. The connections observed suggest that ipsilateral V2a neurons do elicit locomotor control on the contralateral side of the spinal cord through polysynaptic connections made onto V0v and dI6 neurons which then connect onto contralateral neurons (Björnfors & El Manira, 2016; Crone et al., 2008; Kawano et al., 2022; Satou et al., 2012; Satou et al., 2020). Anatomical and physiological connections between V2a neurons onto dI6 had been previously reported (Crone et al., 2008; Guan et al., 2021). Within these experiments, researchers observed loss of coordination during left-right alternation, suggesting that ipsilateral V2a neurons drive inhibition of the contralateral side of the spinal cord through connections onto commissural innervating dI6 neurons (Crone et al., 2008). This claim was further supported when electrophysiological evidence showed that a subset of V2a neurons provide excitatory input on dI6 neurons which then connect onto contralaterally located V2a neurons (Satou et al., 2020). This subtype specificity data aligns with our current results. Among V0v neurons, there is anatomical evidence in the form of retrograde tracing that reveals V2a connections onto V0v neurons (Crone et al., 2008); however, there has been no electrophysiological assessment between the two cell types to date. Our work reveals the first electrophysiological assessment of V2a connections onto V0v, and although there was no clear trend, we did observe some

connections between the two cell types. Further work will be needed to address the impact of this connection, but given the commissural innervation pattern on V0v neurons, we would assume that the connection is required for left-right alternation.

3.5 Acknowledgments

We also acknowledge the Washington University Zebrafish Facility for fish care and Washington University Center for Cellular Imaging (WUCCI) for supporting the confocal imaging experiments. This work is supported by funding through the National Institute of Health (NIH) R01 DC016413 (M.W.B.). M.W.B. is a Pew Biomedical Scholar and a McKnight Foundation Scholar.

3.6 Materials and Methods

Experimental Model and Subject Details:

All fish used for experiments were at the larval stage from 4 – 6 dpf, before onset of sexual differentiation. All experiments and procedures were approved by the Animal Studies Committee at Washington University and adhere to the NIH guidelines. Adult zebrafish (Danio rerio) were maintained at 28.5^{o}C with 14:10 light:dark cycle in the Washington University Zebrafish Facility up to one year following standard care procedures. Larval zebrafish used for experiments were kept in Petri dishes in system water or housed with system water flow. Transgenic animals *Tg*(*chx10:Gal4*;*UAS:CatCh*) were created by crossing the transgenic line *Tg*(*chx10:Gal4;UAS:GFP*) (ZDB-FISH-220828-1) with a stable *Tg*(*UAS:CatCh*) line. For targeting V1 neurons, *Tg*(*eng1b:loxP-DsRed-loxP-GFP*) (ZDB-ALT-191030-2) were crossed to *Tg*(*chx10:Gal4;UAS:CatCh*) to generate a double transgenic *Tg*(*chx10:Gal4;UAS:CatCh; eng1b:loxP-DsRed-loxP-GFP*).

Stochastic Single Cell Labeling by Microinjections:

Embryos were injected with either a *de novo* generated *dmrt3a*:*mCherry* BAC (VectorBuilder, (Satou et al., 2020)) or *evx1*:*mCherry* plasmid (VectorBuilder, (Juárez-Morales et al., 2016)) at the 1 – 2 cell stage. Final plasmid DNA concentrations were 10 – 15 ng/µl. The embryos were transferred to system water, regularly cleaned, and allowed to develop. At 4 dpf, larvae were screened for sparse expression of mCherry in the spinal cord and selected for electrophysiology or fluorescent *in situ* experiments.

Hybridization Chain Reaction – Immunofluorescent *in situ*

Hybridization chain reaction (HCR) fluorescent *in situs* were performed in *WT* larvae injected with either *dmrt3a*:*mCherry* or *evx1*:*mCherry* plasmid to validate neuronal identity of stochastically labeled neurons. Synthesis of RNA probes designed for *dmrt3a* and *evx1* were performed as previously described (Thisse & Thisse, 2008; Tsai et al., 2020). We followed the protocols suggested by Molecular Instruments and adapted from (Tsai et al., 2020) for 4 – 5 dpf larval zebrafish. Hybridized larvae were mounted on slides using Vectashield (ThermoFisher) and cured for >24 hours. Larvae were then imaged using an Olympus FV1200 Confocal microscope and a UAPO 40x W/340 1.15 NA water immersion objective. A transmitted light image was obtained along with laser scanning fluorescent images to identify spinal segments. Sequential scanning was used for multi-wavelength images.

Image Analysis:

Confocal images were analyzed using Imaris (9.8, Bitplane). Three-dimensional (3D) images were reconstructed and analyzed using Imaris. Co-localization of native fluorescence and fluorescent *in situ* label was analyzed manually using the Slice layout of Imaris. Each image was annotated with the measurement function to track labeled neurons. Co-localization frequency

was calculated by taking the percentage of neurons that co-expressed the stated marker out of all neurons with reporter expression.

Electrophysiology:

Whole-cell patch-clamp recordings were performed in larvae at 4 – 6 dpf. Larvae were immobilized with 0.1% α – bungarotoxin and fixed to a Sylgard lined Petri dish with custom-sharpened tungsten pins. One muscle segment overlaying the spinal cord was removed at the mid – body level (segments 8 – 16) using a blunt-end glass electrode and suction (Wen & Brehm, 2010). The larva was then transferred to a microscope (Scientifica SliceScope Pro) equipped with infrared differential interface contrast optics, epifluorescence, and immersion objectives (Olympus: 40x, 0.8 NA). The bath solution consisted of (in mM) 134 NaCl, 2.9 KCl, 1.2 $MgCl_2$, 10 HEPES, 10 glucose, and 2.1 $CaCl_2$. Osmolarity was adjusted to ~295 mOsm and pH to 7.5. Patch pipettes (5–15 MΩ) were filled with internal solution for voltage and current clamp composed of (in mM) 125 K gluconate, 2 $MgCl_2$, 4 KCl, 10 HEPES, 10 EGTA, and 4 Na_2ATP. Additionally, Alexa Fluor 647 hydrazide 0.05–0.1 mM or sulforhodamine (0.02%) was included to visualize morphology of recorded cells post hoc. Osmolarity was adjusted to ~285 mOsm and KOH was used to bring the pH to 7.5. Patch recordings were made in whole-cell configuration using a Multiclamp 700B, filtered at 10 kHz (current clamp) or 2 kHz (voltage clamp). All recordings were digitized at 50 kHz with a Digidata 1440 (Molecular Devices) and acquired with pClamp 10 (Molecular Devices).

Optogenetic Stimulation:

A Polygon 400 Digital Micromirror Device (Mightex) was used to deliver optical stimulation. The projected optical pattern consisted of a 6x5 grid of 30 squares. Each square in the grid approximately measured 20x12 μm. One full stimulus pattern consisted of an ordered sequence

of turning ON and OFF each of the 30 squares sequentially. For each small square, illumination consisted of a 20 ms light pulse (470 nm) at 25% intensity (3.8 – 4.6 µW 40X, 0.8 NA). The sequence was triggered using a TTL pulse from the Digidata to synchronize the stimulation with electrophysiology. The objective was carefully positioned over a single spinal segment prior to stimulus delivery; for each segment, the stage was manually translated and repositioned. V2a spiking calibration was measured by delivering one full stimulus pattern while in current-clamp mode. The same protocol was used for all cell types and in all segments to obtain reliable EPSCs for measurement of synaptic input. For the high frequency stimulation, a 20 Hz train of three 20 ms pulses were performed using the same 30 square stimulus pattern.

Analysis of Electrophysiology Data:

Electrophysiology data were imported into Igor Pro 9 (Wavemetrics) using Neuromatic (Rothman & Silver, 2018). Spikes and EPSCs were detected and analyzed using custom code in Igor and MATLAB. The detection algorithm was based on the event detection instantiated in SpAcAN environment for Igor Pro (Rousseau et al., 2012). Summed synaptic input for evoked responses was calculated by summing all detected EPSC event amplitudes within 100 ms of stimulus onset, and subtracting detected EPSC events within a 100 ms baseline period prior to the stimulus to account for spontaneous activity. All summed synaptic input values were then normalized by the total conductance (inverse of input resistance) of the neuron.

Statistics:

Statistical tests were performed using MATLAB (R2018a, MathWorks). Due to the non-normal distribution of physiological results, we used nonparametric statistics and tests for representations and comparisons. Details of statistical tests, p-values used, and sample size are described in the corresponding figure legends.

3.7 Figures and Legends

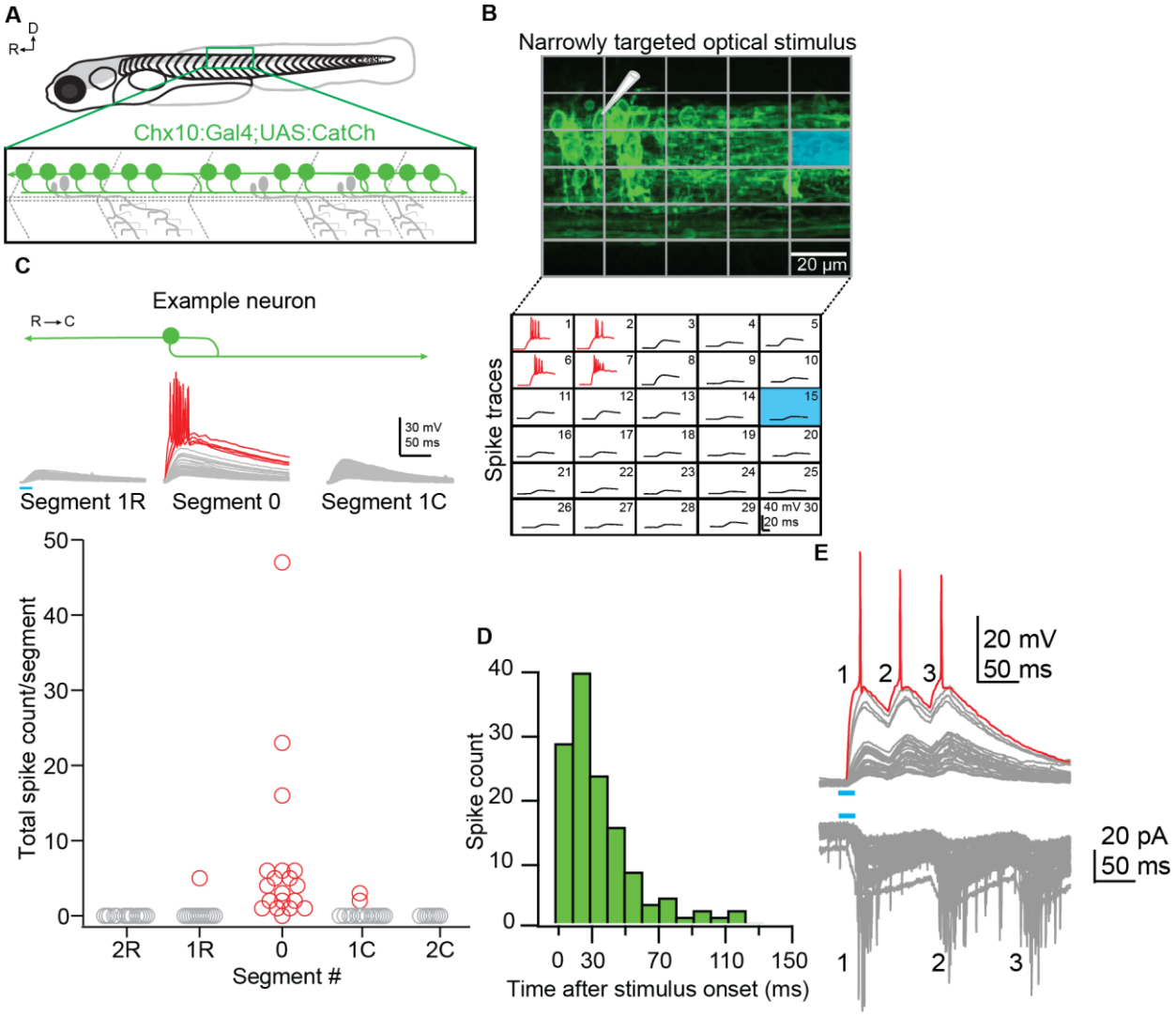

Figure 3.1 Calibration of V2a spiking evoked by optical stimulus

A. Schematic of *Tg*(*chx10:Gal4;UAS:CatCh*) animal used in the experiment. **B.** Schematic of the patterned optical stimulus. A 6x5 grid was overlaid on approximately one segment and each square in the grid (blue square) was optically stimulated in ordered sequence from left to right and top to bottom. Intracellular recordings elicited from optical stimulation in each grid square. Red traces denote spiking **C.** (Top) Representative intracellular recordings of evoked responses from optically stimulated V2a neurons. Segment 0 corresponds to the muscle segment recording site where the V2a cell body is located. Segment 1R and Segment 1C represent intracellular recordings from one muscle segment rostral or caudal to the recording where only axons are

located. Spiking traces are presented as red. No spiking traces are presented as gray. Blue bar represents start and duration of optical stimulus. (Bottom) Scatterplot representing the total V2a spike count and the location of the muscle stimulated. **D.** Histogram representing spike count versus the time after stimulus onset in which the spiking occurred. **E.** (Top) Current clamp intracellular recording depicting the spiking observed when V2a neurons were presented a 3x 20 Hz pulse train. (Bottom) Voltage clamp intracellular recording from a primary motor neuron depicting the 3x stimulus evoking EPSC.

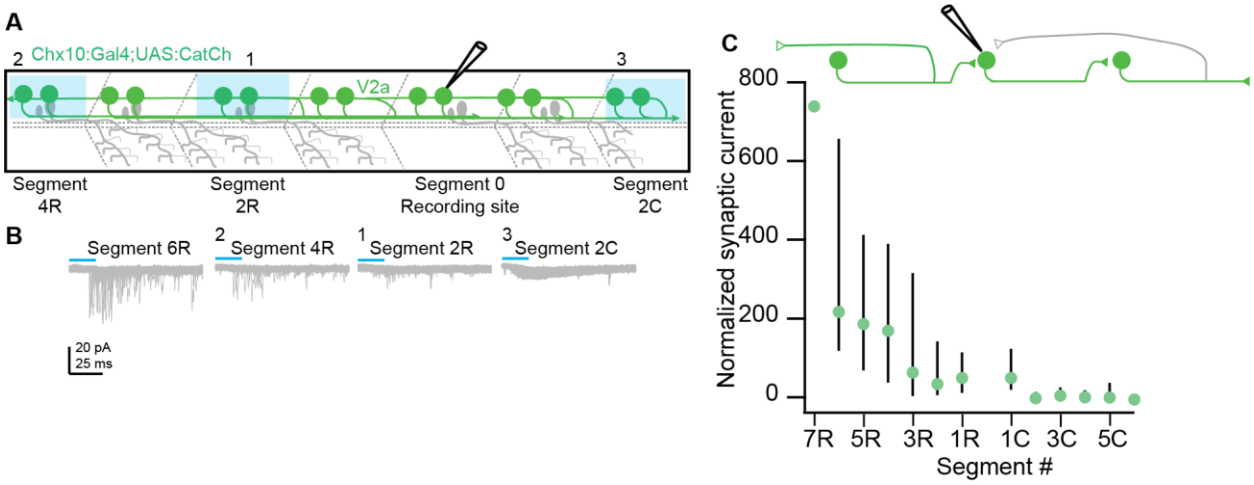

Figure 3.2 V2a neurons receive input from long range V2a neurons

A. Schematic of the experimental design showing intracellular recording from V2a neuron (green) and rostral-caudal sequence of stimulated V2a muscle segments. B. Representative overlay of 30 EPSCs record from V2a neurons during illumination of segments 2, 4, and 6 rostral and segment 2 caudal from the recorded neuron soma. Blue bars represent the duration of the optical stimulus. C. Dot and Whisker plot depicting the normalized synaptic current evoked from V2a neuron spiking along the rostral-caudal axis onto V2a neurons. Green dots represent the median normalized synaptic current. Whiskers represent the 25th and 75th percentile values. n = 20.

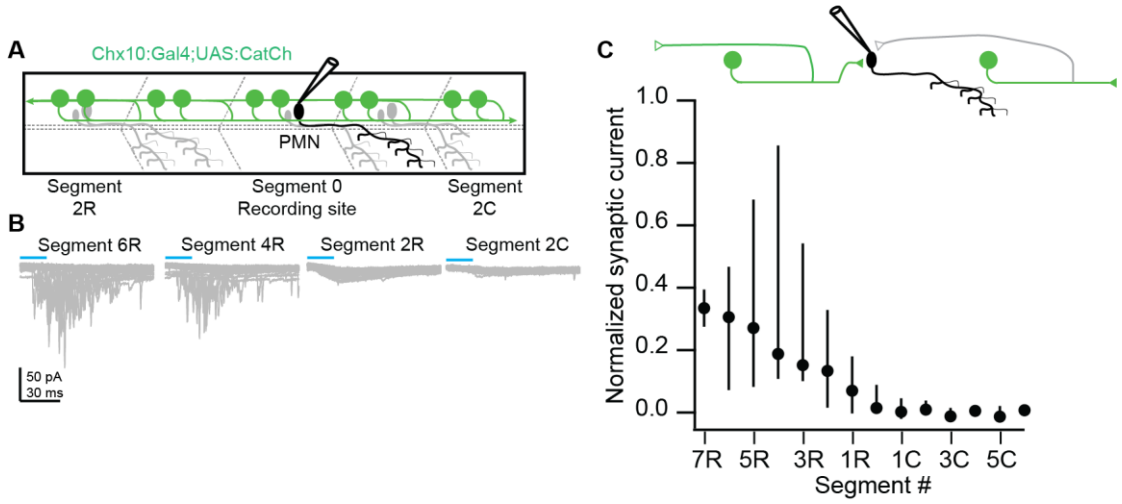

Figure 3.3 Fast motor neurons receive input from long range V2a neurons

A. Schematic of the experimental design showing intracellular recording from fast motor neurons (black). B. Representative overlay of 30 EPSCs record from fast motor neurons during illumination of segments 2, 4, and 6 rostral and segment 2 caudal from the recorded neuron soma. Blue bars represent the duration of the optical stimulus. C. Dot and Whisker plot depicting the normalized synaptic current evoked from V2a neuron spiking along the rostral-caudal axis onto fast motor neurons. Black dots represent the median normalized synaptic current. Whiskers represent the 25^{th} and 75^{th} percentile values. n = 13.

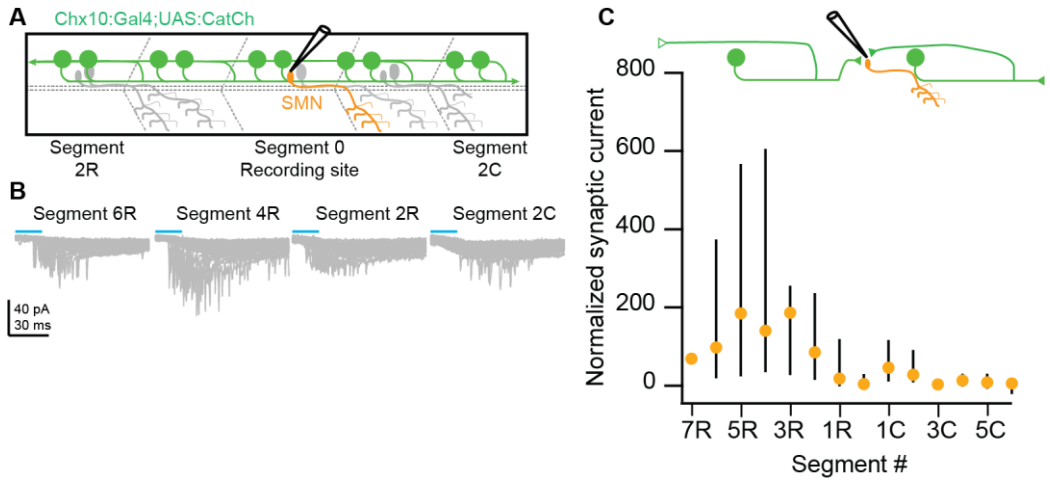

Figure 3.4 Slow motor neurons receive input from long range V2a neurons

A. Schematic of the experimental design showing intracellular recording from slow motor neurons (orange). B. Representative overlay of 30 EPSCs record from slow motor neurons during illumination of segments 2, 4, and 6 rostral and segment 2 caudal from the recorded neuron soma. Blue bars represent the duration of the optical stimulus. C. Dot and Whisker plot depicting the normalized synaptic current evoked from V2a neuron spiking along the rostral-caudal axis onto slow motor neurons. Orange dots represent the median normalized synaptic current. Whiskers represent the 25th and 75th percentile values. n = 20.

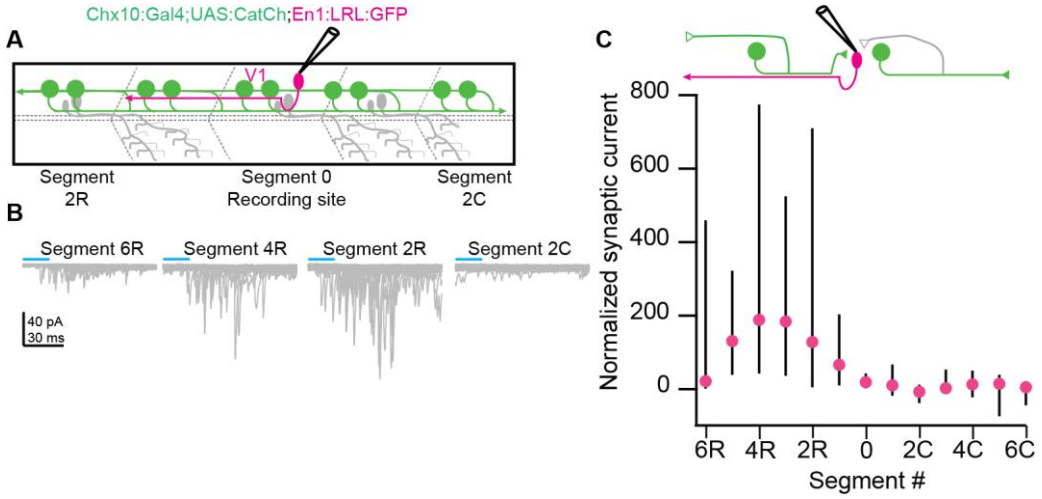

Figure 3.5 V1 neurons receive input from medium range V2a neurons

A. Schematic of the experimental design showing intracellular recording from V1 neurons (pink). B. Representative overlay of 30 EPSCs record from V1 neurons during illumination of segments 2, 4, and 6 rostral and segment 2 caudal from the recorded neuron soma. Blue bars represent the duration of the optical stimulus. C. Dot and Whisker plot depicting the normalized synaptic current evoked from V2a neuron spiking along the rostral-caudal axis onto V1 neurons. Pink dots represent the median normalized synaptic current. Whiskers represent the 25th and 75th percentile values. n = 20.

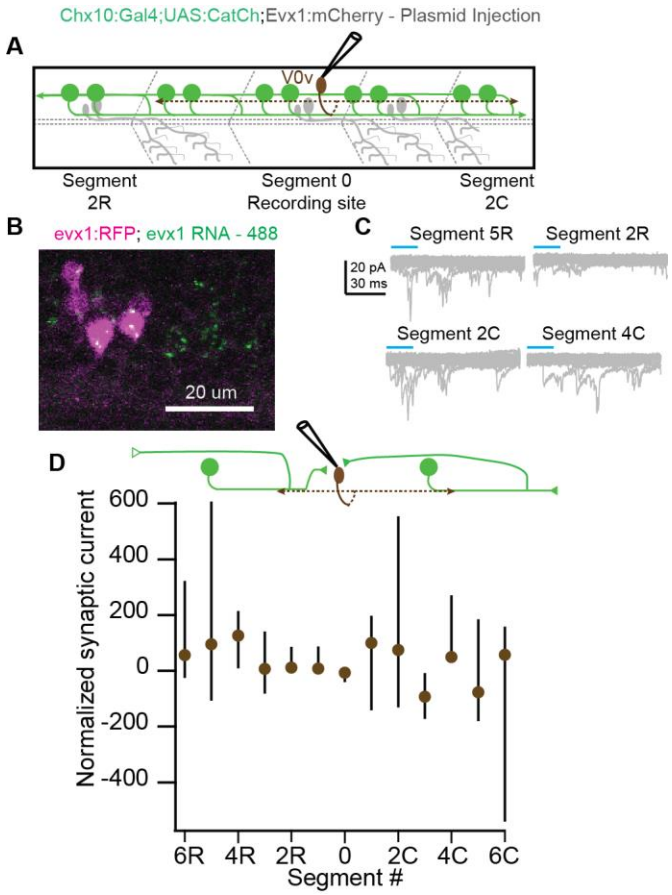

Figure 3.6 V0v neurons receive variable input from V2a neurons

A. Schematic of the experimental design showing intracellular recording from V0v neurons (brown). B. Single – plane confocal image depicting evx1 RFP+ neuron labeled by microinjection and overlap of evx1 (GFP+) fluorescent in situ C. Representative overlay of 30 EPSCs record from V0v neurons during illumination of segments 2 and 5 rostral and segments 2 and 4 caudal from the recorded neuron soma. Blue bars represent the duration of the optical stimulus. D. Dot and Whisker plot depicting the normalized synaptic current evoked from V2a neuron spiking along the rostral-caudal axis onto V0v neurons. Brown dots represent the median normalized synaptic current. Whiskers represent the 25th and 75th percentile values. n = 13.

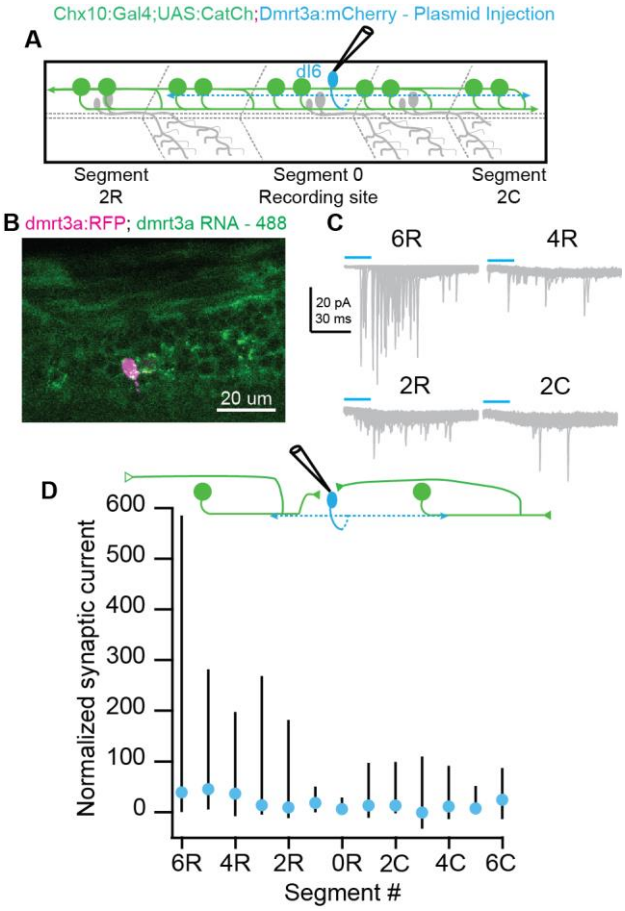

Figure 3.7 dmrt3a+ dI6 neurons receive variable input from V2a neurons

A. Schematic of the experimental design showing intracellular recording from dmrt3a+ dI6 neurons (light blue). B. Single – plane confocal image depicting dmrt3a RFP+ neuron labeled by microinjection and overlap of dmrt3a (GFP+) fluorescent in situ C. Representative overlay of 30 EPSCs record from dI6 neurons during illumination of segments 2, 4, and 6 rostral and segment 2 caudal from the recorded neuron soma. Blue bars represent the duration of the optical stimulus. D. Dot and Whisker plot depicting the normalized synaptic current evoked from V2a neuron spiking along the rostral-caudal axis onto dmrt3a+ dI6 neurons. Blue dots represent the median normalized synaptic current. Whiskers represent the 25th and 75th percentile values. n = 21.

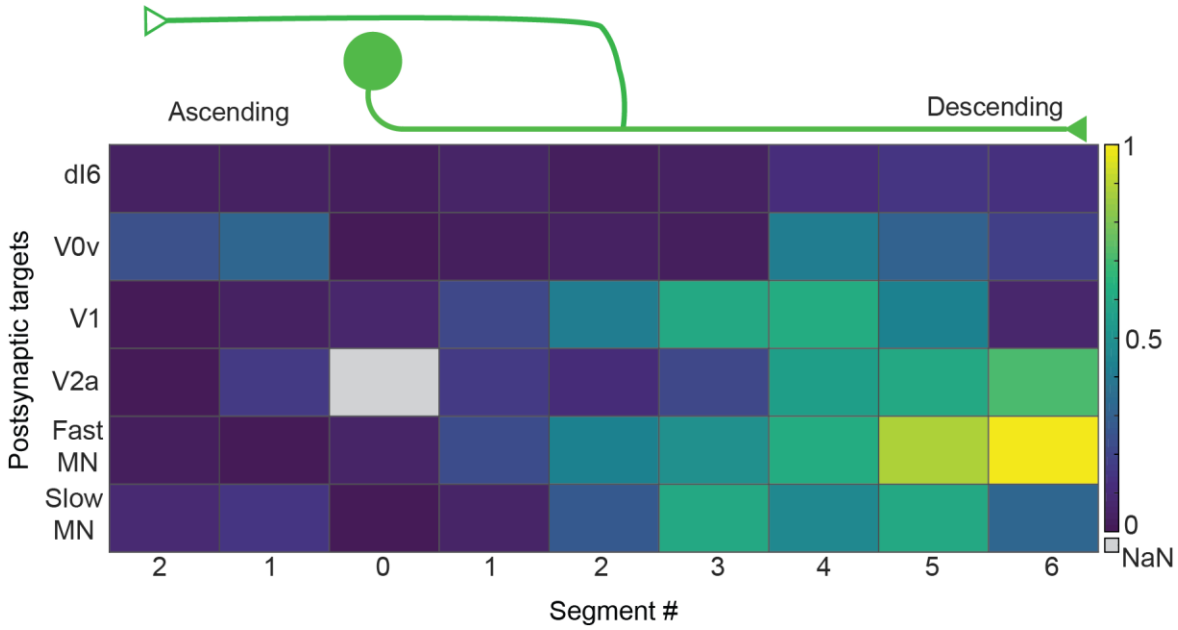

Figure 3.8 Heat map depicting that V2a neurons provide long range descending input

Heat Map summary of V2a connectivity onto different postsynaptic targets along the rostral-caudal axis. The normalized synaptic current for each recorded neuronal was normalized to its measured intrinsic conductance (inverse Rin). Median values of normalized synaptic current for each target cell population are plotted. The resulting values are plotted on the same color scale for all target populations.

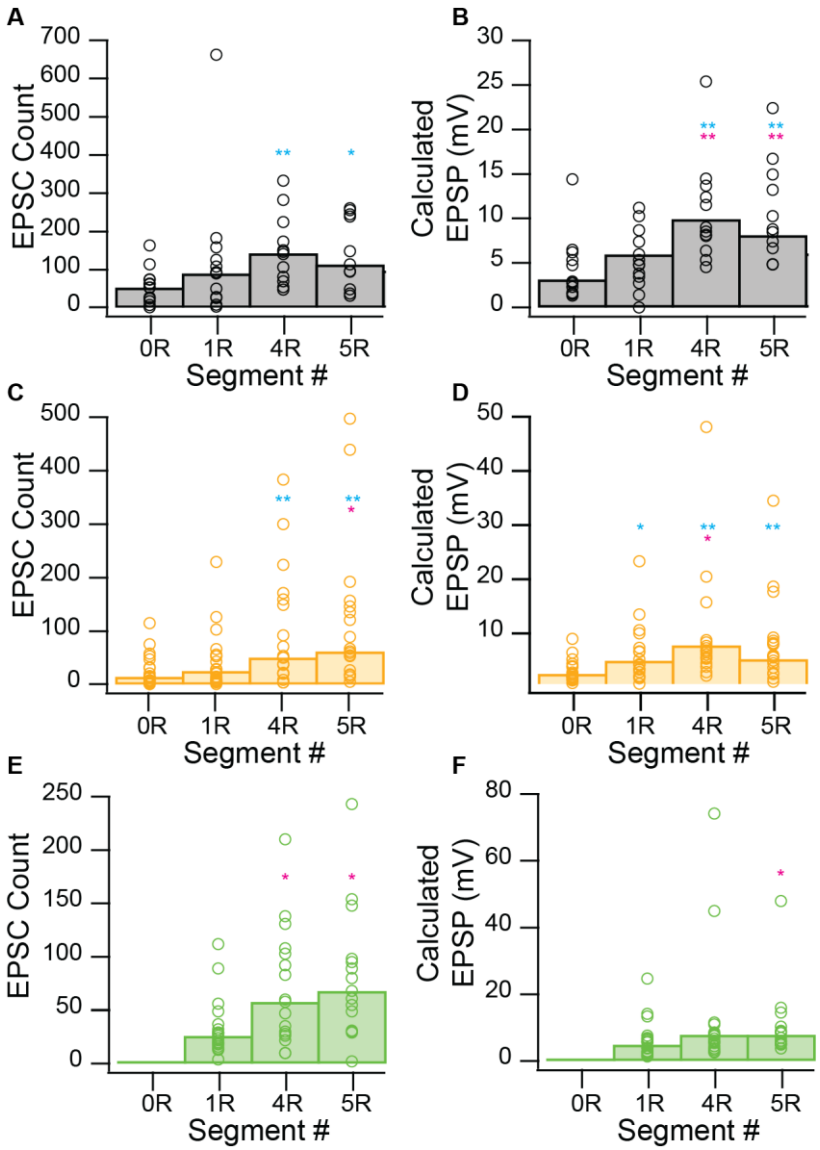

Figure 3.9 V2a neurons provide larger and more EPSCs onto motor neurons and V2a neurons at long ranges

A. Scatterplot depicting the number of detected EPSC events onto a fast motor neuron by optically activating other V2a neurons located 0, 1, 4, and 5 muscle segments rostral to the recording site. Bars depict the median value for each muscle segment. *Wilcoxon signed – rank test (0R – 5R) p=0.0189. **Wilcoxon signed – rank test (0R – 5R) p = 4.3×10^{-3}. B. Scatterplot depicting the calculated EPSP change of fast motor neurons by taking the average of the 95th percentile of evoked EPSC amplitudes and multiplied by the neuron's input resistance (R_{In}). Bars depict median calculated voltage change values. Cyan asterisks denote significant differences compared to segment number 0R. Magenta asterisks denote significant differences compared to segment number 1R. **Wilcoxon signed – rank test (0R – 4R) p= 9.91×10^{-4}; (0R – 5R) p= 9.58×10^{-4}; (1R – 4R) p= 7.1×10^{-3}; (0R – 5R) p= 7.7×10^{-3}. C. Scatterplot depicting the number of

detected EPSC events onto a slow motor neuron by optically activating other V2a neurons located 0, 1, 4, and 5 muscle segments rostral to the recording site. Bars depict the median value for each muscle segment. Cyan asterisks denote significant differences compared to segment number 0R. Magenta asterisks denote significant differences compared to segment number 1R. *Wilcoxon signed – rank test (1R – 5R) p=0.0212. **Wilcoxon signed – rank test (0R – 4R) p = $5.9x10^{-3}$; (0R – 5R) p = $8.6x10^{-4}$. D. Scatterplot depicting the calculated EPSP change of slow motor neurons by taking the average of the 95^{th} percentile of evoked EPSC amplitudes and multiplied by the neuron's input resistance (R_{In}). Bars depict median calculated voltage change values. Cyan asterisks denote significant differences compared to segment number 0R. Magenta asterisks denote significant differences compared to segment number 1R. *Wilcoxon signed – rank test (0R – 1R) p=0.0155; (1R – 4R) p=0.0445; **Wilcoxon signed – rank test (0R – 4R) p = $2.6x10^{-5}$; (0R – 5R) p=$1.2x10^{-3}$. E. Scatterplot depicting the number of detected EPSC events onto a V2a neuron by optically activating other V2a neurons located 0, 1, 4, and 5 muscle segments rostral to the recording site. Bars depict the median value for each muscle segment. No EPSCs could be detected at segment 0 because of the optically induced depolarization. *Wilcoxon signed – rank test (1R – 4R) p=0.0234; (1R – 5R) p = 0.023. F. Scatterplot depicting the calculated EPSP change of V2a neurons by taking the average of the 95^{th} percentile of evoked EPSC amplitudes and multiplied by the neuron's input resistance (R_{In}). Bars depict median calculated voltage change values. *Wilcoxon signed – rank test (1R – 5R) p=0.0443.

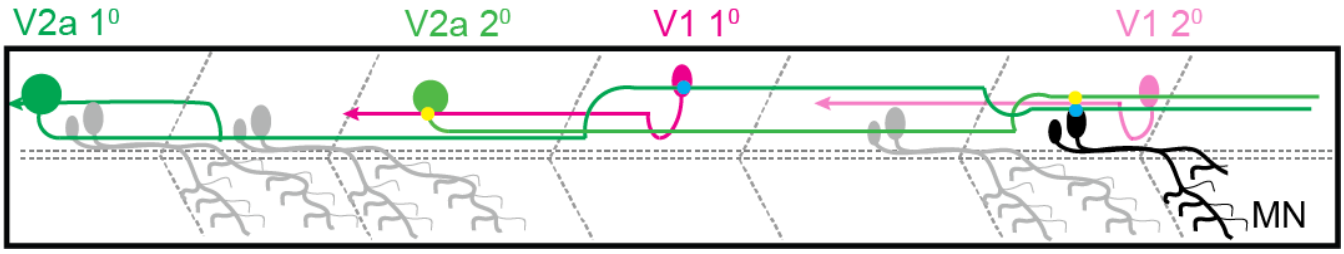

Figure 3.10 Schematic of V2a – V1 – MN Loop according to mapping data only

V2a 1^0 would send an excitatory wave down the spinal cord and synapse onto a V1 neuron 3 – 4 muscle segments away and motor neurons (5 – 6 segments) away, providing excitatory input (cyan circle). V1 1^0 would provide inhibition (yellow dot) onto a local V2a neuron (V2a 2^0). This would prevent the excitatory wave from improperly propagating. After the excitatory wave reaches V2a 2^0, it would excite V1 2^0 which in turn would inhibit the motor neurons activated by V2a 1^0.

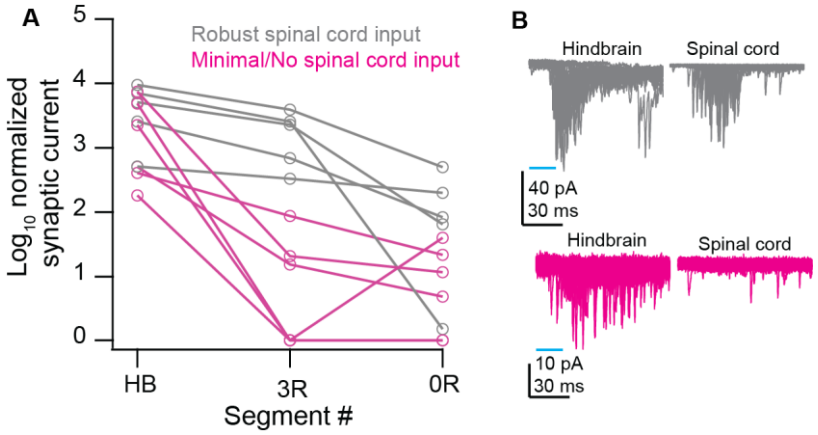

Figure 3.11 Subsets of V1 neurons receive preferential input from the hindbrain

A. Line plot depicting the input onto V1 neurons from optically evoked V2a neurons either 0 or 3 muscle segments rostral to the recording and optically evoked input from *chx10+* neurons located in the hindbrain. Data values were transformed from the normalized synaptic current by Log Base 10. Gray lines represent V1 neurons that receive robust input from the spinal cord. Magenta lines represent V1 neurons that receive minimal/zero input from V2a neurons in the spinal cord. B. Representative traces of example V1 neurons which fit into either category.

Chapter 4: Conclusion and Future Directions

4.1 Conclusion

How does developmental origin determine circuit connectivity within the spinal cord? I used whole-cell electrophysiology, optogenetics, and fluorescence microscopy to investigate the development and neuronal connectivity of V2 neurons in the larval zebrafish spinal cord. My results showed that clonally related, Notch-differentiated V2 neurons exhibit morphological similarities such as soma and axon proximity. However, sister V2 neurons integrate into distinct circuits similar to Notch-differentiated sister neurons in *Drosophila* given that sister V2 neurons receive input from distinct presynaptic sources, do not communicate with each other, and largely connect to distinct downstream targets. This result suggests that although clonally related, sister V2a/b neurons follow a similar circuit development pattern as Notch-differentiated sister neurons in *Drosophila,* supporting a conserved developmental mechanism and potential circuit phenotype for other clonally related, Notch-differentiated neurons in the nervous system.

Given the divergence in postsynaptic targeting, what are the preferential targets of V2a neurons along rostral-caudal axis of the spinal cord? Our assessment of V2a neuron postsynaptic targets revealed that V2a neurons preferentially connect to neurons located 4 – 6 muscles segments away from the V2a somata. The lack of short range V2a targets indicate that V2a neurons cannot function as the predicted local unit burst generators. Instead, we predict that V2a neuron propagate the excitatory wave down the length of the spinal cord to ensure firing of the various motor pools, as well as provide patterned input, such as directing left or right turns. Thus, my study indicates that V2a neurons serve as excitatory drivers of locomotion, but that another

neuronal population within the spinal cord is responsible for establishing the rhythmogenesis of locomotor circuits.

4.2 Effects of Notch on Axon Pathfinding

Notch signaling has been implicated in neuronal development and differentiation of specific cell types within the nervous system (Engerer et al., 2021; Jacobs et al., 2022b; Kageyama et al., 2009; Lathia et al., 2008; Zhang et al., 2021). In *Drosophila*, Notch signaling establishes neuronal clusters which constitute neuronal hemilineages (Artavanis-Tsakonas et al., 1999; Harris et al., 2015; Lacin & Truman, 2016; Lacin et al., 2014). These hemilineages extend and innervate distinct regions within *Drosophila*, presumably establishing a divergence in cellular function through distinct innervation patterns. However, it remains unclear whether Notch signaling continues to play a role in development that extends beyond cellular differentiation and is actually involved in axon pathfinding and circuit formation. There is some evidence that suggests Notch plays a role in axon outgrowth with Notch overexpression resulting in truncated axons (Mizoguchi et al., 2020; Sestan et al., 1999); however, there is no systematic assessment of Notch signaling with regards to circuit formation of Notch – differentiated sister neurons.

Notch Manipulations Alter V2a/b Pathfinding

Our work revealed that sister V2a/b neurons integrate into distinct circuits similar to work performed in *Drosophila*, so an explicit test of the effect of Notch signaling on axon pathfinding would be to temporally manipulate Notch using our V2a/b circuit model. Constitutively active Notch manipulations have only resulted in skewing of V2a/b numbers in the spinal cord (Mizoguchi et al., 2020), so an inducible Notch upregulation or downregulation experiment after V2a/b differentiation would ideally prevent overproduction of either cell type. As a result, any manipulation to Notch would only impact V2a/b axon pathfinding. If Notch

were to have an effect on axon pathfinding, we would hypothesize either a decrease or increase in the axon length of either sister cell. This result would affect the overall synaptic partners that each cell could contact by either shortening or extending their axonal projections.

V2b/s Clonal Circuit Integration

During our evaluation of *vsx1+* progenitors, we identified that a subset of progenitors (~25%) did not give rise to clonally related V2a/b sister cells, but rather, some progenitors differentiated into V2b/s sister pairs. Both V2b/s neurons rely on Notch expression to initiate V2b/s cellular programs (Cucun et al., 2024; Gerber et al., 2019; Mizoguchi et al., 2020), and both cell types share similarities with each other. For example, both cell types are glycinergic and ipsilaterally innervating (Callahan et al., 2019; Gerber et al., 2019), so there is a possibility that both V2b/s neurons function in a similar role in the spinal cord. Additionally, because both V2b/s neurons are $Notch^{ON}$, there is a possibility that both cell types integrate into the same circuit given that V2b/s neurons could integrate into the same $Notch^{ON}$ lineage as seen in *Drosophila*. This outcome would further support the conservation of $Notch^{ON/OFF}$ lineages in nervous system development. Furthermore, this experiment would resemble lineage tracing work performed in vertebrate system which assessed sister neurons that released the same neurotransmitter (Xu et al., 2014; Yu et al., 2009; Zhang et al., 2017).

4.3 Recruitment of Motor Populations via V2a Activation

In vertebrates and in both spinalized cord and intact animals, it has been well documented that V2a neurons provide excitatory drive onto motor neurons, leading to locomotor recruitment of motor pools (Hayashi et al., 2018; Jay et al., 2023; Ljunggren et al., 2014; Menelaou & McLean, 2019; Song et al., 2018; Song et al., 2020). In addition to this excitatory drive, it has been reported in adult zebrafish that V2a neurons function as the main recurrent excitatory

drivers of the unit burst generator model, previously described in lamprey (Grillner, 1985; Grillner & Manira, 2020; Song et al., 2020). In this model, V2a neurons serve as the excitatory source that provides local recurrent excitation to drive locomotor rhythm and excite motor neurons. This recurrent excitation is thought to support rhythmogenesis and direct control of locomotion. The central idea of the unit burst generator model of rhythmogenesis is that recurrent excitatory drive feeds back to excite both the source of the population, and the motor output population (Goulding, 2009; Kiehn, 2016; Kozlov et al., 2009). For V2a neurons to fulfill this role, therefore, we would expect them to make significant synaptic connections onto same segment V2a neurons (recurrence) and motor neurons (output). However, our data suggests that V2a neurons cannot be candidates for this local excitatory population. We did not observe robust V2a input onto local V2a (no recurrence) and motor neuron populations (no output). Instead, the majority of V2a input onto V2a and motor neurons occurred at longer distances (> 4 segments). Although we did observe some short range V2a input, the synaptic amplitudes would not provide enough excitatory drive to alter the firing and recruitment pattern of these neurons relative to the long range input that V2a neurons provide. It still remains to directly test this conclusion with current clamp recordings of the evoked excitatory input.

Optogenetic recruitment of motor neurons

An explicit test of the ability of V2a neurons to drive local vs long-range motor neuron would be to perform current clamp recordings as previously performed in adult zebrafish while using the same optogenetic protocol described in Chapter 3 (Song et al., 2018; Song et al., 2020). From this experiment, we would anticipate that optical activation of V2a neurons located further away (4 – 6 muscle segments) from the target motor neurons would elicit larger changes in the membrane voltage of motor neurons relative to activation of local V2a neurons. Although this

result can be inferred from our already collected data, performing these experiments allow us to make direct comparisons to already published work in adult zebrafish (Song et al., 2018; Song et al., 2020). Ultimately, we hypothesize that the small depolarizations observed in motor neurons of adult zebrafish are caused by the small number of evoked EPSCs that we observed, and that the optogenetic activation of long range V2a neurons will greater influence the depolarization of motor neurons.

Effect of V2a neuron ablation on swim frequency

V2a neurons were presumed to be the recurrent excitatory neuronal source. This conclusion was based not only on the selective connectivity patterns describe above, but also by the functional relationship between V2a neurons and local activity. Researchers ablated V2a neurons along 10 mid – body muscle segments using a high – photon laser, and then they performed ventral root (VR) recordings from both within the ablation area and then a few muscle segments caudal to the ablation area (Eklöf-Ljunggren et al., 2012). From their behavioral assessment, researchers reported that fish could not achieve the same swim speeds prior to the ablation as noted by their VR recordings, and therefore, V2a neurons were crucial for producing locomotion (Eklöf-Ljunggren et al., 2012). Our data suggest an alternate explanation for these results. Given the preferential input from long range V2a neurons onto both V2a and motor neurons, it is possible that the VR recordings within the ablation area are mostly affected the more rostrally located, long range V2a neurons being ablated rather than the more local V2a neurons. Meanwhile, the reduction of VR activity recorded caudal to the ablation area could be accounted for by the loss of V2a neurons within the mid – body, preventing the propagation of the excitatory wave down the spinal cord. Our alternate interpretation could be tested by a refined ablation experiment, targeting cell loss to a 1-2 segment region. This experiment could be

accomplished using a *Tg*(*chx10:Gal4;UAS:KillerRed*) fish line in which all V2a neurons express KillerRed, a chromophore that generates reactive oxygen species under specific light intensities to kill neurons (Liao et al., 2014). The KillerRed will only affect the neurons subjected to this light stimulation, providing spatial control of the ablation. An experiment to test this hypothesis would be to perform VR recordings from one muscle segment directly adjacent to the ablated area (0 – 1 segments caudal) and then another segment located further away from the ablation site (4 – 6 muscle segments caudal). From this experiment, we would expect minimal to zero impact on the firing frequency of the motor nerve adjacent to the ablation site given that V2a neurons provide very little local input. However, we predict robust deficiencies in the more caudal motor nerve given that V2a neurons preferential connect to longer range targets. Ultimately, these experiments would test the difference in impact of V2a neurons on local circuits, versus at longer ranges down the spinal cord.

Identification of the new CPG Candidate Population

Our optical mapping revealed that V2a neurons are very unlikely to be the neuronal population responsible for establishing the innate rhythmic nature of the spinal cord CPG network. This possibility was previously proposed by Kiehn (2016), who stated V2a neurons function downstream of the rhythm generating neurons given V2a ablation did not impact the ongoing locomotor rhythm in mammals (Crone et al., 2008; Crone et al., 2009; Kiehn, 2016). However, evidence still suggests that an ipsilateral, excitatory population is responsible for shaping the rhythmicity in the spinal cord (Cangiano & Grillner, 2003). Researchers arrived at this conclusion when hemicord preparations in lamprey were still able to exhibit burst patterning when glutamate was applied, and additionally, application of glycinergic antagonists did not affect rhythmicity, suggesting that commissural interneurons were not needed for

rhythmogenesis (Cangiano & Grillner, 2003; Grillner, 2003). A possible candidate is the population of Shox2 neurons which are a group of ipsilaterally projecting excitatory neurons found in the spinal cord and have been implicated in rhythm generation in mammals (Dougherty et al., 2013). Shox2 neurons do not comprise their own cardinal class of interneurons, but rather, they are believed to overlap with several neuron groups, including V2a neurons (Dougherty et al., 2013). In mammals, optogenetic silencing of nonV2a Shox2^{+} led to perturbations in rhythm generation, suggesting that Shox2+ neurons function within the CPG network (Dougherty et al., 2013). Furthermore, Shox2+ neurons provide local recurrent excitation onto each other, which is a hallmark of the expected unit burst generator population (Ha & Dougherty, 2018). Thus, we plan on recording from nonV2a Shox2+ neurons in the zebrafish spinal as a possible neuronal candidate of the CPG producing neuron (Kiehn, 2016).

Identification and Electrophysiological Assessment of Shox2 neuron subtypes in zebrafish

Shox2 is expressed in the spinal cord of zebrafish much like in mammals (Laureano et al., 2022), and given the evolutionary conserved nature of the spinal cord, it is very likely that there is heterogeneity within the Shox2+ population of zebrafish. As previously stated, Shox2+ neurons in spinal cord are comprised of several distinct cell types with a subpopulation of Shox2+ being V2a neurons. The identity of the nonV2a Shox2+ is not clear; however, overlap of Lbx1 and Isl1, which are markers of sensory derived populations, make it possible that nonV2a Shox2+ neurons are dorsal dI3, dI4 cell types (Dougherty et al., 2013). Thus, it would be important to perform HCR fluorescent *in situ*s in *Tg*(*shox2:Gal4;UAS:GFP,RFP*) fish to identify subpopulations of Shox2 neurons in zebrafish. This assessment of Shox2 subtypes will help in identifying potential targets during our electrophysiology experiments. During our optical mapping of V2a targets, we did not identify a population of neurons that received local input

from V2a neurons. However, V2a neurons should form synapses onto a local target given that previous experiments showed synaptophysin on portions of the axon that are close the V2a soma and axon hillock (Menelaou et al., 2014). We hypothesize that Shox2+ neurons are the local target of V2a neurons, wherein Shox2+ neurons integrate the excitatory input from V2a neurons which is later converted into the rhythmogenic output needed in the spinal cord. This hypothesis could be tested by performing our V2a optical mapping protocol on Shox2+ neurons. This time, we would expect to see robust input from local V2a neurons onto Shox2+ neurons. Once we have mapped V2a input onto Shox2 neurons, one could perform the same ablation experiments described in the previous section on Shox2+ neurons to examine rhythmogenic deficiencies. Here, we hypothesize that ablation of Shox2+ neurons will lead to local motor defects such as the inability to produce rhythmic swim. Altogether, this will demonstrate the Shox2+ neurons are the rhythmogenic drivers in the spinal cord circuit (Fig 4.1).

4.4 Figures and Legends

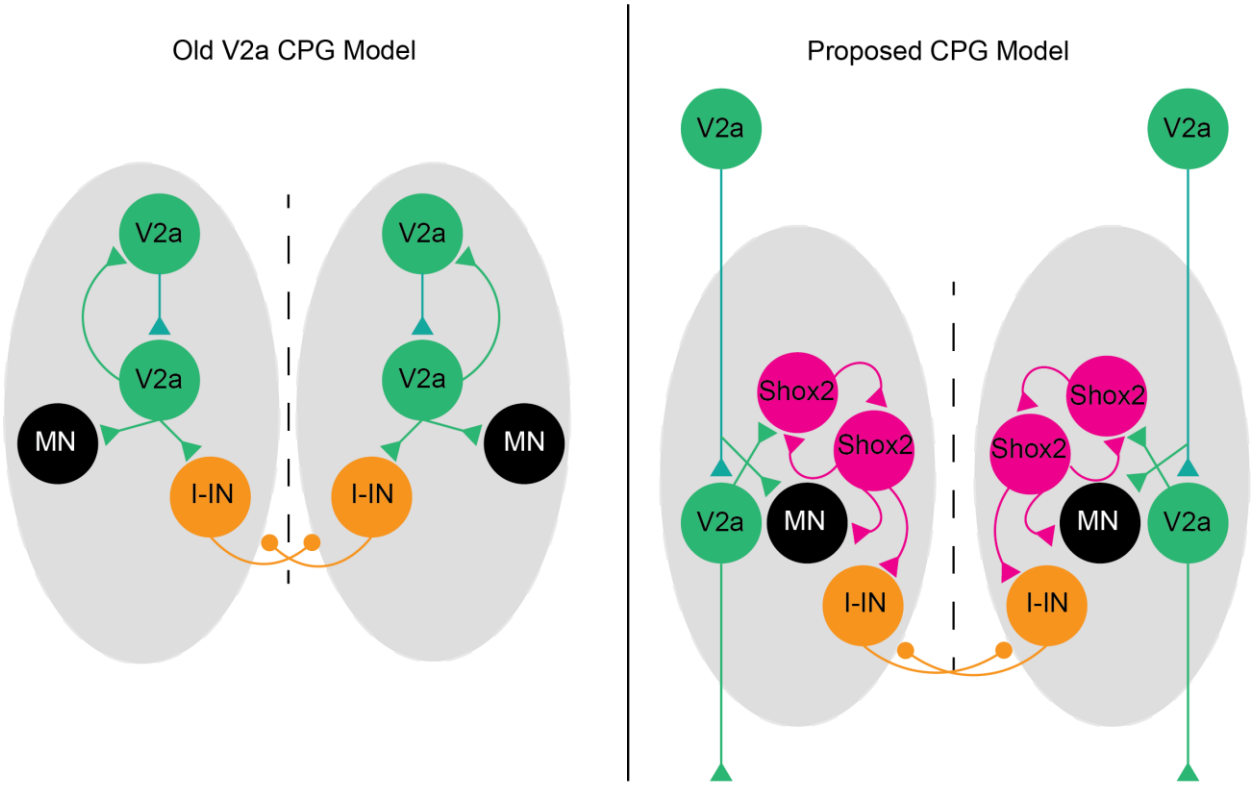

Figure 4.1 Shox2 neurons function as the central pattern generators of the spinal cord

In adult zebrafish, the CPG model predicts that V2a neurons function as the local unit burst generators providing local excitation onto motor neurons (output) and other V2a neurons (recurrence). However, our work disagrees with this current hypothesis. We propose a new model where V2a neurons provide long range excitation onto both V2a and motor neurons as means of excitatory wave propagation. Instead, we hypothesize that Shox2 neurons function as the local recurrent excitatory source that drives rhythmogenesis in the spinal cord.

References

Agha, M. A., Kishore, S., & McLean, D. L. (2024). Cell-type-specific origins of spinal rhythmicity at different locomotor speeds in larval zebrafish. *bioRxiv*, 2024.2001.2011.575271. https://doi.org/10.1101/2024.01.11.575271

Al-Mosawie, A., Wilson, J., & Brownstone, R. (2007). Heterogeneity of V2-derived interneurons in the adult mouse spinal cord. *European Journal of Neuroscience*, *26*(11), 3003-3015.

Alvarez, F. J., Jonas, P. C., Sapir, T., Hartley, R., Berrocal, M. C., Geiman, E. J., Todd, A. J., & Goulding, M. (2005). Postnatal phenotype and localization of spinal cord V1 derived interneurons. *Journal of Comparative Neurology*, *493*(2), 177-192.

Ampatzis, K., Song, J., Ausborn, J., & Abdeljabbar. (2014). Separate Microcircuit Modules of Distinct V2a Interneurons and Motoneurons Control the Speed of Locomotion. *Neuron*, *83*(4), 934-943. https://doi.org/10.1016/j.neuron.2014.07.018

Andersson, L. S., Larhammar, M., Memic, F., Wootz, H., Schwochow, D., Rubin, C.-J., Patra, K., Arnason, T., Wellbring, L., & Hjälm, G. (2012). Mutations in DMRT3 affect locomotion in horses and spinal circuit function in mice. *Nature*, *488*(7413), 642-646.

Andrzejczuk, L. A., Banerjee, S., England, S. J., Voufo, C., Kamara, K., & Lewis, K. E. (2018). Tal1, Gata2a, and Gata3 Have Distinct Functions in the Development of V2b and Cerebrospinal Fluid-Contacting KA Spinal Neurons [Original Research]. *Frontiers in Neuroscience*, *12*. https://doi.org/10.3389/fnins.2018.00170

Antinucci, P., Dumitrescu, A., Deleuze, C., Morley, H. J., Leung, K., Hagley, T., Kubo, F., Baier, H., Bianco, I. H., & Wyart, C. (2020). A calibrated optogenetic toolbox of stable zebrafish opsin lines. *eLife*, *9*. https://doi.org/10.7554/elife.54937

Artavanis-Tsakonas, S., Rand, M. D., & Lake, R. J. (1999). Notch Signaling: Cell Fate Control and Signal Integration in Development. *Science*, *284*(5415), 770-776. https://doi.org/doi:10.1126/science.284.5415.770

Bagnall, M. W., & McLean, D. L. (2014). Modular Organization of Axial Microcircuits in Zebrafish. *Science*, *343*(6167), 197-200. https://doi.org/10.1126/science.1245629

Batista, M. F., Jacobstein, J., & Lewis, K. E. (2008). Zebrafish V2 cells develop into excitatory CiD and Notch signalling dependent inhibitory VeLD interneurons. *Developmental Biology*, *322*(2), 263-275. https://doi.org/https://doi.org/10.1016/j.ydbio.2008.07.015

Bello-Rojas, S., Istrate, A. E., Kishore, S., & McLean, D. L. (2019). Central and peripheral innervation patterns of defined axial motor units in larval zebrafish. *Journal of Comparative Neurology*, *527*(15), 2557-2572. https://doi.org/10.1002/cne.24689

Bhumbra, G. S., Bannatyne, B. A., Watanabe, M., Todd, A. J., Maxwell, D. J., & Beato, M. (2014). The recurrent case for the Renshaw cell. *J Neurosci*, *34*(38), 12919-12932. https://doi.org/10.1523/JNEUROSCI.0199-14.2014

Bikoff, J. B., Gabitto, M. I., Rivard, A. F., Drobac, E., Machado, T. A., Miri, A., Brenner-Morton, S., Famojure, E., Diaz, C., Alvarez, F. J., Mentis, G. Z., & Jessell, T. M. (2016). Spinal Inhibitory Interneuron Diversity Delineates Variant Motor Microcircuits. *Cell*, *165*(1), 207-219. https://doi.org/10.1016/j.cell.2016.01.027

Björnfors, E. R., & El Manira, A. (2016). Functional diversity of excitatory commissural interneurons in adult zebrafish. *eLife*, *5*. https://doi.org/10.7554/eLife.18579

Blacklaws, J., Deska-Gauthier, D., Jones, C. T., Petracca, Y. L., Liu, M., Zhang, H., Fawcett, J. P., Glover, J. C., Lanuza, G. M., & Zhang, Y. (2015). Sim1 is required for the migration

and axonal projections of V3 interneurons in the developing mouse spinal cord. *Dev Neurobiol*, *75*(9), 1003-1017. https://doi.org/10.1002/dneu.22266

Böhm, U. L., Kimura, Y., Kawashima, T., Ahrens, M. B., Higashijima, S. I., Engert, F., & Cohen, A. E. (2022). Voltage imaging identifies spinal circuits that modulate locomotor adaptation in zebrafish. *Neuron*, *110*(7), 1211-1222.e1214. https://doi.org/10.1016/j.neuron.2022.01.001

Bonnot, A., Whelan, P. J., Mentis, G. Z., & O'Donovan, M. J. (2002). Spatiotemporal pattern of motoneuron activation in the rostral lumbar and the sacral segments during locomotor-like activity in the neonatal mouse spinal cord. *J Neurosci*, *22*(3), Rc203. https://doi.org/10.1523/JNEUROSCI.22-03-j0001.2002

Borowska, J., Jones, C. T., Deska-Gauthier, D., & Zhang, Y. (2015). V3 interneuron subpopulations in the mouse spinal cord undergo distinctive postnatal maturation processes. *Neuroscience*, *295*, 221-228. https://doi.org/10.1016/j.neuroscience.2015.03.024

Borowska, J., Jones, C. T., Zhang, H., Blacklaws, J., Goulding, M., & Zhang, Y. (2013). Functional subpopulations of V3 interneurons in the mature mouse spinal cord. *J Neurosci*, *33*(47), 18553-18565. https://doi.org/10.1523/JNEUROSCI.2005-13.2013

Britz, O., Zhang, J., Grossmann, K. S., Dyck, J., Kim, J. C., Dymecki, S., Gosgnach, S., & Goulding, M. (2015). A genetically defined asymmetry underlies the inhibitory control of flexor–extensor locomotor movements. *eLife*, *4*. https://doi.org/10.7554/elife.04718

Callahan, R. A., Roberts, R., Sengupta, M., Kimura, Y., Higashijima, S.-I., & Bagnall, M. W. (2019). Spinal V2b neurons reveal a role for ipsilateral inhibition in speed control. *eLife*, *8*. https://doi.org/10.7554/elife.47837

Cangiano, L., & Grillner, S. (2003). Fast and Slow Locomotor Burst Generation in the Hemispinal Cord of the Lamprey. *Journal of Neurophysiology*, *89*(6), 2931-2942. https://doi.org/10.1152/jn.01100.2002

Carbo-Tano, M., Lapoix, M., Jia, X., Thouvenin, O., Pascucci, M., Auclair, F., Quan, F. B., Albadri, S., Aguda, V., Farouj, Y., Hillman, E. M. C., Portugues, R., Del Bene, F., Thiele, T. R., Dubuc, R., & Wyart, C. (2023). The mesencephalic locomotor region recruits V2a reticulospinal neurons to drive forward locomotion in larval zebrafish. *Nature Neuroscience*. https://doi.org/10.1038/s41593-023-01418-0

Chopek, J. W., Nascimento, F., Beato, M., Brownstone, R. M., & Zhang, Y. (2018). Sub-populations of Spinal V3 Interneurons Form Focal Modules of Layered Pre-motor Microcircuits. *Cell Rep*, *25*(1), 146-156 e143. https://doi.org/10.1016/j.celrep.2018.08.095

Cregg, J. M., Leiras, R., Montalant, A., Wanken, P., Wickersham, I. R., & Kiehn, O. (2020). Brainstem neurons that command mammalian locomotor asymmetries. *Nat Neurosci*, *23*(6), 730-740. https://doi.org/10.1038/s41593-020-0633-7

Crone, S. A., Quinlan, K. A., Zagoraiou, L., Droho, S., Restrepo, C. E., Lundfald, L., Endo, T., Setlak, J., Jessell, T. M., Kiehn, O., & Sharma, K. (2008). Genetic ablation of V2a ipsilateral interneurons disrupts left-right locomotor coordination in mammalian spinal cord. *Neuron*, *60*(1), 70-83. https://doi.org/10.1016/j.neuron.2008.08.009

Crone, S. A., Zhong, G., Harris-Warrick, R., & Sharma, K. (2009). In mice lacking V2a interneurons, gait depends on speed of locomotion. *J Neurosci*, *29*(21), 7098-7109. https://doi.org/10.1523/jneurosci.1206-09.2009

Cucun, G., Köhler, M., Pfitsch, S., & Rastegar, S. (2024). Insights into the mechanisms of neuron generation and specification in the zebrafish ventral spinal cord. *The FEBS Journal*, *291*(4), 646-662. https://doi.org/https://doi.org/10.1111/febs.16913

Danner, S. M., Shevtsova, N. A., Frigon, A., & Rybak, I. A. (2017). Computational modeling of spinal circuits controlling limb coordination and gaits in quadrupeds. *eLife*, *6*. https://doi.org/10.7554/eLife.31050

Debrulle, S., Baudouin, C., Hidalgo-Figueroa, M., Pelosi, B., Francius, C., Rucchin, V., Ronellenfitch, K., Chow, R. L., Tissir, F., Lee, S.-K., & Clotman, F. (2020). Vsx1 and Chx10 paralogs sequentially secure V2 interneuron identity during spinal cord development. *Cellular and Molecular Life Sciences*, *77*(20), 4117-4131. https://doi.org/10.1007/s00018-019-03408-7

Del Barrio, M. G., Taveira-Marques, R., Muroyama, Y., Yuk, D.-I., Li, S., Wines-Samuelson, M., Shen, J., Smith, H. K., Xiang, M., Rowitch, D., & Richardson, W. D. (2007). A regulatory network involving Foxn4, Mash1 and delta-like 4/Notch1 generates V2a and V2b spinal interneurons from a common progenitor pool. *Development*, *134*(19), 3427-3436. https://doi.org/10.1242/dev.005868

Deska-Gauthier, D., Borowska-Fielding, J., Jones, C. T., & Zhang, Y. (2020). The Temporal Neurogenesis Patterning of Spinal p3-V3 Interneurons into Divergent Subpopulation Assemblies. *J Neurosci*, *40*(7), 1440-1452. https://doi.org/10.1523/jneurosci.1518-19.2019

Dessaud, E., McMahon, A. P., & Briscoe, J. (2008). Pattern formation in the vertebrate neural tube: a sonic hedgehog morphogen-regulated transcriptional network.

Dougherty, K. J., Zagoraiou, L., Satoh, D., Rozani, I., Doobar, S., Arber, S., Jessell, T. M., & Kiehn, O. (2013). Locomotor rhythm generation linked to the output of spinal shox2 excitatory interneurons. *Neuron*, *80*(4), 920-933.

Eccles, J. C. (1957). The physiology of nerve cells. In *The physiology of nerve cells* (pp. ix, 270-ix, 270).

Eisen, J., Pike, S., & Romancier, B. (1990). An identified motoneuron with variable fates in embryonic zebrafish. *The Journal of Neuroscience*, *10*(1), 34-43. https://doi.org/10.1523/jneurosci.10-01-00034.1990

Eklöf-Ljunggren, E., Haupt, S., Ausborn, J., Dehnisch, I., Uhlén, P., Higashijima, S.-I., & El Manira, A. (2012). Origin of excitation underlying locomotion in the spinal circuit of zebrafish. *Proceedings of the National Academy of Sciences*, *109*(14), 5511-5516. https://doi.org/10.1073/pnas.1115377109

Endo, K., Aoki, T., Yoda, Y., Kimura, K.-I., & Hama, C. (2007). Notch signal organizes the Drosophila olfactory circuitry by diversifying the sensory neuronal lineages. *Nature Neuroscience*, *10*(2), 153-160. https://doi.org/10.1038/nn1832

Engerer, P., Petridou, E., Williams, P. R., Suzuki, S. C., Yoshimatsu, T., Portugues, R., Misgeld, T., & Godinho, L. (2021). Notch-mediated re-specification of neuronal identity during central nervous system development. *Current Biology*, *31*(21), 4870-4878.e4875. https://doi.org/10.1016/j.cub.2021.08.049

Falgairolle, M., & O'Donovan, M. J. (2019). V1 interneurons regulate the pattern and frequency of locomotor-like activity in the neonatal mouse spinal cord. *PLoS Biology*, *17*(9), e3000447.

Fedirchuk, B., Nielsen, J., Petersen, N., & Hultborn, H. (1998). Pharmacologically evoked fictive motor patterns in the acutely spinalized marmoset monkey (Callithrix jacchus). *Experimental Brain Research*, *122*(3), 351-361. https://doi.org/10.1007/s002210050523

Forli, A., Vecchia, D., Binini, N., Succol, F., Bovetti, S., Moretti, C., Nespoli, F., Mahn, M., Baker, C. A., Bolton, M. M., Yizhar, O., & Fellin, T. (2018). Two-Photon Bidirectional Control and Imaging of Neuronal Excitability with High Spatial Resolution In Vivo. *Cell Reports*, *22*(11), 3087-3098. https://doi.org/https://doi.org/10.1016/j.celrep.2018.02.063

Francius, C., Hidalgo-Figueroa, M., Debrulle, S., Pelosi, B., Rucchin, V., Ronellenfitch, K., Panayiotou, E., Makrides, N., Misra, K., Harris, A., Hassani, H., Schakman, O., Parras, C., Xiang, M., Malas, S., Chow, R. L., & Clotman, F. (2016). Vsx1 Transiently Defines an Early Intermediate V2 Interneuron Precursor Compartment in the Mouse Developing Spinal Cord [Original Research]. *Frontiers in Molecular Neuroscience*, *9*. https://doi.org/10.3389/fnmol.2016.00145

Gerber, V., Yang, L., Takamiya, M., Ribes, V., Gourain, V., Peravali, R., Stegmaier, J., Mikut, R., Reischl, M., Ferg, M., Rastegar, S., & Strähle, U. (2019). The HMG box transcription factors Sox1a and b specify a new class of glycinergic interneurons in the spinal cord of zebrafish embryos. *Development*, *146*(4), dev172510. https://doi.org/10.1242/dev.172510

Gosgnach, S., Lanuza, G. M., Butt, S. J., Saueressig, H., Zhang, Y., Velasquez, T., Riethmacher, D., Callaway, E. M., Kiehn, O., & Goulding, M. (2006). V1 spinal neurons regulate the speed of vertebrate locomotor outputs. *Nature*, *440*(7081), 215-219.

Goulding, M. (2009). Circuits controlling vertebrate locomotion: moving in a new direction. *Nature Reviews Neuroscience*, *10*(7), 507-518. https://doi.org/10.1038/nrn2608

Goulding, M., & Lamar, E. (2000). Neuronal patterning: Making stripes in the spinal cord. *Current Biology*, *10*(15), R565-R568. https://doi.org/https://doi.org/10.1016/S0960-9822(00)00615-1

Grillner, S. (1985). Neurobiological Bases of Rhythmic Motor Acts in Vertebrates. *Science*, *228*(4696), 143-149. https://doi.org/doi:10.1126/science.3975635

Grillner, S. (2003). The motor infrastructure: from ion channels to neuronal networks. *Nat Rev Neurosci*, *4*(7), 573-586. https://doi.org/10.1038/nrn1137

Grillner, S., Kozlov, A., Dario, P., Stefanini, C., Menciassi, A., Lansner, A., & Kotaleski, J. H. (2007). Modeling a vertebrate motor system: pattern generation, steering and control of body orientation. *Progress in brain research*, *165*, 221-234.

Grillner, S., & Manira, A. E. (2020). Current Principles of Motor Control, with Special Reference to Vertebrate Locomotion. *Physiological Reviews*, *100*(1), 271-320. https://doi.org/10.1152/physrev.00015.2019

Guan, N. N., Xu, L., Zhang, T., Huang, C.-X., Wang, Z., Dahlberg, E., Wang, H., Wang, F., Pallucchi, I., Hua, Y., El Manira, A., & Song, J. (2021). A specialized spinal circuit for command amplification and directionality during escape behavior. *Proceedings of the National Academy of Sciences*, *118*(42), e2106785118. https://doi.org/doi:10.1073/pnas.2106785118

Ha, N. T., & Dougherty, K. J. (2018). Spinal Shox2 interneuron interconnectivity related to function and development. *eLife*, *7*. https://doi.org/10.7554/eLife.42519

Hägglund, M., Borgius, L., Dougherty, K. J., & Kiehn, O. (2010). Activation of groups of excitatory neurons in the mammalian spinal cord or hindbrain evokes locomotion. *Nature Neuroscience*, *13*(2), 246-252. https://doi.org/10.1038/nn.2482

Harris, R. M., Pfeiffer, B. D., Rubin, G. M., & Truman, J. W. (2015). Neuron hemilineages provide the functional ground plan for the Drosophila ventral nervous system. *eLife*, *4*, e04493. https://doi.org/10.7554/eLife.04493

Hayashi, M., Gullo, M., Senturk, G., Di Costanzo, S., Nagasaki, S. C., Kageyama, R., Imayoshi, I., Goulding, M., Pfaff, S. L., & Gatto, G. (2023). A spinal synergy of excitatory and inhibitory neurons coordinates ipsilateral body movements. In: Cold Spring Harbor Laboratory.

Hayashi, M., Hinckley, C. A., Driscoll, S. P., Moore, N. J., Levine, A. J., Hilde, K. L., Sharma, K., & Pfaff, S. L. (2018). Graded Arrays of Spinal and Supraspinal V2a Interneuron Subtypes Underlie Forelimb and Hindlimb Motor Control. *Neuron*, *97*(4), 869-884.e865. https://doi.org/10.1016/j.neuron.2018.01.023

Heckman, C., & Enoka, R. M. (2012). Motor unit. *Comprehensive physiology*(4), 2629-2682.

Henneman, E. (1957). Relation between Size of Neurons and Their Susceptibility to Discharge. *Science*, *126*(3287), 1345-1347. https://doi.org/doi:10.1126/science.126.3287.1345

Henneman, E., Clamann, H. P., Gillies, J. D., & Skinner, R. D. (1974). Rank order of motoneurons within a pool: law of combination. *Journal of Neurophysiology*, *37*(6), 1338-1349.

Henneman, E., & Mendell, L. M. Functional Organization of Motoneuron Pool and its Inputs. In *Comprehensive physiology* (pp. 423-507). https://doi.org/https://doi.org/10.1002/cphy.cp010211

Henneman, E., Somjen, G., & Carpenter, D. O. (1965). FUNCTIONAL SIGNIFICANCE OF CELL SIZE IN SPINAL MOTONEURONS. *Journal of Neurophysiology*, *28*(3), 560-580. https://doi.org/10.1152/jn.1965.28.3.560

Higashijima, S., Masino, M. A., Mandel, G., & Fetcho, J. R. (2004). Engrailed-1 expression marks a primitive class of inhibitory spinal interneuron. *J Neurosci*, *24*(25), 5827-5839. https://doi.org/10.1523/jneurosci.5342-03.2004

Huang, K. H., Ahrens, M. B., Dunn, T. W., & Engert, F. (2013). Spinal projection neurons control turning behaviors in zebrafish. *Curr Biol*, *23*(16), 1566-1573. https://doi.org/10.1016/j.cub.2013.06.044

Jacobs, C. T., Kejriwal, A., Kocha, K. M., Jin, K. Y., & Huang, P. (2022a). Temporal cell fate determination in the spinal cord is mediated by the duration of Notch signalling. *Developmental Biology*, *489*, 1-13. https://doi.org/https://doi.org/10.1016/j.ydbio.2022.05.010

Jacobs, C. T., Kejriwal, A., Kocha, K. M., Jin, K. Y., & Huang, P. (2022b). Temporal cell fate determination in the spinal cord is mediated by the duration of Notch signalling. *Developmental Biology*. https://doi.org/https://doi.org/10.1016/j.ydbio.2022.05.010

Jankowska, E. (2001). Spinal interneuronal systems: identification, multifunctional character and reconfigurations in mammals. *The Journal of Physiology*, *533*(1), 31-40.

Jankowska, E., & Edgley, S. (1993). Interactions between pathways controlling posture and gait at the level of spinal interneurones in the cat. *Progress in brain research*, *97*, 161-171.

Jay, M., MacIver, M. A., & McLean, D. L. (2023). Spinal Basis of Direction Control during Locomotion in Larval Zebrafish. *The Journal of Neuroscience*, *43*(22), 4062-4074. https://doi.org/10.1523/jneurosci.0703-22.2023

Jessell, T. M. (2000). Neuronal specification in the spinal cord: inductive signals and transcriptional codes. *Nature Reviews Genetics*, *1*(1), 20-29. https://doi.org/10.1038/35049541

Juárez-Morales, J. L., Schulte, C. J., Pezoa, S. A., Vallejo, G. K., Hilinski, W. C., England, S. J., de Jager, S., & Lewis, K. E. (2016). Evx1 and Evx2 specify excitatory neurotransmitter fates and suppress inhibitory fates through a Pax2-independent mechanism. *Neural Development*, *11*(1), 5. https://doi.org/10.1186/s13064-016-0059-9

Kageyama, R., Ohtsuka, T., Shimojo, H., & Imayoshi, I. (2009). Dynamic regulation of Notch signaling in neural progenitor cells. *Curr Opin Cell Biol*, *21*(6), 733-740. https://doi.org/10.1016/j.ceb.2009.08.009

Kandler, K., Clause, A., & Noh, J. (2009). Tonotopic reorganization of developing auditory brainstem circuits. *Nat Neurosci*, *12*(6), 711-717. https://doi.org/10.1038/nn.2332

Kawano, K., Kato, K., Sugioka, T., Kimura, Y., Tanimoto, M., & Higashijima, S. I. (2022). Long descending commissural V0v neurons ensure coordinated swimming movements along the body axis in larval zebrafish. *Sci Rep*, *12*(1), 4348. https://doi.org/10.1038/s41598-022-08283-0

Kiehn, O. (2006). LOCOMOTOR CIRCUITS IN THE MAMMALIAN SPINAL CORD. *Annual Review of Neuroscience*, *29*(1), 279-306. https://doi.org/10.1146/annurev.neuro.29.051605.112910

Kiehn, O. (2016). Decoding the organization of spinal circuits that control locomotion. *Nature Reviews Neuroscience*, *17*(4), 224-238. https://doi.org/10.1038/nrn.2016.9

Kimura, Y., & Higashijima, S. I. (2019). Regulation of locomotor speed and selection of active sets of neurons by V1 neurons. *Nat Commun*, *10*(1), 2268. https://doi.org/10.1038/s41467-019-09871-x

Kimura, Y., Okamura, Y., & Higashijima, S.-i. (2006). alx, a Zebrafish Homolog of Chx10, Marks Ipsilateral Descending Excitatory Interneurons That Participate in the Regulation of Spinal Locomotor Circuits. *Journal of Neuroscience*, *26*(21), 5684-5697. https://doi.org/10.1523/jneurosci.4993-05.2006

Kimura, Y., Satou, C., & Higashijima, S.-I. (2008). V2a and V2b neurons are generated by the final divisions of pair-producing progenitors in the zebrafish spinal cord. *Development*, *135*(18), 3001-3005. https://doi.org/10.1242/dev.024802

Kishore, S., Cadoff, E. B., Agha, M. A., & McLean, D. L. (2020). Orderly compartmental mapping of premotor inhibition in the developing zebrafish spinal cord. *Science*, *370*(6515), 431-436. https://doi.org/doi:10.1126/science.abb4608

Kjaerulff, O., & Kiehn, O. (1997). Crossed rhythmic synaptic input to motoneurons during selective activation of the contralateral spinal locomotor network. *Journal of Neuroscience*, *17*(24), 9433-9447.

Kozak, E. L., Palit, S., Miranda-Rodríguez, J. R., Janjic, A., Böttcher, A., Lickert, H., Enard, W., Theis, F. J., & López-Schier, H. (2020). Epithelial Planar Bipolarity Emerges from Notch-Mediated Asymmetric Inhibition of Emx2. *Current Biology*, *30*(6), 1142-1151.e1146. https://doi.org/10.1016/j.cub.2020.01.027

Kozlov, A., Huss, M., Lansner, A., Kotaleski, J. H., & Grillner, S. (2009). Simple cellular and network control principles govern complex patterns of motor behavior. *Proceedings of the National Academy of Sciences*, *106*(47), 20027-20032.

Lacin, H., Chen, H.-M., Long, X., Singer, R. H., Lee, T., & Truman, J. W. (2019). Neurotransmitter identity is acquired in a lineage-restricted manner in the Drosophila CNS. *eLife*, *8*, e43701. https://doi.org/10.7554/eLife.43701

Lacin, H., & Truman, J. W. (2016). Lineage mapping identifies molecular and architectural similarities between the larval and adult Drosophila central nervous system. *eLife*, *5*. https://doi.org/10.7554/elife.13399

Lacin, H., Zhu, Y., Wilson, B. A., & Skeath, J. B. (2014). Transcription factor expression uniquely identifies most postembryonic neuronal lineages in the Drosophila thoracic central nervous system. *Development*, *141*(5), 1011-1021. https://doi.org/10.1242/dev.102178

Lanuza, G. M., Gosgnach, S., Pierani, A., Jessell, T. M., & Goulding, M. (2004). Genetic identification of spinal interneurons that coordinate left-right locomotor activity necessary for walking movements. *Neuron*, *42*(3), 375-386.

Lathia, J. D., Mattson, M. P., & Cheng, A. (2008). Notch: from neural development to neurological disorders. *J Neurochem*, *107*(6), 1471-1481. https://doi.org/10.1111/j.1471-4159.2008.05715.x

Laureano, A. S., Flaherty, K., Hinman, A. M., Jadali, A., Nakamura, T., Higashijima, S. I., Sabaawy, H. E., & Kwan, K. Y. (2022). shox2 is required for vestibular statoacoustic neuron development. *Biol Open*, *11*(12). https://doi.org/10.1242/bio.059599

Le Dréau, G., & Martí, E. (2012). Dorsal–ventral patterning of the neural tube: a tale of three signals. *Developmental Neurobiology*, *72*(12), 1471-1481.

Lee, K. J., & Jessell, T. M. (1999). The specification of dorsal cell fates in the vertebrate central nervous system. *Annual Review of Neuroscience*, *22*(1), 261-294.

Leto, K., Arancillo, M., Becker, E. B., Buffo, A., Chiang, C., Ding, B., Dobyns, W. B., Dusart, I., Haldipur, P., Hatten, M. E., Hoshino, M., Joyner, A. L., Kano, M., Kilpatrick, D. L., Koibuchi, N., Marino, S., Martinez, S., Millen, K. J., Millner, T. O., . . . Hawkes, R. (2016). Consensus Paper: Cerebellar Development. *Cerebellum*, *15*(6), 789-828. https://doi.org/10.1007/s12311-015-0724-2

Li, S., Misra, K., & Xiang, M. (2010). A Cre transgenic line for studying V2 neuronal lineages and functions in the spinal cord. *Genesis*, *48*(11), 667-672. https://doi.org/10.1002/dvg.20669

Li, W.-C., Higashijima, S.-i., Parry, D. M., Roberts, A., & Soffe, S. R. (2004). Primitive Roles for Inhibitory Interneurons in Developing Frog Spinal Cord. *The Journal of Neuroscience*, *24*(25), 5840-5848. https://doi.org/10.1523/jneurosci.1633-04.2004

Li, W. C., Roberts, A., & Soffe, S. R. (2009). Locomotor rhythm maintenance: electrical coupling among premotor excitatory interneurons in the brainstem and spinal cord of young Xenopus tadpoles. *J Physiol*, *587*(Pt 8), 1677-1693. https://doi.org/10.1113/jphysiol.2008.166942

Li, W. C., Soffe, S. R., Wolf, E., & Roberts, A. (2006). Persistent responses to brief stimuli: feedback excitation among brainstem neurons. *J Neurosci*, *26*(15), 4026-4035. https://doi.org/10.1523/jneurosci.4727-05.2006

Li, W. Y., Deng, L. X., Zhai, F. G., Wang, X. Y., Li, Z. G., & Wang, Y. (2023). Chx10+V2a interneurons in spinal motor regulation and spinal cord injury. *Neural Regen Res*, *18*(5), 933-939. https://doi.org/10.4103/1673-5374.355746

Liao, Z. X., Li, Y. C., Lu, H. M., & Sung, H. W. (2014). A genetically-encoded KillerRed protein as an intrinsically generated photosensitizer for photodynamic therapy. *Biomaterials*, *35*(1), 500-508. https://doi.org/10.1016/j.biomaterials.2013.09.075

Liu, Z., Hildebrand, D. G. C., Morgan, J. L., Jia, Y., Slimmon, N., & Bagnall, M. W. (2022). Organization of the gravity-sensing system in zebrafish. *Nature Communications*, *13*(1), 5060. https://doi.org/10.1038/s41467-022-32824-w

Ljunggren, E. E., Haupt, S., Ausborn, J., Ampatzis, K., & El Manira, A. (2014). Optogenetic activation of excitatory premotor interneurons is sufficient to generate coordinated locomotor activity in larval zebrafish. *J Neurosci*, *34*(1), 134-139. https://doi.org/10.1523/jneurosci.4087-13.2014

Lundfald, L., Restrepo, C. E., Butt, S. J., Peng, C. Y., Droho, S., Endo, T., Zeilhofer, H. U., Sharma, K., & Kiehn, O. (2007). Phenotype of V2-derived interneurons and their relationship to the axon guidance molecule EphA4 in the developing mouse spinal cord. *European Journal of Neuroscience*, *26*(11), 2989-3002.

Ma, J., Shen, Z., Yu, Y. C., & Shi, S. H. (2018). Neural lineage tracing in the mammalian brain. *Curr Opin Neurobiol*, *50*, 7-16. https://doi.org/10.1016/j.conb.2017.10.013

Mark, B., Lai, S.-L., Zarin, A. A., Manning, L., Pollington, H. Q., Litwin-Kumar, A., Cardona, A., Truman, J. W., & Doe, C. Q. (2021). A developmental framework linking neurogenesis and circuit formation in the Drosophila CNS. *eLife*, *10*. https://doi.org/10.7554/elife.67510

Mayer, C., Bandler, Rachel C., & Fishell, G. (2016). Lineage Is a Poor Predictor of Interneuron Positioning within the Forebrain. *Neuron*, *92*(1), 45-51. https://doi.org/https://doi.org/10.1016/j.neuron.2016.09.035

Mayer, C., Jaglin, X. H., Cobbs, L. V., Bandler, R. C., Streicher, C., Cepko, C. L., Hippenmeyer, S., & Fishell, G. (2015). Clonally Related Forebrain Interneurons Disperse Broadly across Both Functional Areas and Structural Boundaries. *Neuron*, *87*(5), 989-998. https://doi.org/10.1016/j.neuron.2015.07.011

McLean, D. L., Fan, J., Higashijima, S., Hale, M. E., & Fetcho, J. R. (2007). A topographic map of recruitment in spinal cord. *Nature*, *446*(7131), 71-75. https://doi.org/10.1038/nature05588

McLean, D. L., & Fetcho, J. R. (2009). Spinal interneurons differentiate sequentially from those driving the fastest swimming movements in larval zebrafish to those driving the slowest ones. *J Neurosci*, *29*(43), 13566-13577. https://doi.org/10.1523/jneurosci.3277-09.2009

Menelaou, E., & McLean, D. L. (2012). A gradient in endogenous rhythmicity and oscillatory drive matches recruitment order in an axial motor pool. *J Neurosci*, *32*(32), 10925-10939. https://doi.org/10.1523/JNEUROSCI.1809-12.2012

Menelaou, E., & McLean, D. L. (2019). Hierarchical control of locomotion by distinct types of spinal V2a interneurons in zebrafish. *Nature Communications*, *10*(1). https://doi.org/10.1038/s41467-019-12240-3

Menelaou, E., Vandunk, C., & McLean, D. L. (2014). Differences in the morphology of spinal V2a neurons reflect their recruitment order during swimming in larval zebrafish. *Journal of Comparative Neurology*, *522*(6), 1232-1248. https://doi.org/10.1002/cne.23465

Mizoguchi, T., Fukada, M., Iihama, M., Song, X., Fukagawa, S., Kuwabara, S., Omaru, S., Higashijima, S.-I., & Itoh, M. (2020). Transient activation of the Notch-her15.1 axis plays an important role in the maturation of V2b interneurons. *Development*, *147*(16), dev191312. https://doi.org/10.1242/dev.191312

Okigawa, S., Mizoguchi, T., Okano, M., Tanaka, H., Isoda, M., Jiang, Y.-J., Suster, M., Higashijima, S.-i., Kawakami, K., & Itoh, M. (2014). Different combinations of Notch ligands and receptors regulate V2 interneuron progenitor proliferation and V2a/V2b cell

fate determination. *Developmental Biology*, *391*(2), 196-206. https://doi.org/https://doi.org/10.1016/j.ydbio.2014.04.011

Panayi, H., Panayiotou, E., Orford, M., Genethliou, N., Mean, R., Lapathitis, G., Li, S., Xiang, M., Kessaris, N., Richardson, W. D., & Malas, S. (2010). Sox1 is required for the specification of a novel p2-derived interneuron subtype in the mouse ventral spinal cord. *J Neurosci*, *30*(37), 12274-12280. https://doi.org/10.1523/jneurosci.2402-10.2010

Passini, M. A., Kurtzman, A. L., Canger, A. K., Asch, W. S., Wray, G. A., Raymond, P. A., & Schechter, N. (1998). Cloning of zebrafish vsx1: Expression of a paired-like homeobox gene during CNS development. *Developmental Genetics*, *23*(2), 128-141. https://doi.org/https://doi.org/10.1002/(SICI)1520-6408(1998)23:2<128::AID-DVG5>3.0.CO;2-8

Peng, C.-Y., Yajima, H., Burns, C. E., Zon, L. I., Sisodia, S. S., Pfaff, S. L., & Sharma, K. (2007). Notch and MAML Signaling Drives Scl-Dependent Interneuron Diversity in the Spinal Cord. *Neuron*, *53*(6), 813-827. https://doi.org/10.1016/j.neuron.2007.02.019

Pierani, A., Moran-Rivard, L., Sunshine, M., Littman, D., Goulding, M., & Jessell, T. (2001). Control of interneuron fate in the developing spinal cord by the progenitor homeodomain protein Dbx1. *Neuron*, *29*(2), 367-384.

Pinto-Teixeira, F., & Desplan, C. (2014). Notch activity in neural progenitors coordinates cytokinesis and asymmetric differentiation. *Science Signaling*, *7*(348), pe26-pe26. https://doi.org/doi:10.1126/scisignal.2005980

Preibisch, S., Saalfeld, S., & Tomancak, P. (2009). Globally optimal stitching of tiled 3D microscopic image acquisitions. *Bioinformatics*, *25*(11), 1463-1465. https://doi.org/10.1093/bioinformatics/btp184

Radosevic, M., Willumsen, A., Petersen, P. C., Lindén, H., Vestergaard, M., & Berg, R. W. (2019). Decoupling of timescales reveals sparse convergent CPG network in the adult spinal cord. *Nature Communications*, *10*(1), 2937. https://doi.org/10.1038/s41467-019-10822-9

Rothman, J. S., & Silver, R. A. (2018). NeuroMatic: An Integrated Open-Source Software Toolkit for Acquisition, Analysis and Simulation of Electrophysiological Data [Technology Report]. *Frontiers in Neuroinformatics*, *12*. https://doi.org/10.3389/fninf.2018.00014

Rousseau, C. V., Dugué, G. P., Dumoulin, A., Mugnaini, E., Dieudonné, S., & Diana, M. A. (2012). Mixed Inhibitory Synaptic Balance Correlates with Glutamatergic Synaptic Phenotype in Cerebellar Unipolar Brush Cells. *The Journal of Neuroscience*, *32*(13), 4632-4644. https://doi.org/10.1523/jneurosci.5122-11.2012

Roussel, Y., Gaudreau, S. F., Kacer, E. R., Sengupta, M., & Bui, T. V. (2021). Modeling spinal locomotor circuits for movements in developing zebrafish. *eLife*, *10*. https://doi.org/10.7554/eLife.67453

Russ, D. E., Cross, R. B. P., Li, L., Koch, S. C., Matson, K. J. E., Yadav, A., Alkaslasi, M. R., Lee, D. I., Le Pichon, C. E., Menon, V., & Levine, A. J. (2021). A harmonized atlas of mouse spinal cord cell types and their spatial organization. *Nature Communications*, *12*(1), 5722. https://doi.org/10.1038/s41467-021-25125-1

Sagner, A., & Briscoe, J. (2019). Establishing neuronal diversity in the spinal cord: a time and a place. *Development*, *146*(22). https://doi.org/10.1242/dev.182154

Satou, C., Kimura, Y., & Higashijima, S. (2012). Generation of multiple classes of V0 neurons in zebrafish spinal cord: progenitor heterogeneity and temporal control of neuronal

diversity. *J Neurosci*, *32*(5), 1771-1783. https://doi.org/10.1523/JNEUROSCI.5500-11.2012

Satou, C., Sugioka, T., Uemura, Y., Shimazaki, T., Zmarz, P., Kimura, Y., & Higashijima, S. I. (2020). Functional Diversity of Glycinergic Commissural Inhibitory Neurons in Larval Zebrafish. *Cell Rep*, *30*(9), 3036-3050.e3034. https://doi.org/10.1016/j.celrep.2020.02.015

Saueressig, H., Burrill, J., & Goulding, M. (1999). Engrailed-1 and netrin-1 regulate axon pathfinding by association interneurons that project to motor neurons. *Development*, *126*(19), 4201-4212. https://doi.org/10.1242/dev.126.19.4201

Schild, L. C., & Glauser, D. A. (2015). Dual Color Neural Activation and Behavior Control with Chrimson and CoChR in Caenorhabditis elegans. *Genetics*, *200*(4), 1029-1034. https://doi.org/10.1534/genetics.115.177956

Schindelin, J., Arganda-Carreras, I., Frise, E., Kaynig, V., Longair, M., Pietzsch, T., Preibisch, S., Rueden, C., Saalfeld, S., Schmid, B., Tinevez, J.-Y., White, D. J., Hartenstein, V., Eliceiri, K., Tomancak, P., & Cardona, A. (2012). Fiji: an open-source platform for biological-image analysis. *Nature Methods*, *9*(7), 676-682. https://doi.org/10.1038/nmeth.2019

Sengupta, M., & Bagnall, M. W. (2022). V2b neurons act via multiple targets in spinal motor networks. *bioRxiv*, 2022.2008.2001.502410. https://doi.org/10.1101/2022.08.01.502410

Sengupta, M., & Bagnall, M. W. (2023). Spinal Interneurons: Diversity and Connectivity in Motor Control. *Annu Rev Neurosci*. https://doi.org/10.1146/annurev-neuro-083122-025325

Sengupta, M., Daliparthi, V., Roussel, Y., Bui, T. V., & Bagnall, M. W. (2021). Spinal V1 neurons inhibit motor targets locally and sensory targets distally. *Current Biology*, *31*(17), 3820-3833.e3824. https://doi.org/https://doi.org/10.1016/j.cub.2021.06.053

Sestan, N., Artavanis-Tsakonas, S., & Rakic, P. (1999). Contact-dependent inhibition of cortical neurite growth mediated by notch signaling. *Science*, *286*(5440), 741-746.

Sherrington, C. (1904). Correlation of reflexes and the principle of the common path. Presidential address to the physiological section of the British Association for the Advancement of Science. *British Association Reports*.

Skeath, J. B., & Doe, C. Q. (1998). Sanpodo and Notch act in opposition to Numb to distinguish sibling neuron fates in the Drosophila CNS. *Development*, *125*(10), 1857-1865. https://doi.org/10.1242/dev.125.10.1857

Song, J., Dahlberg, E., & El Manira, A. (2018). V2a interneuron diversity tailors spinal circuit organization to control the vigor of locomotor movements. *Nat Commun*, *9*(1), 3370. https://doi.org/10.1038/s41467-018-05827-9

Song, J., Pallucchi, I., Ausborn, J., Ampatzis, K., Bertuzzi, M., Fontanel, P., Picton, L. D., & El Manira, A. (2020). Multiple Rhythm-Generating Circuits Act in Tandem with Pacemaker Properties to Control the Start and Speed of Locomotion. *Neuron*, *105*(6), 1048-1061.e1044. https://doi.org/10.1016/j.neuron.2019.12.030

Stokke, M. F., Nissen, U. V., Glover, J. C., & Kiehn, O. (2002). Projection patterns of commissural interneurons in the lumbar spinal cord of the neonatal rat. *Journal of Comparative Neurology*, *446*(4), 349-359.

Talpalar, A. E., Bouvier, J., Borgius, L., Fortin, G., Pierani, A., & Kiehn, O. (2013). Dual-mode operation of neuronal networks involved in left–right alternation. *Nature*, *500*(7460), 85-88. https://doi.org/10.1038/nature12286

Thisse, C., & Thisse, B. (2008). High-resolution in situ hybridization to whole-mount zebrafish embryos. *Nature Protocols*, *3*(1), 59-69. https://doi.org/10.1038/nprot.2007.514

Tootell, R. B., Silverman, M. S., Switkes, E., & De Valois, R. L. (1982). Deoxyglucose analysis of retinotopic organization in primate striate cortex. *Science*, *218*(4575), 902-904. https://doi.org/10.1126/science.7134981

Truman, J. W., Moats, W., Altman, J., Marin, E. C., & Williams, D. W. (2010). Role of Notch signaling in establishing the hemilineages of secondary neurons in Drosophila melanogaster. *Development*, *137*(1), 53-61. https://doi.org/10.1242/dev.041749

Tsai, T. Y.-C., Sikora, M., Xia, P., Colak-Champollion, T., Knaut, H., Heisenberg, C.-P., & Megason, S. G. (2020). An adhesion code ensures robust pattern formation during tissue morphogenesis. *Science*, *370*(6512), 113-116. https://doi.org/doi:10.1126/science.aba6637

Tunstall, M. J., & Roberts, A. (1994). A longitudinal gradient of synaptic drive in the spinal cord of Xenopus embryos and its role in co-ordination of swimming. *The Journal of Physiology*, *474*(3), 393-405.

Uemura, Y., Kato, K., Kawakami, K., Kimura, Y., Oda, Y., & Higashijima, S.-i. (2020). Neuronal Circuits That Control Rhythmic Pectoral Fin Movements in Zebrafish. *The Journal of Neuroscience*, *40*(35), 6678-6690. https://doi.org/10.1523/jneurosci.1484-20.2020

Usseglio, G., Gatier, E., Heuzé, A., Hérent, C., & Bouvier, J. (2020). Control of Orienting Movements and Locomotion by Projection-Defined Subsets of Brainstem V2a Neurons. *Current Biology*, *30*(23), 4665-4681.e4666. https://doi.org/https://doi.org/10.1016/j.cub.2020.09.014

Wen, H., & Brehm, P. (2010). Paired Patch Clamp Recordings from Motor-neuron and Target Skeletal Muscle in Zebrafish. *JoVE*(45), e2351. https://doi.org/doi:10.3791/2351

Wenner, P., O'Donovan, M. J., & Matise, M. P. (2000). Topographical and physiological characterization of interneurons that express engrailed-1 in the embryonic chick spinal cord. *Journal of Neurophysiology*.

Wiggin, T. D., Peck, J. H., & Masino, M. A. (2014). Coordination of fictive motor activity in the larval zebrafish is generated by non-segmental mechanisms. *PLoS One*, *9*(10), e109117. https://doi.org/10.1371/journal.pone.0109117

Willenberg, R., & Steward, O. (2015). Nonspecific labeling limits the utility of Cre-Lox bred CST-YFP mice for studies of corticospinal tract regeneration. *J Comp Neurol*, *523*(18), 2665-2682. https://doi.org/10.1002/cne.23809

Wilson, D., & Wyman, R. (1965). Motor output patterns during random and rhythmic stimulation of locust thoracic ganglia. *Biophysical Journal*, *5*(2), 121-143.

Wolf, E., Soffe, S. R., & Roberts, A. (2009). Longitudinal neuronal organization and coordination in a simple vertebrate: a continuous, semi-quantitative computer model of the central pattern generator for swimming in young frog tadpoles. *J Comput Neurosci*, *27*(2), 291-308. https://doi.org/10.1007/s10827-009-0143-9

Worthy, A. E., Anderson, J. T., Lane, A. R., Gomez-Perez, L., Wang, A. A., Griffith, R. W., Rivard, A. F., Bikoff, J. B., & Alvarez, F. J. (2023). SPINAL V1 INHIBITORY INTERNEURON CLADES DIFFER IN BIRTHDATE, PROJECTIONS TO MOTONEURONS AND HETEROGENEITY. *bioRxiv*, 2023.2011.2029.569270. https://doi.org/10.1101/2023.11.29.569270

Xu, H.-T., Han, Z., Gao, P., He, S., Li, Z., Shi, W., Kodish, O., Shao, W., Keith, Huang, K., & Shi, S.-H. (2014). Distinct Lineage-Dependent Structural and Functional Organization of the Hippocampus. *Cell*, *157*(7), 1552-1564. https://doi.org/10.1016/j.cell.2014.03.067

Yang, C., Li, S., Li, X., Li, H., Li, Y., Zhang, C., & Lin, J. (2019). Effect of sonic hedgehog on motor neuron positioning in the spinal cord during chicken embryonic development. *J Cell Mol Med*, *23*(5), 3549-3562. https://doi.org/10.1111/jcmm.14254

Yu, Y.-C., Bultje, R. S., Wang, X., & Shi, S.-H. (2009). Specific synapses develop preferentially among sister excitatory neurons in the neocortex. *Nature*, *458*(7237), 501-504. https://doi.org/10.1038/nature07722

Zhang, H., Shevtsova, N. A., Deska-Gauthier, D., Mackay, C., Dougherty, K. J., Danner, S. M., Zhang, Y., & Rybak, I. A. (2022). The role of V3 neurons in speed-dependent interlimb coordination during locomotion in mice. *eLife*, *11*. https://doi.org/10.7554/eLife.73424

Zhang, J., Guillermo, Britz, O., Wang, Z., Valerie, Zhang, Y., Velasquez, T., Francisco, Frank, E., & Goulding, M. (2014). V1 and V2b Interneurons Secure the Alternating Flexor-Extensor Motor Activity Mice Require for Limbed Locomotion. *Neuron*, *82*(1), 138-150. https://doi.org/10.1016/j.neuron.2014.02.013

Zhang, T., Liu, T., Mora, N., Guegan, J., Bertrand, M., Contreras, X., Hansen, A. H., Streicher, C., Anderle, M., Danda, N., Tiberi, L., Hippenmeyer, S., & Hassan, B. A. (2021). Generation of excitatory and inhibitory neurons from common progenitors via Notch signaling in the cerebellum. *Cell Reports*, *35*(10), 109208. https://doi.org/10.1016/j.celrep.2021.109208

Zhang, X.-J., Li, Z., Han, Z., Sultan, K. T., Huang, K., & Shi, S.-H. (2017). Precise inhibitory microcircuit assembly of developmentally related neocortical interneurons in clusters. *Nature Communications*, *8*(1), 16091. https://doi.org/10.1038/ncomms16091

Zhang, Y., Narayan, S., Geiman, E., Lanuza, G. M., Velasquez, T., Shanks, B., Akay, T., Dyck, J., Pearson, K., Gosgnach, S., Fan, C. M., & Goulding, M. (2008). V3 spinal neurons establish a robust and balanced locomotor rhythm during walking. *Neuron*, *60*(1), 84-96. https://doi.org/10.1016/j.neuron.2008.09.027

Zholudeva, L. V., Karliner, J. S., Dougherty, K. J., & Lane, M. A. (2017). Anatomical Recruitment of Spinal V2a Interneurons into Phrenic Motor Circuitry after High Cervical Spinal Cord Injury. *J Neurotrauma*, *34*(21), 3058-3065. https://doi.org/10.1089/neu.2017.5045